AD-A164 354

DTIC
SELECTED
FEB 1 4 1986
S D
D

DYNAMIC RESPONSE OF FLUID
TRANSMISSION LINES

THESIS

Stephen J. McKenna
Major, Canadian Armed Forces

AFIT/GAE/AA/85S-1

DEPARTMENT OF THE AIR FORCE

AIR UNIVERSITY

AIR FORCE INSTITUTE OF TECHNOLOGY

Wright-Patterson Air Force Base, Ohio

86 2 14 017

AFIT/GAE/AA/85S-1

DYNAMIC RESPONSE OF FLUID
TRANSMISSION LINES

THESIS

Stephen J. McKenna
Major, Canadian Armed Forces

AFIT/GAE/AA/85S-1

AFIT/GAE/AA/85S-1

DYNAMIC RESPONSE OF FLUID TRANSMISSION LINES

THESIS

Presented to the Faculty of the School of Engineering

of the Air Force Institute of Technology

Air University

In Partial Fulfillment of the

Requirements for the Degree of

Master of Science in Aeronautical Engineering

Stephen J. McKenna, B. Chem. Eng.

Major, Canadian Armed Forces

September 1985

Accesion For	
NTIS CRA&I	☑
DTIC TAB	☐
Unannounced	☐
Justification	
By	
Distribution /	
Availability Codes	
Dist	Avail a d/or Special
A-1	

Preface

The analysis of the dynamic response of pneumatic transmission lines has been the subject of an ongoing series of studies at the Air Force Institute of Technology, School of Engineering. This thesis is the latest in this series. The purpose of the study has been to examine specific areas in an attempt to answer questions raised in the earlier studies. The emphasis has been on the continuation of work conducted by Captain P. G. Wilkins in 1984.

I would like to take this opportunity to thank several individuals without whose assistance this study would not have been possible. My thesis advisor, Dr. M. E. Franke, provided invaluable guidance and advice. Dr. W. Elrod and Captain W. Cox also contributed welcome assistance in specific areas. Captain Phil Wilkins, whose earlier thesis provided a basis and direction for this study, gladly answered my questions and offered insights into the subject. I would also like to take this opportunity to express a special thank you to my wife Suzanne for her encouragement and confidence which has made my studies at AFIT so much easier.

— Stephen J. McKenna

ii

Table of Contents

List of Figures

ix

List of Tables

List of Symbols

Symbol	Description	Units
A	line cross-sectional area	in^2
a	adiabatic speed of sound	in/sec
B	phase angle	radians
C	capacitance/unit length	in^4/lbf
C_a	adiabatic capacitance/unit length	in^4/lbf
C_i	isothermal capacitance/unit length	in^4/lbf
C_T	turbulent capacitance/unit length	in^4/lbf
D	inside line diameter	in
f	friction factor	dimensionless
G	conductance/unit length	in^4/lbf-sec
g	pressure gain	dimensionless
g_{db}	Pressure gain in decibels	decibels
h_t	temperature distribution factor	dimensionless
h_v	velocity distribution factor	dimensionless
Im	imaginary part of a complex number	dimensionless
j	$(-1)^{\frac{1}{2}}$	dimensionless
k	ratio of specific heats	dimensionless
K_{LT}	inertance constant	dimensionless
L	inertance/unit length	lbf-sec^2/in^6
L_a	adiabatic inertance unit length	lbf-sec^2/in^6

xi

Symbol	Description	Units
L_T	turbulent inertance/unit length	$lbf\text{-}sec^2/in^6$
M	mass flow rate	lbm/sec
n	polytropic exponent	dimensionless
P	pressure	psia
P_a	ambient pressure	psia
P_{in}	inlet pressure	psia
P_L	pressure drop across load	psi
P_R	receiving pressure	psig
P_S	sending pressure	psig
P_T	static line pressure	psig
ΔP	pressure drop along a line	psi
Q	volumetric flow rate	in^3/sec
R	resistance/unit length	$lbf\text{-}sec/in^6$
R_{AC}	AC resistance/unit length	$lbf\text{-}sec/in^6$
R_{DC}	DC resistance/unit length	$lbf\text{-}sec/in^6$
R_g	gas constant for air	$in^2/sec^2\text{-}R$
Re	Reynolds number	dimensionless
Re	real part of a complex number	dimensionless
r	inside line radius	in
T_a	ambient temperature	R
u	velocity	in/sec
V	volume	in^3
W	reflection coefficient	dimensionless

Symbol	Description	Units
x	distance in downstream direction	in
Y	admittance/unit length	$in^4/lbf\text{-}sec$
z	impedance/unit length	$lbf\text{-}sec/in^6$
z_c	characteristic impedance/unit length	$lbf\text{-}sec/in^6$
z_{in}	input impedance	$lbf\text{-}sec/in^5$
z_L	terminal impedance	$lbf\text{-}sec/in^5$
z_R	radiation impedance	$lbf\text{-}sec/in^5$
α	attenuation/unit length	neper/in
β	phase shift/unit length	rad/in
Γ	propagation operator/unit length	in^{-1}
μ	dynamic viscosity	$lbf\text{-}sec/in^2$
ν	kinematic viscosity	in^2/sec
Ω	nondimensional frequency	dimensionless
Ω_B	nondimensional break frequency	dimensionless
ω	angular frequency	rad/sec
ω_ν	characteristic frequency	rad/sec
ρ	density	$lbf\text{-}sec^2/in^4$
σ	(Prandtl number)$^{\frac{1}{2}}$	dimensionless
θ_o	radiation function, real	dimensionless
χ_o	radiation function, imaginary	dimensionless

Abstract

The theoretical predictions of the dynamic response of circular cross-section pneumatic transmission lines were compared with experimental results. Tests were conducted in blocked line situations as well as in both laminar and turbulent mean flow conditions. The lines used in the study were 24 in. in length with inside diameters of 0.041, 0.119, and 0.195 in. Tests were conducted over the frequency range 20-1000 Hz and over a range of mean flow Reynolds numbers from 0-16000.

Theoretical solutions were obtained from computer simulations using a laminar flow model and two turbulent flow models. These models were developed from the Navier-Stokes equation and include components to account for viscosity and radial heat transfer in the fluid.

An examination of the turbulent models was conducted based on a nondimensional frequency and attenuation. This led to modification of one of the turbulent models to include a frequency dependent term in the conductance.

The effect of flow conditions upstream of the test line and the effect of orifice design on the dynamic response were studied.

Experimental results showed good agreement with
results of earlier studies. The use of a bypass device
upstream of the test line was found to have no effect on
line response.

The reconfiguration of the orifice devices to more
closely match theoretical models produced no noticeable
change in the results.

DYNAMIC RESPONSE OF FLUID TRANSMISSION LINES

I. Introduction

Background

The behavior of periodic pressure signals in fluid
lines has been the topic of many studies in the past. The
results of these studies are important in applications
such as pneumatic and liquid control systems in aircraft,
jet engine test facilities and measuring systems. Both
analytical and experimental studies have been conducted in
an effort to develop accurate models for the prediction of
the dynamic response of fluid filled lines.

As a signal travels along a fluid line, the magni-
tude and phase angle of the signal are modified, depending
on such parameters as the line length, diameter, signal
frequency and fluid characteristics. The ratio of the
downstream magnitude to the upstream magnitude is referred
to as the gain and the change in the phase angle is
referred to as the phase shift. The ability to accurately
predict the gain and phase shift is of major importance in
many system designs.

Studies have shown that the model developed by
Nichols (Ref 1), and modified by Krishnaiyer and Lechner

1

(Ref 2) accurately predicts the response of signals in lines with blocked and laminar mean flow conditions. Attempts to extend the use of this model to turbulent mean flow conditions have shown good agreement at high frequency but result in lower attenuation than observed experimentally at low frequencies. Studies by Brown, Margolis and Shaw (Ref 3), Moore (Ref 4), Briski (Ref 5) and Wilkins (Ref 6) have concentrated on the development of a model which can accurately predict the response under turbulent flow conditions. Briski (Ref 5) and Wilkins (Ref 6) worked with the model developed by Moore (Ref 4) to produce modified models which provide accurate and relatively simple means of predicting line response under turbulent mean flow conditions.

Objectives

The following objectives were established to study the dynamic response of pneumatic transmission lines.

1. Review current models to ensure proper application of theory to experimental conditions.

2. Verify experimental procedures and extend results obtained in previous studies.

3. Investigate the effect of conditions upstream of the test line on line response.

4. Revise existing computer program to incorporate revised models and improve documentation.

5. Investigate effect of improved orifice termination devices on correlation of theoretical and experimental results.

II. Theory

Electrical Transmission Line Analogy

The theory of electrical transmission lines is well developed and may be found in many references. This theory may be used in the analysis of fluid transmission lines by considering pressure and volumetric flow rate in fluid systems to be analogous to potential and current respectively in electrical systems. With this analogy Ohms law becomes

$$\Delta P = ZQ \tag{1}$$

or

$$Q = Y\Delta P \tag{2}$$

where

ΔP = change in pressure

Q = volumetric flow rate

Z = complex series impedance

Y = complex shunt admittance = $1/Z$

The complex impedance is composed of the resistance and inertance, while the admittance is composed of the conductance and capacitance. Using these components, the

4

above equations may be expressed in terms of the distance along the line as

$$\frac{dP}{dx} = ZQ = (R + j\omega L)Q \tag{3}$$

and
$$\frac{dQ}{dx} = YP = (G + j\omega C)P \tag{4}$$

where

R = resistance

L = inertance

G = conductance

C = capacitance

all taken per unit length.

Based on these equations, the analogous electrical circuit to a fluid transmission line is shown in Figure 1.

Blocked and Laminar Flow

The equations developed by Nichols (Ref 1) provide a means of calculating values of Z and Y for circular lines with either laminar mean flow or blocked line conditions. These equations, however, involve the use of Bessel functions, and the calculations can become complicated. Krishnaiyer and Lechner (Ref 2) have presented algebraically simplified equations which provide accurate results over the frequency range $0.1\ \omega_\nu < \omega < \infty$. The characteristic frequency ω_ν, is defined as
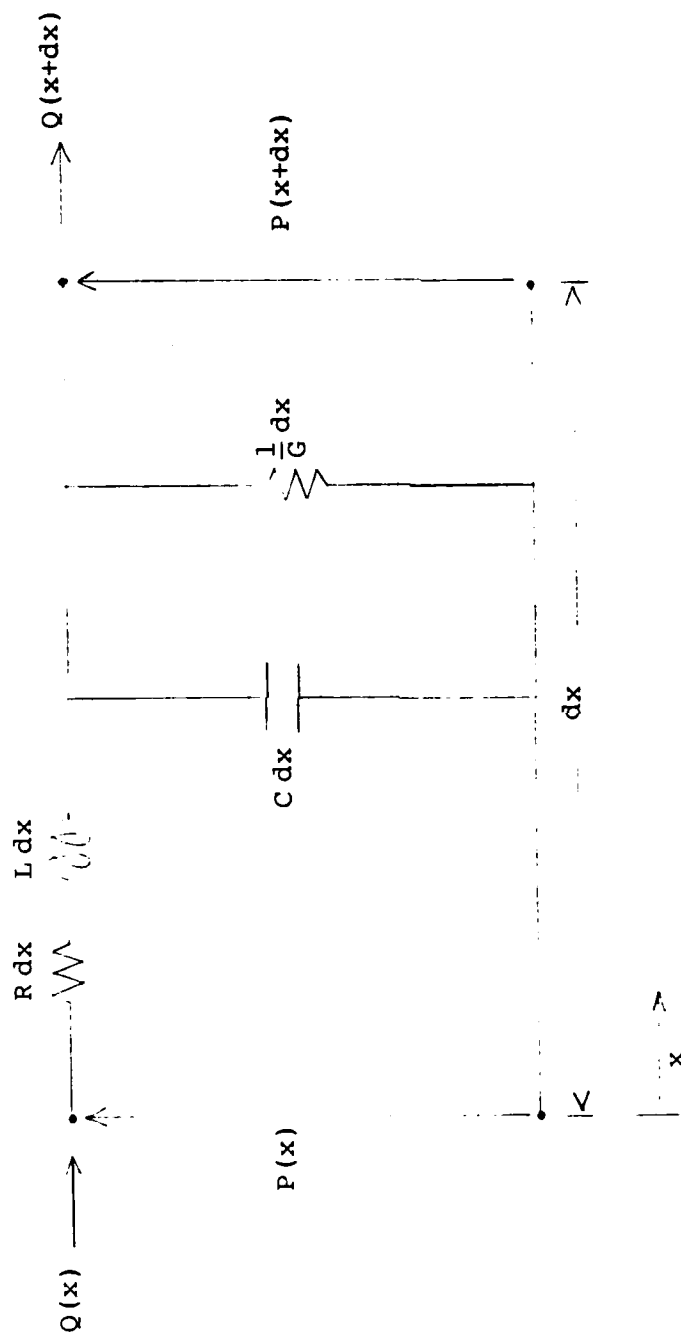
Fig. 1. Electrical Analogy to Fluid Transmission Line

6

$$\omega_\nu = \frac{8\pi\nu}{A} \tag{5}$$

where A is the line cross-sectional area.

The modified equations for Z and Y are

$$Z = \frac{8\pi\mu}{A^2}(DR) + j\left[\frac{\omega\rho}{A} + \frac{8\pi\mu}{A^2}(DL)\right] \tag{6}$$

and

$$Y = \frac{-[\omega(k-1)A/kP(DG)]}{(DC)^2 + (DG)^2} + j\omega\left[\frac{A}{kP} + \frac{(k-1)A/kP(DC)}{(DC)^2 + (DG)^2}\right] \tag{7}$$

with the expressions DR, DL, DG and DC described as

$$DR = \frac{3}{8} + \frac{h_\nu}{4} + \frac{3}{8h_\nu} \tag{8}$$

$$DL = \frac{h_\nu}{4} - \frac{15}{64h_D} \tag{9}$$

$$DG = \frac{h_t}{2} - \frac{1}{4h_t} \tag{10}$$

$$DC = \frac{1}{4} + \frac{h_t}{2} + \frac{1}{4h_t} \tag{11}$$

where $\qquad h_\nu = 2(\omega/\omega_\nu)^{\frac{1}{2}} \tag{12}$

$$h_t = \sigma h_\nu \tag{13}$$

are velocity and temperature distribution parameters respectively.

7

The transmission line may now be described by the propagation operator Γ and the characteristic impedance Z_c.

$$\Gamma = (ZY)^{\frac{1}{2}} = \alpha + j\beta \tag{14}$$

$$Z_c = \left(\frac{Z}{Y}\right)^{\frac{1}{2}} \tag{15}$$

where

α = attenuation per unit length

β = phase shift per unit length

For the general case of a line with terminal impedance Z_L, as shown in Figure 2, Kirshner and Katz (Ref 7) express the input impedance as

$$Z_{in} = \frac{P_{in}}{Q_{in}} = Z_c \left[\frac{Z_L \cosh(\Gamma\ell) + Z_c \sinh(\Gamma\ell)}{Z_L \sinh(\Gamma\ell) + Z_c \cosh(\Gamma\ell)} \right] \tag{16}$$

The pressure transfer function relating the pressure at a distance x along the line to the input pressure is

$$\frac{P}{P_{in}} = \frac{\sinh\Gamma\ell(1-x/\ell) + (Z_L/Z_c)\cosh\Gamma\ell(1-x/\ell)}{\sinh\Gamma\ell + (Z_L/Z_c)\cosh\Gamma\ell} \tag{17}$$

and the pressure gain is defined as the magnitude of the transfer function

$$g = \left| \frac{P}{P_{in}} \right| \tag{18}$$

8
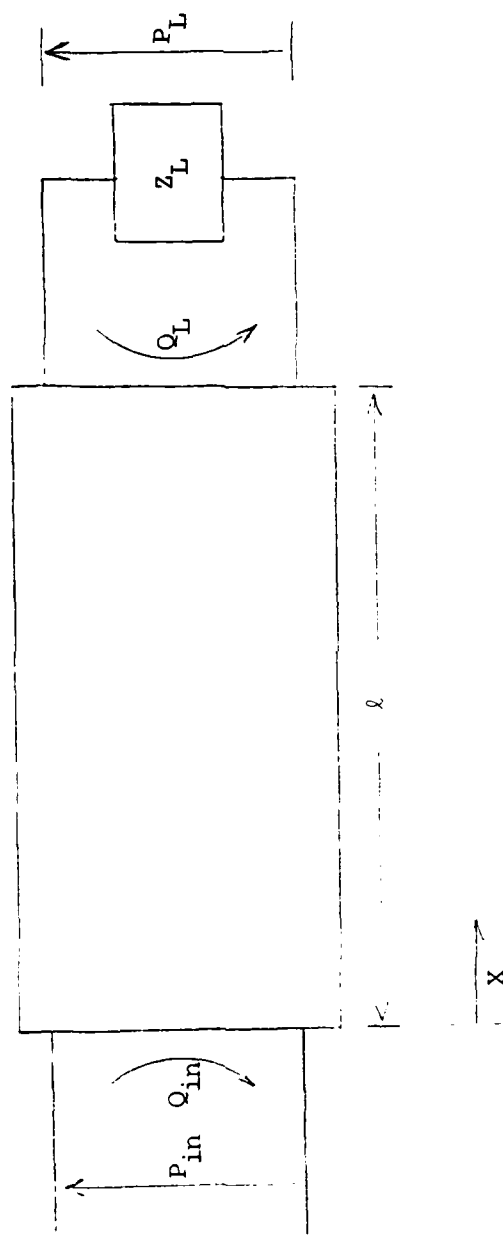
Fig. 2. Generalized Transmission Line with Terminal Impedance

or, in decibels,

$$g_{dB} = 20 \log g \tag{19}$$

The phase shift is defined as the angle formed by
the real part and the complex part of the transfer function
in the complex plane

$$B = \tan^{-1} \left[\frac{I_m (P/P_{in})}{Re (P/P_{in})} \right] \tag{20}$$

Turbulent Flow

While Equations (6) and (7) have proven accurate
for use in blocked line and laminar flow cases, it has been
shown that their use in the turbulent flow case results
in attenuation values lower than those observed experi-
mentally (Refs 3-5).

The velocity profile for fully developed laminar
steady state flow is parabolic with the boundary layer
thickness equal to the tube radius. When a periodic
signal is applied to the steady state flow a dynamic boun-
dary layer is created. As the frequency of the signal is
increased this dynamic boundary layer becomes thinner and
the velocity gradients near the wall increase. As a result,
the dynamic layer is thinner than the steady state boundary
layer at frequencies of practical interest and dictates
the line response (Ref 13).

In turbulent flow the steady state velocity pro-
file exhibits a dependency on the Reynolds number. The
boyndary layer thickness decreases with increasing Reynolds
number and at the limit of an infinite Reynolds number a
uniform profile, or slug flow, is obtained. With this
variation in steady state boundary layer thickness, the
dynamic boundary layer created by the application of a
periodic signal will no longer necessarily be thinner than
the steady state boundary layer. With the response deter-
mined by the thinner of the two layers, it is clear that
variations in Reynolds number and signal frequency would
affect line response.

In order to classify the response based on Reynolds
number and frequency, Brown et al. (Ref 3) presented a
plot of nondimensional attenuation versus nondimensional
frequency. An example of this type of plot is shown in
Figure 3. The two nondimensional parameters are defined as

$$\text{nondimensional attenuation} = \frac{r^2 a\alpha}{\nu} \tag{21}$$

$$\text{nondimensional frequency } \Omega = \frac{r^2 \omega}{\nu} = 8 \frac{\omega}{\omega_\nu} \tag{22}$$

This plot has been divided into three frequency regions
by Moore (Ref 4) as suggested by Brown et al. (Ref 3).
In the low frequency region, the dynamic boundary layer is
thicker than the steady state boundary layer. In the
mid frequency region, the dynamic layer and the steady

11
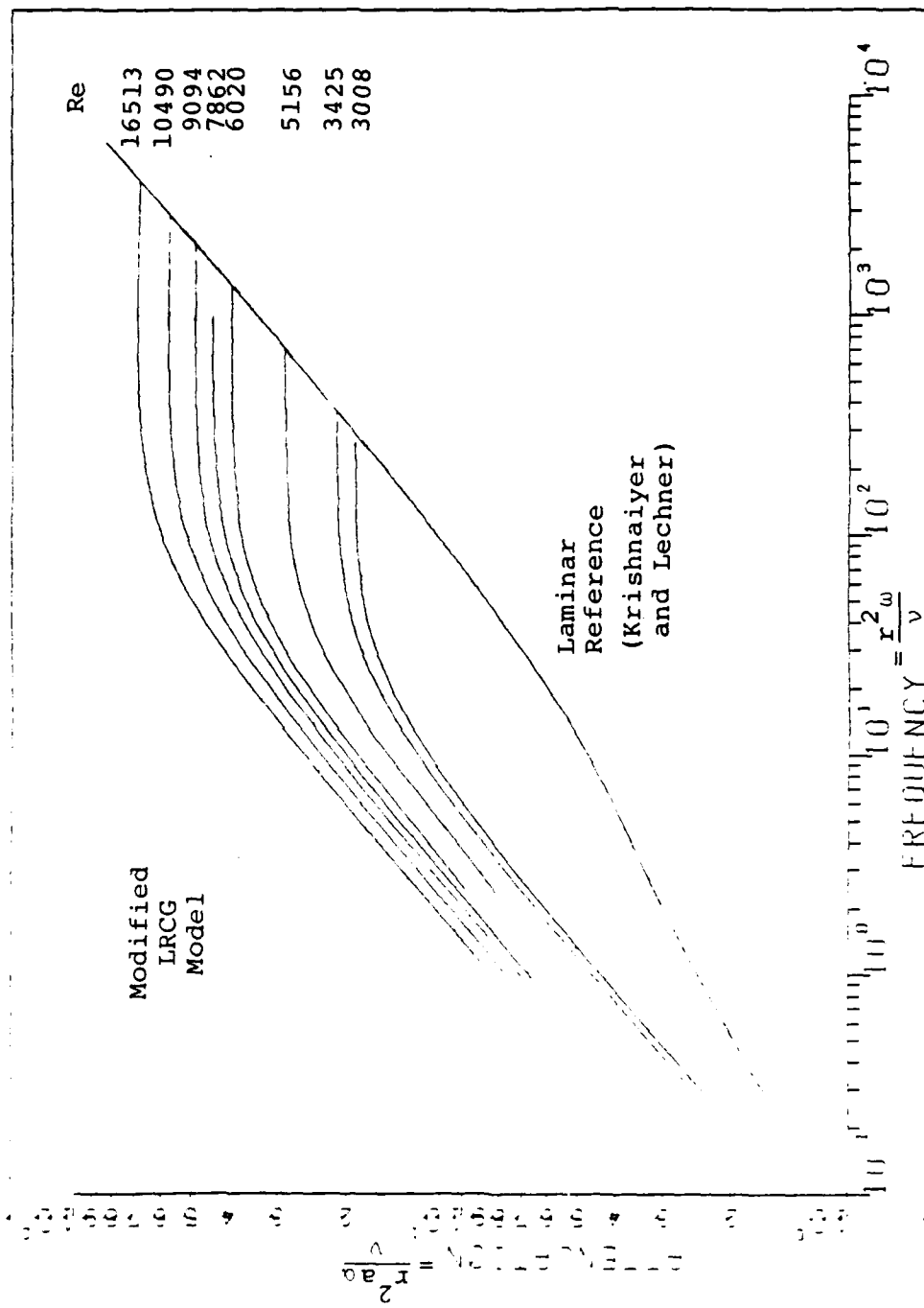
Fig. 3. Nondimensional Plot of Attenuation vs Frequency

12

layer are of comparable thickness. In the high frequency region the dynamic layer has become much thinner than the steady state layer and as a result the behavior in this region is the same as in laminar flow. The frequency at which the steady state layer becomes the thicker of the two and the response transitions to laminar behavior is termed the break frequency, Ω_B.

Several turbulent models have been suggested to predict dynamic response. Moore applied a constant LRC model to the low and mid frequency regions, the components of which were selected based on analysis of the low frequency laminar flow case (Ref 4). The adiabatic inertance was defined as

$$L_a = \rho/A \tag{23}$$

A steady state (DC) resistance was defined as

$$R_{DC} = \frac{fRe\mu}{2Ad^2} \tag{24}$$

and using the Blasius resistance formula for turbulent flow in smooth lines

$$f = 0.3164 \ Re^{-0.25} \tag{25}$$

This was rewritten as

$$R_{DC} = \frac{0.1582 \ Re^{0.75}\mu}{Ad^2} \tag{26}$$

13

The capacitance was defined as

$$C = \frac{k}{n} C_a \tag{27}$$

where n is the polytropic exponent and the adiabatic capacitance. C_a is defined as

$$C_a = A/kP \tag{28}$$

The value of n is seen to vary from k at high frequencies to 1.0 at low frequencies.

Wilkins presented modifications to the constant LRC model in an attempt to improve the attenuation predictions of his model. The attenuation curve in the mid frequency region of Figure 3 is seen to be dependent only on the Reynolds number. The modifications to the resistance, inertance and capacitance proposed by Wilkins were based on this variation in attenuation with Reynolds number. A linearized (AC) resistance suggested in Ref 8

$$R_{AC} = R_{DC} + Re \left[\frac{\partial R_{DC}}{\partial Re} \right] \tag{29}$$

was used which using the R_{DC} in Equation (26) reduces to

$$R_{AC} = 1.75 \ R_{DC} \tag{30}$$

Moore and Franke have proposed a turbulent inertance to reflect the effect of the velocity profile on

14

the inertance (Ref 9). This turbulent inertance is defined as

$$L_T = K_{LT} L_a \tag{31}$$

where K_{LT} is the inertance constant defined as

$$K_{LT} = \frac{(f^{0.5}+1)(f^{0.5}+2)^2}{4(2f^{0.5}+1)} \tag{32}$$

L_T is now seen to be a function of the Reynolds number through the friction factor f.

The turbulent capacitance was formed by combining the imaginary part of the conductance with the isothermal capacitance. The conductance accounts for the effects of radial heat transfer in a gas. In laminar flow the increased attenuation due to this effect is well understood and has been included in the equations by Krishnaiyer and Lechner (Equations (6) and (7)).

The conductance for turbulent flow as presented by Brown et al. (Ref 3) as

$$G = \frac{(k-1)C_a L_a \omega^2}{R_{AC} + j\omega L_T} \tag{33}$$

If the quantity R_{AC}/ω is assumed to be much less than L_T, Wilkins (Ref 6) showed that after some algebraic manipulation, this reduces to

15

$$G = (k-1) \frac{R_{AC}C_a L_a}{L_T^2} - j\omega(k-1) \frac{C_a K_{LT} L_a^2}{L_T^2} \qquad (34)$$

From this expression, the turbulent capacitance is written as

$$C_T = C_i - (k-1) \frac{C_a K_{LT} L_a^2}{L_T^2}$$

$$= kC_a - (k-1) \frac{C_a K_{LT} L_a^2}{L_T^2}$$

$$= C_a \left[k - \frac{k-1}{K_{LT}} \right] \qquad (35)$$

which is again seen to be dependent on the Reynolds number through the inertance constant.

The second turbulent model presented by Wilkins (Ref 6) was the constant LRCG model. This model uses the same resistance, inertance and capacitance components as the modified constant LRC but also includes the real part of the conductance from Equation (34). Each component of these models is seen to be independent of the signal frequency and a function of only the Reynolds number.

If the quantity $\frac{R_{AC}}{\omega}$ cannot be assumed to be much less than LT, the complete equation for G must be utilized (Equation (33)). Expansion of this expression gives

16

$$G = \frac{(k-1)R_{AC}C_aL_a\omega^2 - j\omega^3(k-1)L_TL_aC_a}{R_{AC}^2 + \omega^2L_T^2} \qquad (36)$$

It should be noted that use of the full expression results in a component that is dependent on frequency as well as the Reynolds number.

If, as before, a portion of the imaginary part of G is combined with C_i to form the turbulent capacitance, the following result is obtained.

$$C_T = C_i - \frac{\omega^2(k-1)L_TL_aC_a}{R_{AC}^2 + \omega^2L_T^2}$$

$$= C_a\left[k - \frac{\omega^2(k-1)L_TL_a}{R_{AC}^2 + \omega^2L_T^2}\right] \qquad (37)$$

The turbulent capacitance thus formed is also seen to be frequency dependent in contrast to the component used by Wilkins in the Constant LRCG model.

A new model can be formed by using the frequency dependent expression for G and C_T in place of the respective frequency independent terms in the Constant LRCG model. The resulting expressions will be referred to as the Modified LRCG model.

It must be noted that although the expression for the conductance used in both LRCG models is based upon that presented by Brown et al. (Ref 3), there is an

17

important difference between the components as defined by Brown and those used in this study. As an example, Brown defines the effective inertia, I (equivalent to the adiabatic inductance) as

$$I = \rho \tag{38}$$

as compared to the definition of L_a in Equation (23). The two components are seen to differ by the area factor such that

$$I = L_a A \tag{39}$$

A similar multiplicative factor must be included in the resistance components used in this study to obtain Brown's results.

Similarly, Brown's admittance components are related to those used in this study by

$$Y_{Brown} = \frac{Y}{A} \tag{40}$$

Though the admittance and impedance terms each differ by a factor of the area, these factors cancel out when the two components are combined to form the propagation operator Γ producing the same result regardless of the method that is used. Care must be taken, however, to ensure that the two types of components are not combined without regard to the multiplicative factor by which they differ.

18

Terminal Impedance

Several methods have been proposed to accurately model the terminal impedance of a dynamic system. Using a linearized DC expression such as that proposed by Franke, Malanowski and Martin (Ref 10)

$$Z_L = \frac{\Delta P_L}{\Delta Q_L} \tag{41}$$

shows that in the limiting cases, for an open line, $\Delta P_L = 0$ and $Z_L = 0$; while for the blocked line case, $\Delta Q_L = 0$ and $Z_L = \infty$.

In this study two primary methods have been used to model terminal impedance. In the open line case, the radiation impedance as suggested by acoustic theory has been employed.

The air at the end of the transmission line is described as a massless piston which transmits some of the energy into free space while reflecting some energy back into the line. This finite impedance is seen to differ from the zero impedance resulting from the linearized impedance model mentioned above. Morse and Ingard (Ref 11) define the radiation impedance as

$$Z_R = (\frac{\rho a}{A}) \; (\theta_o - j \chi_o) \tag{42}$$

19

where θ_o and χ_o are radiation functions. For the case of a flanged exit (a flush opening in an infinite wall) these functions may be approximated as

$$\theta_o = 0 \tag{43}$$

$$\chi_o = 0.4\ D\omega/a \tag{44}$$

Using these approximate values results in an expression for the terminal impedance of

$$Z_R = -0.4j\omega\rho D/A \tag{45}$$

The second method used to model the terminal impedance involves the use of reflection coefficients. The orifice of the transmission line was modeled as illustrated at Figure 4. Kensler and Frey (Ref 12) give the terminal impedance for this situation as

$$Z_L = \left(\frac{\rho a}{A}\right)_1 \left(\frac{1 + W}{1 - W}\right) \tag{46}$$

where W is the reflection coefficient for the sudden change in line area between 1 and 2. The reflection coefficient for the situation where line 2 is terminated by its characteristic impedance is given as

$$W = (A_1 - A_2)/(A_1 + A_2) \tag{47}$$

20
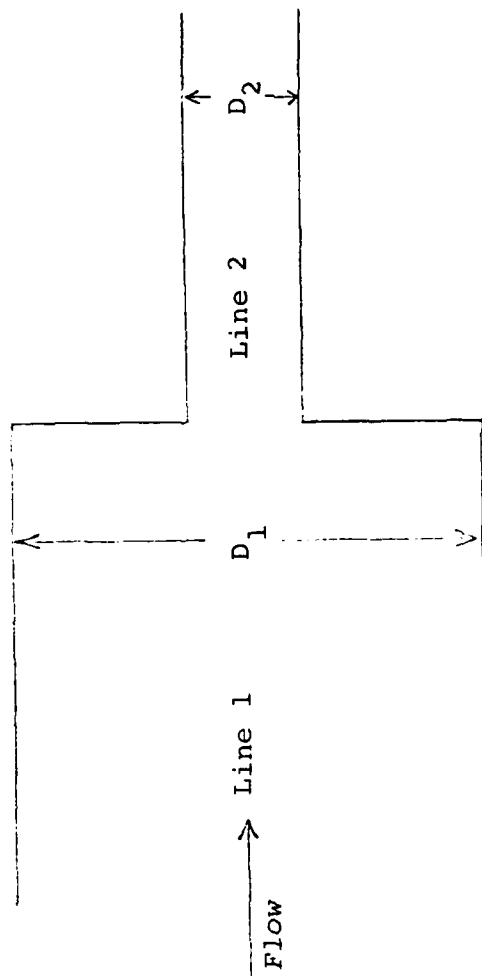
Fig. 4. Orifice Model

21

Compressible flow theory states that waves which reflect from a boundary and travel at the speed of sound will not be able to propagate upstream against a sonic flow. The reflected waves will be swept downstream by the flow and the presence of the orifice will not be sensed at the input. The line will appear to be of infinite length and Equation (47) may be applied.

In those situations where the flow was found to be choked by the orifice, the above analysis was assumed to be applicable and Equation (47) was used to determine the reflection coefficient.

In those situations where choked flow conditions are not present, the orifice was represented as an infinitesimally short open line and the remainder of area 1 (Figure 4) was treated as a blocked line. The reflection coefficients for the two areas were taken respectively to be -1 and 1. These two values were averaged by area to obtain a composite reflection coefficient

$$W = (A_1 - 2A_2) / (A_1 + A_2) \tag{48}$$

Effect of Upstream Conditions

A review of the various equations describing the dynamic response of a pneumatic transmission line reveals dependence only on the conditions at the line inlet.

22

Schlichting (Ref 13) gives the presssure drop along a
line as

$$\Delta P = -f(\Delta x) \rho (u^2/2D) \qquad (49)$$

and by substituting the applicable expression for the
friction factor, the following results may be obtained.

$$\text{laminar flow} \quad \Delta P = -0.106 (\Delta x) \mu M/D^4 \rho \qquad (50)$$

$$\text{turbulent flow} \quad \Delta P = -(7.18 \times 10^{-6}) \Delta x \mu^{.25} M^{1.75}/D^{4.75} \rho \qquad (51)$$

From these expressions it can be seen that, for a
given fluid at ambient conditions and a given line con-
figuration, the mass flow rate is dependent only on the
pressure drop along the line. In test situations where
an upstream bypass device is used to simulate a branch
line in a more complex system, the pressure drop along the
test line may be used to establish a required mass flow
rate.

Error Analysis

In order to properly assess the correlation of
theoretical predictions with experimental results, a deter-
mination of the error due to the readability of measurement
instruments is necessary. In this study the method of
absolute error was used to calculate this error (Ref 15).

For some quantity F, defined by

$$F = F(e_1, e_2, \ldots, e_n) \qquad (52)$$

23

where e_1, e_2, ..., e_n are independent measured quantities, the absolute error in F due to instrument readability is

$$\Delta F = \sum_{i=1}^{n} \left| \Delta e_i \frac{\partial F}{\partial e_i} \right| \tag{53}$$

where Δe_i is the readability of the instrument used to measure e_i.

The absolute error may be used to determine the accuracy of experimental results. If the error analysis shows an error of 5 percent in a calculation, for example, the effort spent on resolving a difference of 2 percent between experimental and theoretical results might be better spent improving instrumentation or experimental techniques.

Computer Simulation

The computer program developed by Malanowski (Ref 14) and modified by Briski (Ref 5) and Wilkins (Ref 6) was used to provide theoretical simulations for comparison with experimental results.

The test line is divided into several short segments over which the properties are assumed to remain constant. Using Schlichting's equation for the pressure drop along a line (Equation (49)) and the respective expressions for the friction factor for laminar and turbulent flow, Wilkins developed expressions to determine the

24

pressure drop along a line segment of known length given
the mass flow rate and the inlet pressure. The final
expressions are, for laminar and turbulent flow respec-
tively.

$$\Delta P = P_{in} - \left[P_{in}^2 + 64x\mu^2 \frac{ReT_aT_g}{D^3} \right]^{\frac{1}{2}} \qquad (54)$$

$$\Delta P = P_{in} - \left[P_{in}^2 + 0.3164x\mu^2 \frac{Re^{1.75}T_aT_g}{D^3} \right]^{\frac{1}{2}} \qquad (55)$$

Using the appropriate expression the program calcu-
lates the pressure drop for each segment in succession
and thereby the inlet pressure for each of the line seg-
ments. The program then uses the segment pressures and
other properties to calculate the propagation operator and
from this, the theoretical gain and phase shift.

The program is interactive and offers the choice
between the laminar model (Equations (6) and (7)) and
either the Modified Constant LRC or Modified LRCG models.
For the turbulent models, the attenuation is calculated
by both the selected turbulent model and the laminar model.
The program compares the two values and selects the larger
for the calculation of gain and phase shift. In this
manner the program is able to identify the break frequency
between the mid frequency and high frequency ranges and
then use the laminar model for calculations beyond the
break frequency.

The program also contains an interactive module to allow the selection of the appropriate reflection coefficient expression. The radiation impedance is used for open line cases.

The expressions for the ratio of turbulent/ adiabatic capacitances and the inertance constant were added to the program to reduce the amount of input data required.

The documentation and layout of the program were improved to make it more easily understood and to provide a more useful analytical tool for future studies in this area. A complete listing of the program is included at Appendix B.

III. Experiment

Apparatus

The test sections used in this study consisted of
24-inch lengths of stainless steel line which were per-
manently mounted in plexiglass blocks at each end. Three
inside line diameters were used: 0.041, 0.119 and 0.195 in.
The mounting blocks were machined to provide fittings for
air input line, static pressure transducer, and dynamic
pressure transducer. The bypass device and several features
of the upstream mounting block as listed below are shown in
Figure 5.

        A - Bypass device
        B - Static pressure transducer
        C - Dynamic pressure transducer
        D - Test line

A typical test line is shown in Figure 6 and the actual line
dimensions are listed in Table I. The downstream mounting
block was also machined to allow the fitting of different
termination devices. There were four termination devices
for each test line; a blocked line fitting, an open line
fitting and two orifice fittings with diameters of 0.0135 in.
and 0.016 in. (Figure 7). Dimensions of the termination
devices are also shown in Table I.

A plexiglass calibration block shown in Figure 8
was used to calibrate the dynamic pressure transducer/

27
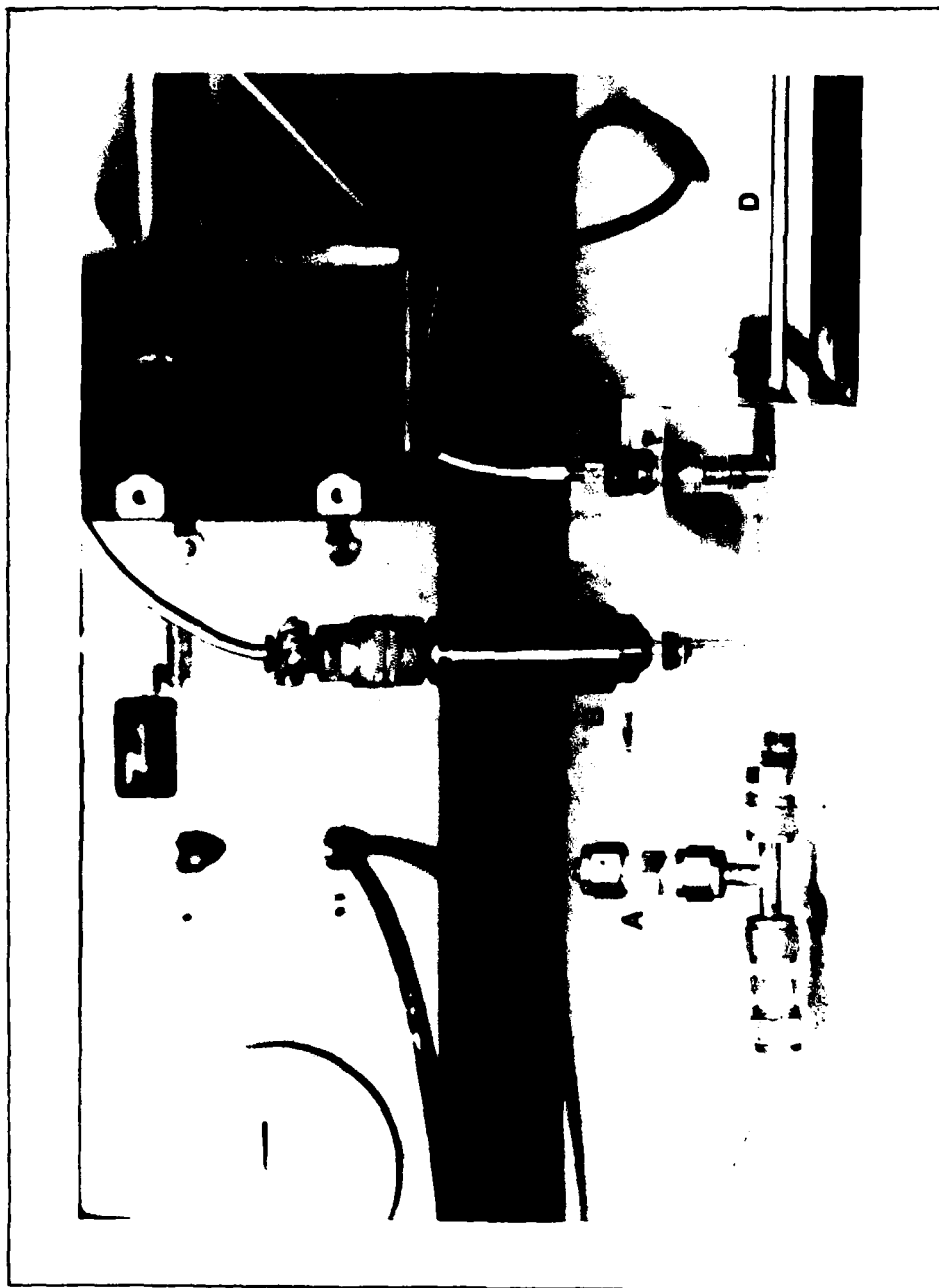
Fig. 5. Upstream Mounting Block and Bypass Device
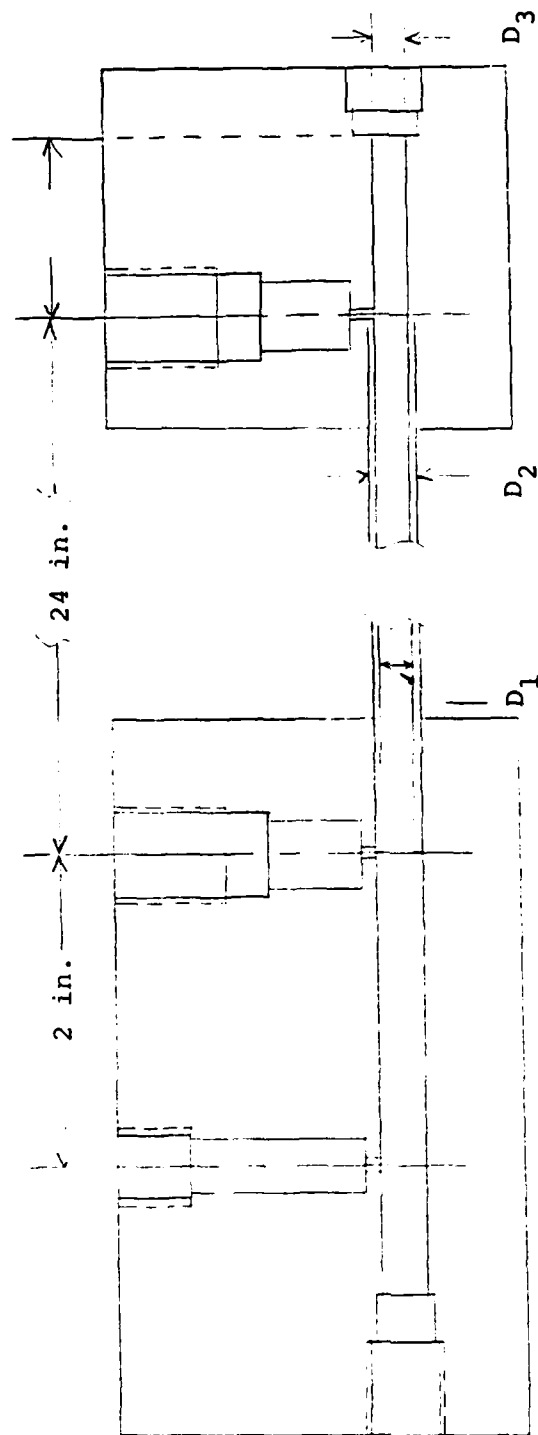
Fig. 6. Test Line Dimensions

29
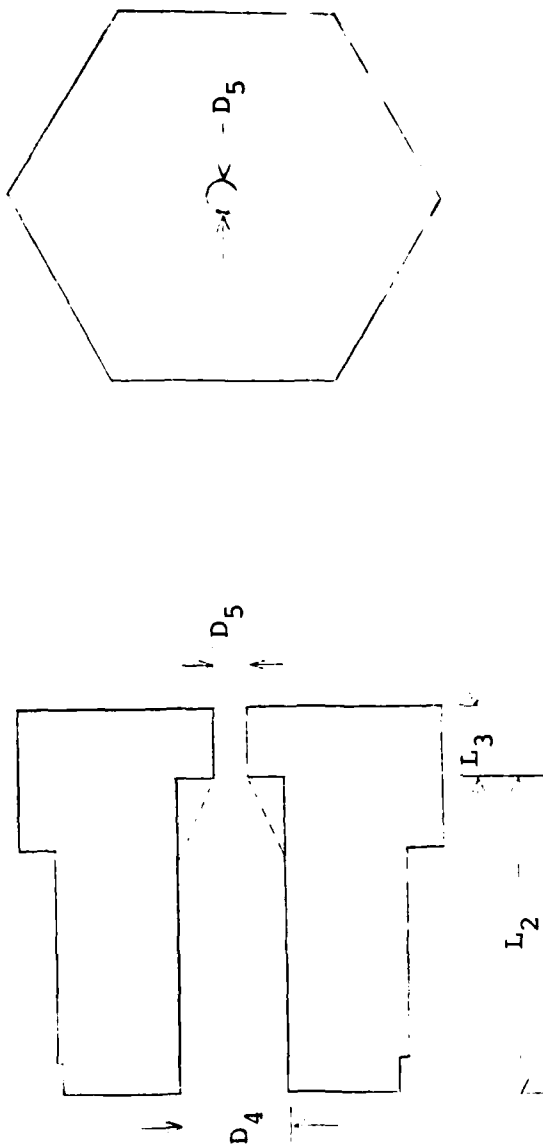
Fig. 7. Orifice Device Dimensions

TABLE I

TEST LINE AND ORIFICE DEVICE DIMENSIONS

Line Number	Termination Number	D_1	D_2	D_3	D_4	D_5	L_1	L_2	L_3
1	0	0.041	0.065	0.0426	0	0	1.006	0	0
	1	"	"	"	0.043	0.0135	"	0.600	0.0633
	2	"	"	"	"	0.016	"	0.603	0.0647
	3	"	"	"	"	0.043	"	0.6655	0
2	0	0.119	0.190	0.1218	0	0	0.998	0	0
	1	"	"	"	0.120	0.0135	"	0.625	0.0359
	2	"	"	"	"	0.016	"	0.613	0.0525
	3	"	"	"	"	0.120	"	0.6634	0
3	0	0.195	0.251	0.1964	0	0	1.007	0	0
	1	"	"	"	0.196	0.0135	"	0.593	0.0730
	2	"	"	"	"	0.016	"	0.599	0.0683
	3	"	"	"	"	0.196	"	0.6630	0

Note: All dimensions in inches.

31
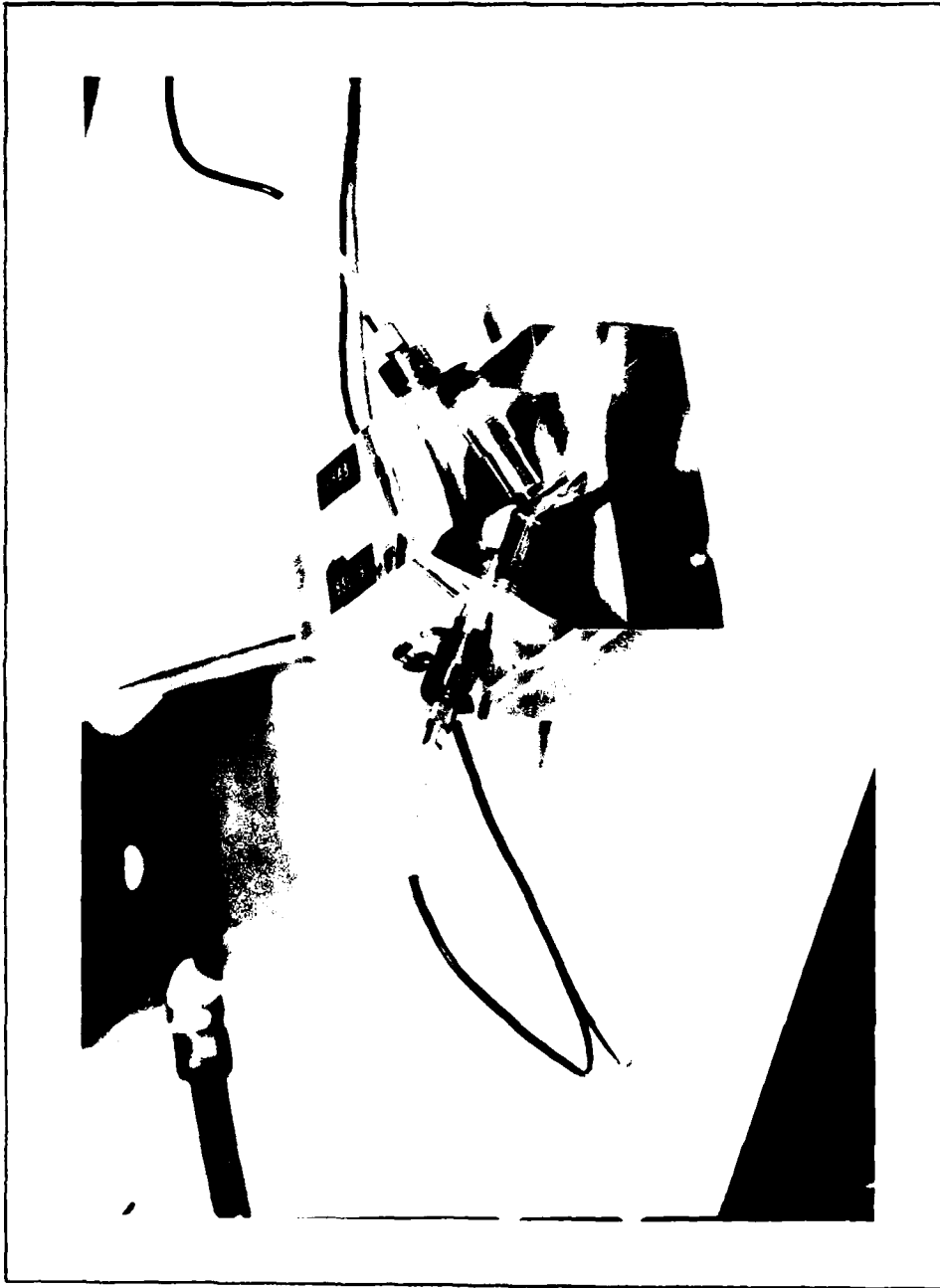
Fig. 8. Calibration Block

charge amplifier combinations. The calibration block positioned the transducers at the same point in the line to allow comparison of the measured signals. The block was machined similar to the test line mounting blocks for an air supply line connection.

The experimental instrumentation used in the study is shown in Figures 9 and 10. The equipment is also illustrated in schematic form in Figure 11.

The sending wave analyzer provided a sinusoidal input signal of variable frequency, which was measured by a frequency counter, to the amplifier/power supply and the pneumatic driver. This input signal was suitably conditioned and passed to the pneumatic driver itself which imposed a sinusoidal pressure signal on the mean air flow passing through the driver. The pressure signal was measured at upstream and downstream locations by piezoelectric dynamic pressure transducers. The charge output of each dynamic transducer was fed to a charge amplifier where it was converted to a voltage and input to a wave analyzer where it was displayed as a RMS voltage. The charge amplifier output was also input to a digital recording oscilloscope where the waveforms could be compared and recorded if desired. A static pressure transducer mounted in the upstream mounting block provided a measure of the static line pressure at that point. The pneumatic driver, test line and charge amplifiers are shown in Figure 12.

33
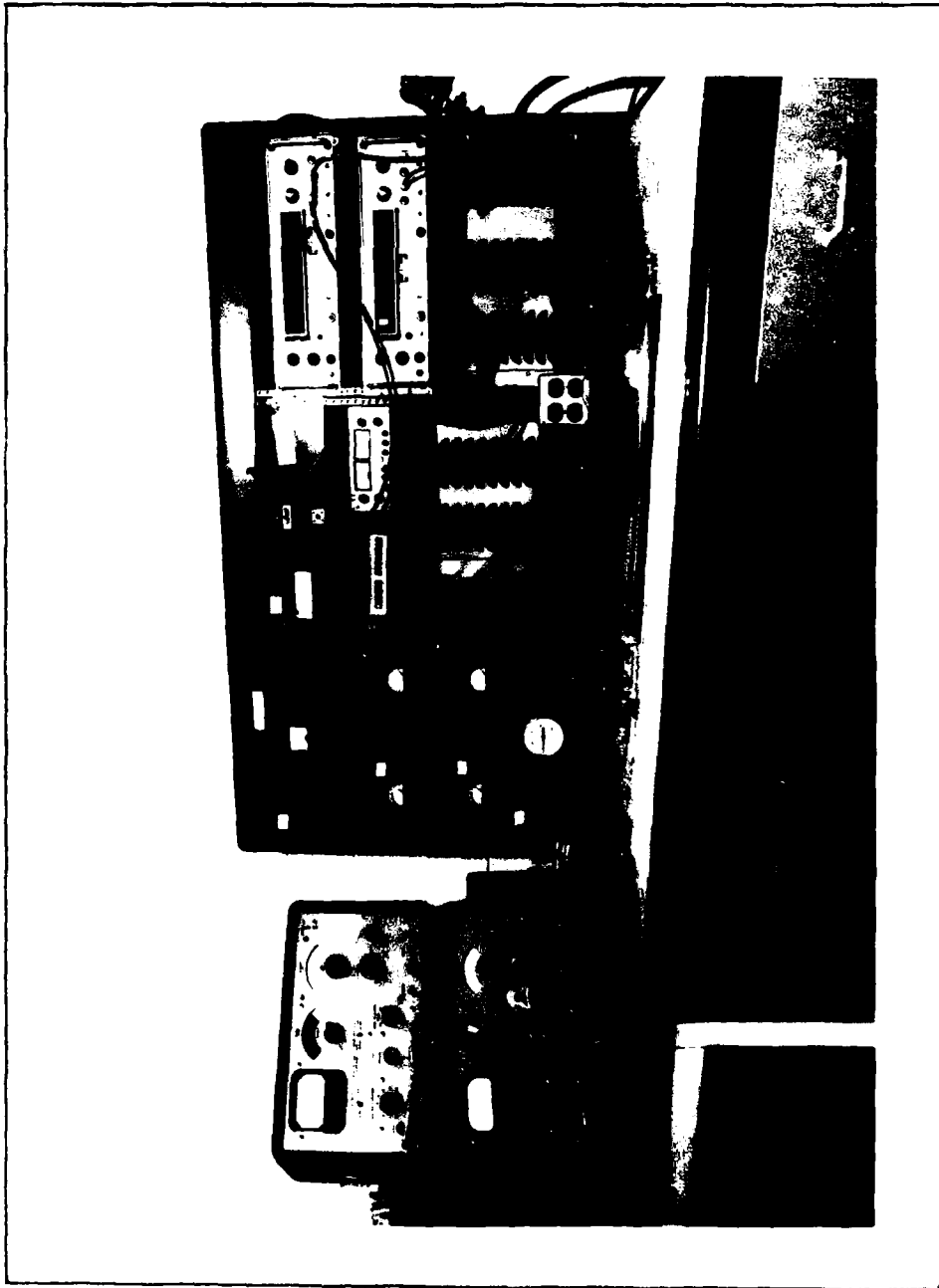
Fig. 9. Experimental Equipment Configuration
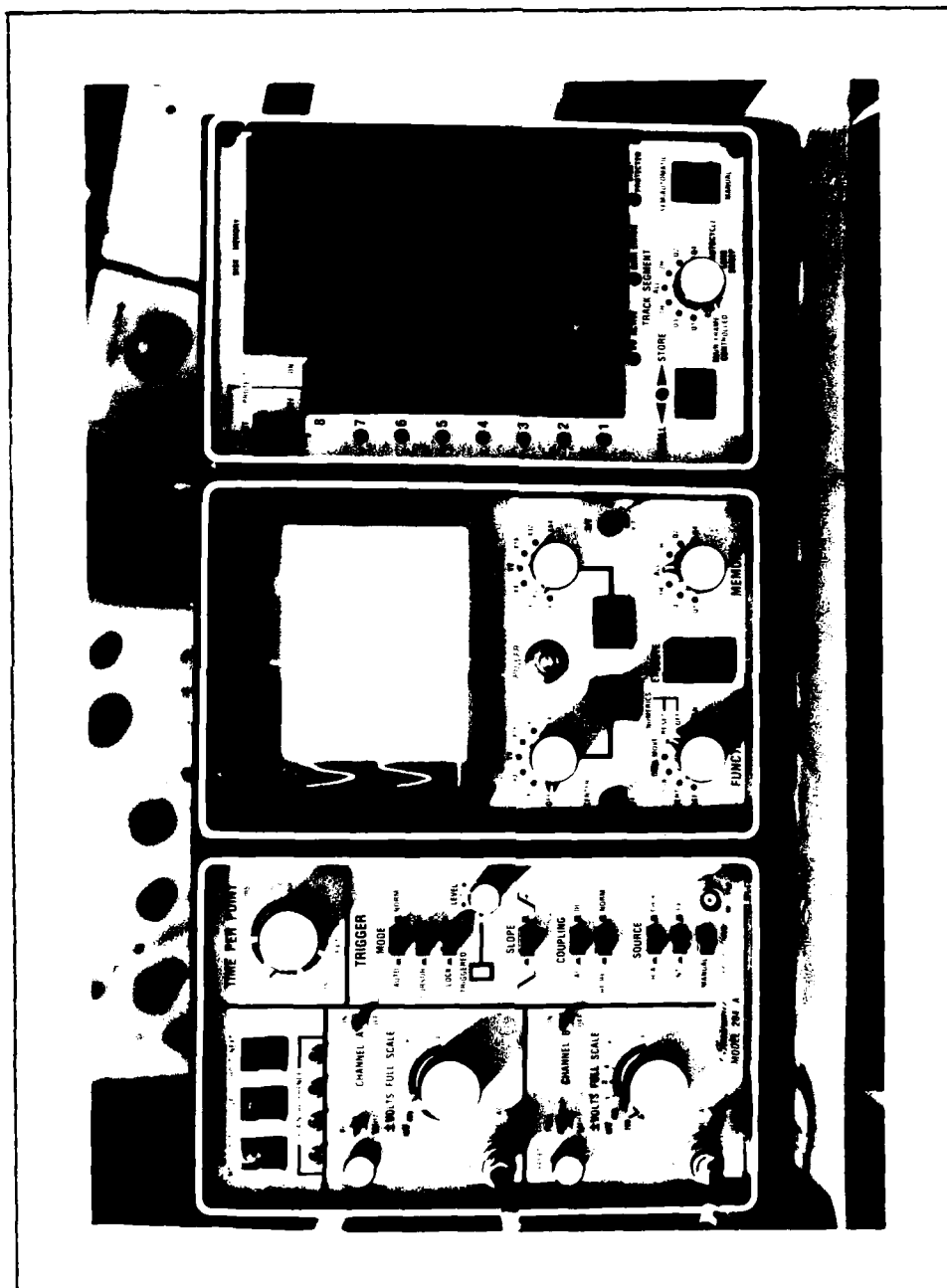
Fig. 10. Nicolet Digital Oscilloscope

35
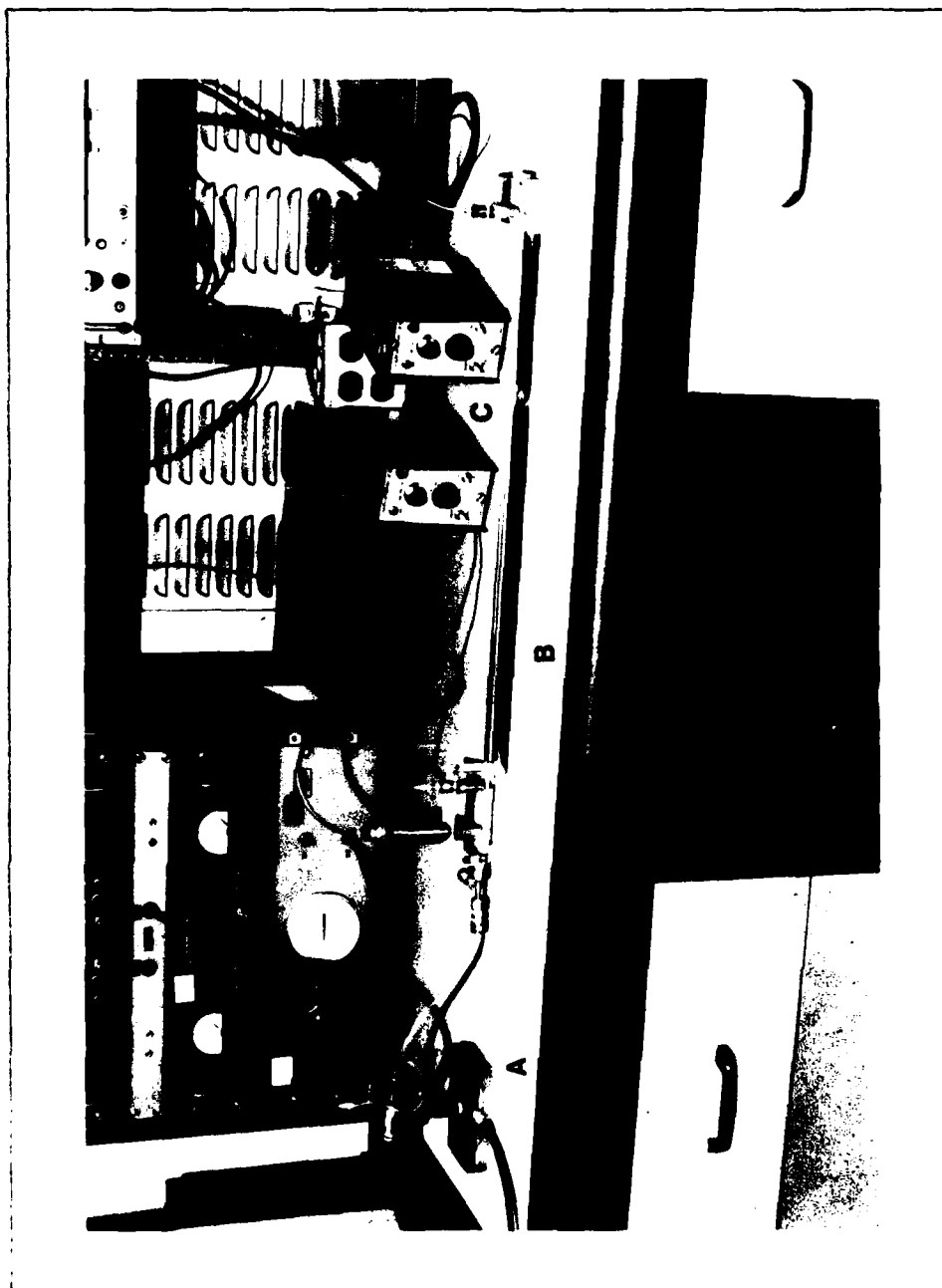
Fig. 12.   Pneumatic Driver (A), Test Line (B) and Charge Amplifiers (C)

37

For those runs involving bypass flow upstream of the test line, a complete bypass device (Figure 5) was used. This device consisted of a tee fitting located between the pneumatic driver and the upstream mounting block. The bypass outlet of the tee was fitted with an inside threaded cap with a floating disc. Adjustment of the threaded cap allowed varying amounts of the flow to escape providing increased flow through the pneumatic driver for a given flow through the test line. This device was also used for the blocked line cases where the entire flow was diverted from the test line.

A calibrated rotometer was used to measure the mass flow rate through the test line. As the presence of the rotometer downstream of the test line altered the line's response, flow measurements were made and the rotometer removed before data was taken. When the bypass device was being used, the rotometer again could not be used as its presence changed the respective flows through the test line and the bypass device. To determine the mass flow through the test line with the bypass device open, it was assumed that the difference between a given upstream static pressure and atmospheric pressure resulted in a given flow through the line.

With the bypass device closed, the air supply was adjusted to give the desired static pressure reading. The rotometer was then used to measure the flow and

38

removed. The bypass device was then opened and the air

supply increased until the previous static pressure read-

ing was re-established.

A complete listing of the instrumentation and

ancillary equipment used in this study is provided in

Appendix C.

Procedures

Dynamic Transducer Calibration. Throughout the

study each dynamic pressure transducer was paired with a

specific charge amplifier and the combination treated as a

single unit. To calibrate the transducer/amplifier units

the transducers were mounted in the calibration block which

was then connected to the air supply line in place of the

test line. The remainder of the experimental equipment

was set up as for a normal test run. At a selected fre-

quency, the signals from the transducers were displayed

on the oscilloscope and positioned such that the signals

overlayed each other. With the magnitude switches for

each channel set to the same setting, the sensitivity dial

on the downstream charge amplifier was adjusted until the

signal traces on the oscilloscope exactly matched. The

amplitude of the signals was verified by setting the down-

stream wave analyzer frequency to obtain maximum voltage.

It was found that using the procedure of matching the signals visually on the oscilloscope produced voltages on the wave analyzers which were equal to within the accuracy of the analyzer meters.

This sensitivity setting was then verified over a range of frequencies and air supply levels. In all cases the signals displayed negligible differences over the range of frequency and air supply levels used in this study. After calibration the transducers were transferred to the applicable test line and the line connected in place of the calibration block.

This calibration procedure was repeated each time the transducers were placed in a new test line. Initial tests using the calibration block showed that the same results were obtained regardless of the position in which the transducers were placed. Calibration tests were repeated with the transducer positions reversed without measurable differences.

Experimental Procedure. The experimental data collected during this study consisted of the sending (upstream) pressure, the receiving (downstream) pressure and the phase shift between the two pressure signals. The data was measured as a function of the frequency over the frequency range 20 to 1000 Hz.

40

Given a selected Reynolds number, the required
static pressure setting was determined from Equations (50)
or (51). Following the warmup period of the pneumatic
driver amplifier/power supply and the zeroing of the wave
analyzers, the air pressure was adjusted to obtain the
correct reading on the voltmeter connected to the static
pressure transducer. The voltage reading was converted
to psig using the calibration equation determined for the
transducer. The ambient-atmospheric pressure and tempera-
ture were recorded with the atmospheric pressure being
corrected for temperature and gravity effects.

The frequency was selected on the sending wave
analyzer using the frequency counter as the measuring
device. The frequency on the receiving wave analyzer was
adjusted until a maximum voltage was obtained. This pro-
cedure was used rather than simply matching the frequen-
cies using the frequency counters because it was dis-
covered early in the study that there were sometimes differ-
ences of up to 7 Hz between the sending frequency and the
receiving frequency at which the maximum voltage was mea-
sured. In many instances if the frequencies were simply
matched, the receiving pressure signal would decrease from
a maximum of anywhere from 50 to 300 mV to almost zero mV.
This problem is attributed to the wave analyzers used in
this study. The problem should be eliminated by the
scheduled acquisition of new wave analyzers.

41

When the maximum voltage was obtained, both charge amplifiers were grounded using the ground button on the front panel to ensure accurate readings and the two pressure signal voltages recorded.

The storage feature of the Nicolet oscilloscope was utilized to record the traces of the pressure signals. The time difference between identifiable common points on the two signals was determined using the movable cursor and the digital display of the oscilloscope. Any traces which showed distinctive or unusual features were stored on the oscilloscope's magnetic disc for later review and analysis. This procedure was repeated over the usable frequency range of the pneumatic driver of 20 to 1000 Hz at varying intervals.

The flow rate through the test line was measured using the rotometer before and after the test run. The rotometer measurement was converted to a mass flow rate using calibration curves previously prepared for the rotometer. The calibration of the most commonly used rotometer tube was verified during this study.

The air supply was monitored using the static pressure transducer output. Fluctuations in the pressure signal voltage readings could be related to sharp fluctuations in the supply line pressure. Data measurements were not taken during periods of line pressure fluctuation.

The precaution of grounding the charge amplifiers before taking the readings was implemented after it was noted that the output of the amplifiers would decay significantly over a period of time. Although the length of time required for this effect to occur was longer than that usually taken to obtain the readings, this precaution was taken to ensure accurate readings in the event that there was some delay.

In the cases where the bypass device was used, the required static pressure reading was obtained with the bypass device closed by adjusting the air supply and the flow rate was measured. The bypass device was then opened the optimum amount to provide maximum pressure signal voltages and clear oscilloscope traces and the air supply increased to re-establish the static pressure reading.

Test Designation

A five-digit numeric code was assigned to each test run. The code was the same as that used by Wilkins (Ref 6) to allow direct comparison of experimental results and to maintain consistency within the data base.

The first digit identifies the line used; 1 for the 0.041, 2 for the 0.119 and 3 for the 0.195 in. diameter line. The second digit identifies the line termination condition; 0 for blocked, 1 and 2 respectively for the

43

0.0135 and 0.016 in. diameter orifices, and 3 for open. The last three digits indicate the nominal Reynolds number in hundreds.

An alpha character suffix was used in some instances to identify significant test characteristics. The characters and their meaning are listed below.

     b - bypass device open

     n - modified orifice device

     r - transducer positions reversed

IV. Results and Discussions

Test Conditions

A summary of line configurations and ambient conditions for which experimental tests were conducted is presented in Table II. The shaded area of Figure 13 shows the portion of the nondimensional frequency vs. attenuation region covered by these results ($3.52 < \Omega < 9201.8$).

Analysis of Instrument Error

Table III presents the absolute error in the experimental gain for typical pressure measurements. This error is based solely on the readability of the wave analyzers and was determined by analysis of Equation (19) using the method of Equation (53).

A similar analysis was conducted for the phase angle calculation based on the readability of the Nicolet oscilloscope and the frequency counters. The experimental phase shift is calculated from the equation

$$B = -0.36(freq)(phd) \tag{56}$$

where   freq = signal frequency in Hz

phd = phase delay in msec.

The resultant absolute error for typical phase delay measurements is presented in Table IV.
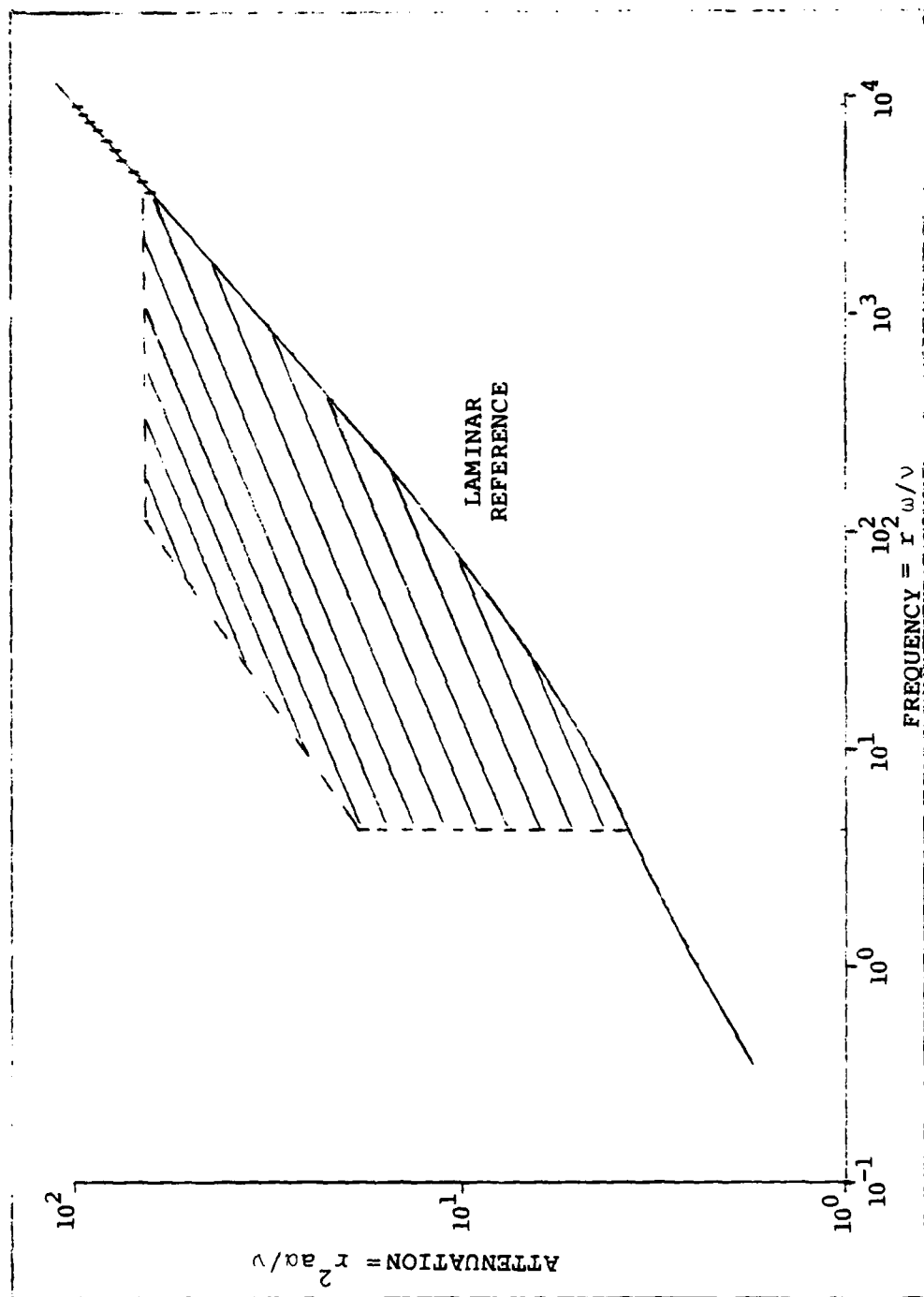
Fig. 13. Range of Experimental Nondimensional Results

46

TABLE II

TEST SUMMARY

Case	P_a (psia)	P_T (psig)	T_a (°F)	M (lb_m/sec x 10^4)	Re	Ω_{min}	Ω_{max}
10000	14.18	9.03	76.1	0	0	3.46	172.8
11006	14.23	8.09	72.5	2.07	620	3.35	167.3
11012	14.24	14.56	76.1	.393	1180	4.29	214.3
11012b	14.24	14.56	76.1	.393	1180	4.29	214.3
11014n	14.20	16.47	84.2	.473	1402	4.50	224.9
11014nb	14.20	16.47	84.2	.473	1402	4.50	224.9
11020	14.20	21.78	75.2	.712	2100	5.37	268.3
11020b	14.20	21.78	75.2	.712	2100	5.37	268.3
11030n	14.20	21.67	82.4	1.002	2969	5.28	263.8
11033	14.15	33.73	83.3	1.11	3337	7.03	351.6
11033b	14.15	33.73	83.3	1.11	3337	7.03	351.6
12018n	14.17	16.15	77.0	.592	1780	4.51	225.3
12034n	14.20	30.36	82.4	1.15	3425	6.56	327.9
12034nb	14.20	30.36	82.4	1.15	3425	6.56	327.9
21004	14.19	13.03	75.7	.433	445	34.3	1715.9
21004b	14.21	13.13	76.1	.433	404	34.3	1714.6
21007	14.21	17.04	81.5	.632	654	38.8	1940.3
21007b	14.21	17.04	81.5	.632	654	38.8	1940.3

TABLE II--Continued

Case	P_a (psia)	P_T (psig)	T_a (°F)	M ($lb_m/sec \times 10^4$)	Re	Ω_{min}	Ω_{max}
21015n	14.27	40.79	78.8	1.47	1521	68.7	3436.0
21015nr	14.27	40.79	80.6	1.47	1480	68.5	3424.6
22020nr	14.29	48.83	80.6	1.99	2060	78.5	3925.3
23090	14.31	1.32	77.9	9.14	9094	19.5	975.5
23105	14.27	1.69	81.5	10.37	10490	19.7	989.5
23107	14.19	1.87	82.4	10.38	10736	19.9	993.4
23107b	14.19	1.87	82.4	10.38	10736	19.9	993.4
23129	14.31	2.37	77.9	12.1	12934	20.8	1039.7
23165	14.22	3.519	77.9	14.6	16513	22.1	1105.5
30000	14.45	11.51	79.1	0	0	86.9	4346.5
31003b	14.24	14.64	77.0	.473	300	97.1	4854.6
31009	14.34	26.35	77.9	1.43	927	136.6	6828.4
31009b	14.34	26.35	77.9	1.43	927	136.3	6816.8
31009n	14.28	41.14	83.8	1.43	927	184.0	9201.8
32003b	14.17	7.74	77.0	.473	300	73.7	3683.7
32010n	14.32	32.63	78.8	1.51	979	157.3	7866.6
33052	14.11	.12	77.0	10.46	5156	47.8	2391.4
33060	14.23	.155	77.0	10.78	6020	48.4	2420.4
33079	14.23	.244	78.8	14.0	7862	49.0	2448.9

48

TABLE III

ABSOLUTE ERROR IN EXPERIMENTAL GAIN
DUE TO INSTRUMENT READABILITY

P_S (mV)	P_R (mV)	Gain (dB)	Error (dB)	%
6.2	22.0	11.0	.34	3.1
69	27.0	-8.1	.29	3.5
230	410	5.02	.40	8.0
730	340	-6.64	.37	5.6
9.5	7.2	-2.4	.21	8.8
46	81	4.9	.30	6.0
300	200	-3.52	.36	10.3
1700	870	-5.82	.36	6.1
1605	1450	-1.122	.56	50.2

TABLE IV

ABSOLUTE ERROR IN EXPERIMENTAL PHASE SHIFT
DUE TO INSTRUMENT READABILITY

Freq (Hz)	(msec)	Phase Shift (deg)	Error (deg)	(%)
60	1.2	-25.9	5.5	21.3
100	2.5	-90.0	6.1	6.8
460	2.0	-331.2	5.3	1.6
720	0.58	-510.3	5.8	1.1
860	0.78	-601.5	7.0	1.2
1000	0.96	-705.6	4.6	0.6

Though the Nicolet oscilloscope features sample rates up to 50×10^{-9} secs., the sample rates used in this study were determined largely by the signal frequency. It was necessary to select a sample rate which provided a display of several cycles to allow a significant number of phase delay measurements to be made at each frequency.

The major source of error in the phase shift calculation is the determination of the actual peak location on the upstream signal in certain situations. In these instances the signal either degenerated into a multipeak signal as illustrated in Figure 14 or displayed random noise which obscured the location of the peak. The range of possible peak locations in these situations was several sample steps wide and presents significant error in addition to that resulting from instrument readability. Almost all cases where the experimental phase shift data differs significantly from theoretical predictions can be traced to situations where this problem was evident.

General Gain and Phase
Shift Results

All cases presented in Table II were evaluated using the computer simulation to compare experimental results with theoretical predictions. Figures 15-32 present the correlation between experimental and theoretical results for some representative cases from this study. The results of the remaining cases will be used to

50
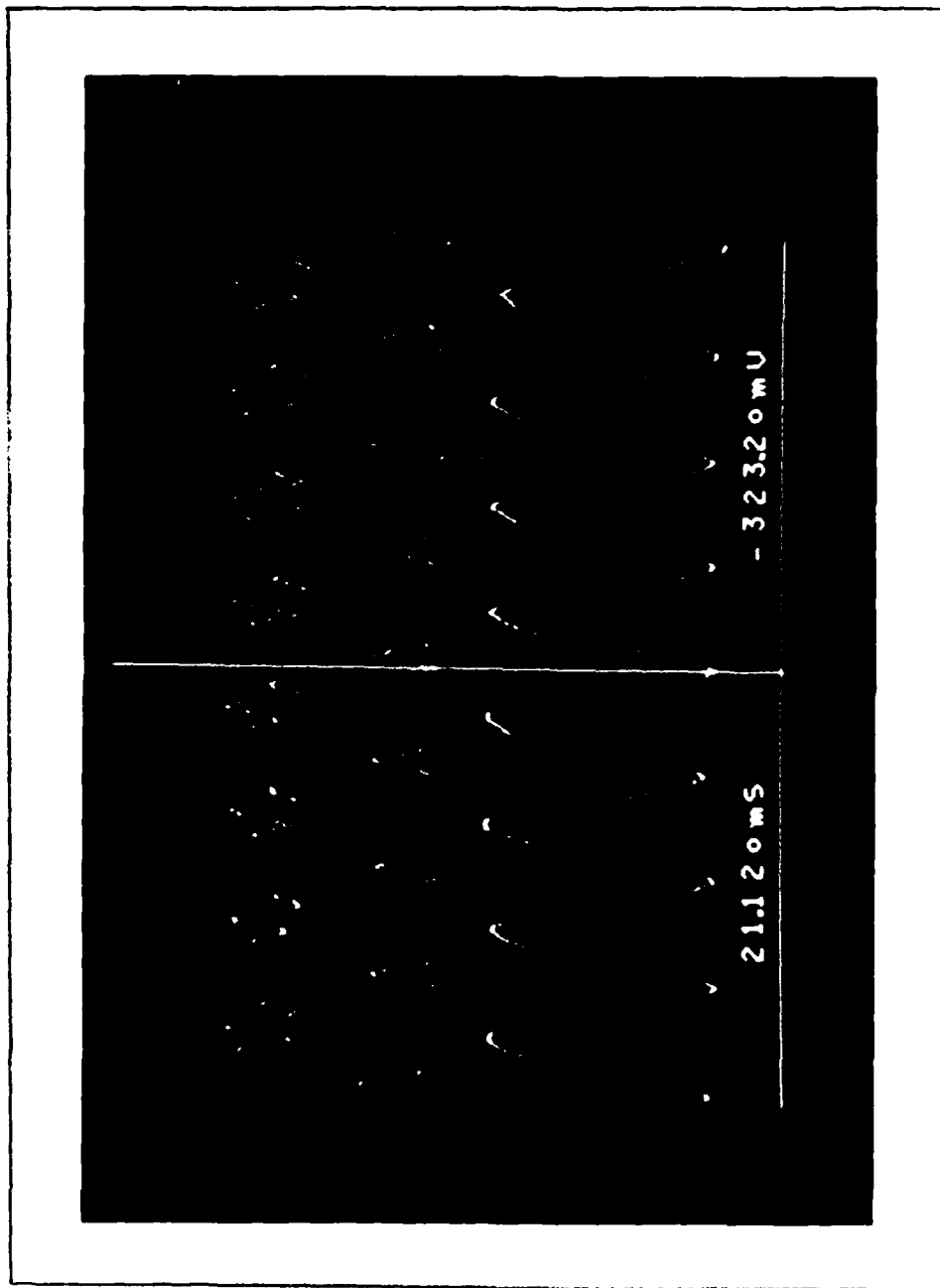
Fig. 14. Atypical Sending Pressure Signal (Upper Signal)

51

illustrate points discussed in the following sections. In most cases the experimental results show good agreement with the results of Briski (Ref 5) and Wilkins (Ref 6). Blocked line and laminar mean flow experimental results show close correlation with laminar theory predictions (Figures 15-18 and 27-30), while in turbulent mean flow cases the laminar theory predicts significantly lower attenuation than observed experimentally (Figures 19-26 and 31-32). The Modified Constant LRC model (MCLRC) developed by Wilkins (Ref 6) predicts increased attenuation in turbulent mean flow cases but the attenuation is still below experimental results. The use of the Constant LRCG model (Ref 6) results in a further increase in attenuation over that predicted by the MCLR model, but in most cases the theoretical attenuation still results in peak gain magnitudes less than those observed experimentally. The phase shift results are generally in close agreement between experimental and theoretical models with some deviation at high Reynolds numbers. The deviations are consistent with results obtained by Wilkins (Ref 6) but are of unknown cause at this time.

Analysis of Radiation Impedance

For the open line cases in this study the radiation impedance was used in the computer simulation to determine the terminal impedance. A comparison of the

radiation impedance and the assumption that $Z_L = 0$ for an open line (Ref 10) was made and the effect of each method on the line response was studied. For the line configurations and conditions of this study the value of the radiation impedance was between -1×10^{-6} and -3×10^{-3} with the largest value occurring at high frequency in the 0.119 in. diameter line. Figures 33-39 show the relative effects of the two impedances on the results of the MCLRC model and the Constant LRCG model. In all cases setting $Z_L = 0$ caused a slight increase in the gain over the entire frequency range. The increase was so small, however, that it is considered insignificant in relation to the differences between experimental and theoretical results. The effect of the radiation impedance is seen to be negligible from these results.

Effect of Upstream Conditions

Several test runs were conducted to confirm that variations in the conditions upstream of the test section would not affect line response. The variation in upstream conditions was obtained by diverting a significant amount of the mass flow out of the line upstream of the test section. The input flow rate was increased to maintain the same flow rate through the test section in both situations. Operation of the system in the bypass configuration would simulate a branch line upstream of the test section.

Figures 40-48 show the comparison of experimental gain between the bypass and no-bypass conditions.

The experimental results match very closely in most cases confirming that flow variations upstream of the test section have no effect on line response.

The results of Case 21004 (Figure 45), however, show an unexpected positive offset of the gain over the entire frequency range in the bypass condition. This off-set resulted from a switch of the transducer locations and indicated that there was a difference in sensitivity between the two transducer/charge amplifier pairs despite the same settings being used on both amplifiers. This difference was confirmed by the results of two other sets of runs where the transducer positions were reversed. These results led to the implementation of the calibration procedure discussed in Chapter III. Results obtained after calibration of the transducers show no such offset. The theoretical gain has not been plotted for those cases con-ducted before transducer calibration as the difference in sensitivity caused an offset of both the bypass and no-bypass results from the actual values.

Effect of Modified Orifice Devices

Due to the machining methods used in their produc-tion, the original orifice devices did not match the char-acteristics of the orifice model shown in Figure 4. The

orifice devices contained a significant length of area
reduction before the actual orifice as shown by the dotted
lines of Figure 7. The devices were modified to more
closely match the model by machining out the inlet passage
to a constant diameter. The dimensions noted on Figure 7
and listed in Table I apply to the modified orifice devices.

The gain and phase shift results in Figures 49-60
show close correlation with results of similar cases pre-
sented by Wilkins with the exception of Case 12034 (Figures
66-67). The experimental gain data from this case shows
significant deviation from Wilkins' results in similar
cases (12020 and 12050). The results show higher peak
gains over the frequency range 20-500 Hz. Particularly
noticeable is the peak gain of 6.89 dB at 350 Hz compared
with values of approximately zero in Wilkins' results.
The gain results over the remainder of the frequency range
and the phase shift results show good agreement with
Wilkins' results. The deviation between the experimental
results and the theoretical predictions is generally the
same as displayed in Wilkins' results. The reason for this
anomaly is not known but the almost exact agreement between
Cases 12034 and 12034b reduces the likelihood of experi-
mental error. It should be noted that there is a signifi-
cant difference in the Reynolds numbers between this case
and comparable cases of Wilkins (3425 vs. 2044 and 4992).

Modified LRCG Model

Analysis of theoretical results obtained using the Constant LRCG model developed by Wilkins (Ref 6) revealed that this model did not display the characteristic decrease in nondimensional attenuation at low nondimensional frequency as described by Brown et al. (Ref 5). (All further references to attenuation and frequency will refer to the nondimensional parameters unless otherwise specified.) A similar analysis of the MCLRC model showed that the MCLRC model did exhibit the expected decrease in attenuation. This led to a review of the development of the Constant LRCG model to determine the cause of the deviation.

The assumption that RAC/ω is much less than L_T was used by Wilkins to simplify the model and remove any dependency on the frequency. In his results Wilkins (Ref 6, p. 41) discusses the limitations imposed on the model by the assumption. A review of Wilkins' cases reveals that for a wide range of line configurations and Reynolds numbers this assumption is not valid over a significant portion of the frequency range under consideration. Table V presents a review of cases from both this study and Wilkins and illustrates the frequency limitation of this assumption for various line configurations and flow conditions.

TABLE V

COMPARISON OF R_{AC} VS. L_T

Case	Re	R_{AC} $(\frac{lb_f\text{-}s}{in^6})\times10^4$	L_T $(\frac{lb_f\text{-}s^2}{in^6})\times10^4$	ω_b $(\frac{rad}{s})$	(Hz)
11030*	2968	1434.8	2.1388	6283	1000
12018n	1780	906.96	1.8190	4986	794
23070*	7326	40.542	.10723	3781	602
23090	9094	43.857	.10892	4027	641
23100*	10450	48.683	.11197	4348	692
23105	10490	48.812	.11037	4423	704
23165	16513	68.598	.12297	5578	888
31003b	300	.46812	.086477	54.1	8.6
31009	927	1.0746	.11011	97.6	15.5
31052	5156	3.9743	.037176	1069	170
32010n	979	1.1190	.12665	88.4	14.1
33020*	1818	1.8192	.037723	482	76.8
33070*	7177	5.5296	.038131	1450	231
33079	7862	5.3430	.037187	1437	229

*denotes cases from Wilkins (Ref 6).

ω_b is defined as the frequency at which RAC/ω = 0.1(L_T) and above which the assumption RAC/ω much less than L_T is taken to be valid.

The results in Table V show that the assumption is invalid for the 0.041 in. diameter line over most of the frequency range except at very low Reynolds numbers. In the case of the 0.195 in. diameter line the assumption is generally valid except at low frequencies (<200 Hz) and high Reynolds numbers (>7000).

Results obtained using the Modified LRCG model which incorporates the full expression for G (Equation 36)) display the expected decrease in attenuation with negligible changes in attenuation at higher frequencies. Figures 61-63 show comparisons of the attenuation predicted by the Constant LRCG model with that predicted by the Modified LRCG model. The difference in attenuation at low frequencies is immediately obvious.

Though the inclusion of the frequency dependent term drastically alters the nondimensional behavior of the model, the effect on the gain and phase shift predictions is less significant. Figures 64-73 compare the effect of the Modified LRCG model versus the Constant LRCG model for typical cases from this study. These figures indicate an increase in the gain over that predicted by the Constant LRCG model, particularly at low frequency. The increase in the gain depends on the line configuration and signal frequency and generally reflects the validity of the limiting assumption discussed earlier. Review of the theoretical data from Case 11033 (Figure 64), for example,

shows an increase of 3.5 dB at 1 Hz and of 0.9 dB at 100 Hz. The differences decreases with increasing frequency and in this case is negligible above about 700 Hz. This increase in the gain produces better agreement with experimental results yet a significant difference still remains between theoretical and experimental results.

Examination of the expression for the modified C_T (Equation (37)) shows that as ω varies from 0 to infinity, C_T varies from kC_a to $(k - \frac{k-1}{K_{LT}})C_a$. The latter value is the same as the original expression for C_T (Equation (35)). As illustrated in Table VI the use of Equation (37) results in an increase in C_T of from approximately 38 percent at 1 Hz to less than 1 percent at 1000 Hz over the value of C_T determined by Equation (35). It is also noted that the value of the original C_T is less than 2 percent greater than C_a for the cases examined in this study.

Table VII shows the effect of the modification of C_T on the attenuation predicted by the Modified LRCG model. To obtain this data the Modified LRCG model was used with values of C_T calculated from Equations (35) and (37). The use of Equation (37) results in an increase in the attenuation over that predicted using Equation (35). Though the percentage increase is large at low frequencies, the absolute increase is on the order of 2 dB and is much less significant when compared with the 25-55 dB (300-600 percent) decrease in attenuation resulting from the use of

59

TABLE VI

VARIATION OF C_T DUE TO FREQUENCY

Case	Re	C_T (Eq 35) $(\frac{in^4}{lb_f} \times 10^4)$	Range of C_T (Eq 37) $(\frac{in^4}{lb_f} \times 10^4)$ **
11012	1180	.334	.459 - .337
12018n	1780	.315	.435 - .318
23070*	7326	5.285	7.308 - 5.292
23090	9094	5.151	7.126 - 5.159
23105	10490	5.038	6.972 - 5.048
23110*	10450	5.048	6.986 - 5.058
23165	16513	4.537	6.286 - 4.551

*denotes case from Wilkins (Ref 6).

**$(1 < \omega < 1000)$.

TABLE VII

PERCENT INCREASE IN ATTENUATION (MODIFIED LRCG MODEL)
DUE TO MODIFIED C_T (EQ 37) OVER C_T (EQ 35)

Frequency (Hz)	Case				
	11033	23090	23105	23165	33079
1	17.6	17.5	17.5	17.6	17.3
50	9.9	7.8	8.5	10.4	1.65
100	4.5	3.0	3.5	4.9	0.44
200	1.4	0.84	1.0	1.6	0.11
300	0.64	0.38	0.46	0.73	0.05
500	0.24	0.14	0.17	0.27	0.02
1000	-	0.04	0.04	0.07	-

the Modified LRCG model vice the Constant LRCG model. This indicates that the largest part of the difference in attenuation between the two LRCG models is due to the use of the full expression for Re (G).

Correlation of Modified LRCG Model with Brown's Modified IRC Model

In Reference 3, Brown et al. present the results of their Modified IRC model for turbulent flow accounting for heat transfer. The laminar reference curve (Figure 3) produced using the simplified equations developed by Krishnaiyer and Lechner (Ref 3) matches the laminar references shown in Figure 9 of Reference 3 and in Wilkins (Ref 6) except for the difference in the slope of the reference compared to the Modified LRCG curves in the low frequency region. Brown shows a change in the slope of the laminar reference at $\Omega = 2.5$ which does not appear in the laminar reference produced using the equations of Krishnaiyer and Lechner (Equations (6) and (7)).

The mid frequency range attenuation levels predicted by the Modified LRCG model agree with those shown on Brown's figure to within the resolution allowed by the figure.

Brown (Ref 3) gives an expression for the break frequency between the mid and high frequency regions as

$$\Omega_b = 2.5 \times 10^{-3} \, Re^{1.6} \tag{57}$$

This expression identifies a point of inflection on Brown's curves rather than the intersection of the turbulent model curves and the laminar reference curve. The results of this study give the expression for the intersection point for the Modified LRCG model as

$$\Omega_b = 9.68 \times 10^{-4} \, Re^{1.58} \qquad (58)$$

assuming a power form solution as presented by Brown. This break frequency agrees closely with the actual intersection point of the curves in Brown's figure.

Correlation of Results with Nichols (Ref 1)

Figure 74 presents a comparison of the attenuation predicted by the modified equations of Krishnaiyer and Lechner (Equations (6) and (7)) with that given by Nichols (Ref 1, Figure 6). The large deviation shown is attributed to the use of an approximation to the Bessel functions used to derive Equations (6) and (7). The simplified equations are stated to be limited to the region $\omega/\omega_v > 0.1$. This is confirmed by Figure 74.

Figures 75 and 76 compare the attenuation predictions of the various models discussed in this study. The deviation of the Constant LRCG at low frequencies is again seen to be significant. The MCLRC model and the Modified LRCG model show comparable behavior with the Modified LRCG model displaying the higher attenuation of the two models.

V. Conclusions

1. Changes in conditions upstream of the test section as represented by a bypass device with variable flow rates did not affect the line response as measured experimentally. This was determined to be true in both laminar and turbulent mean flow conditions.

2. The elimination of small differences between the orifice devices and the orifice model used to determine the reflection coefficient caused no change in the experimental results.

3. The absolute error in the experimental calculations due to instrument readability was determined to be approximately 0.5 dB in the gain calculations and approximately 5 degrees in the phase shift calculations. With the current experimental apparatus these values represent realistic limits on the resolution of differences between theoretical predictions and experimental results.

4. The effect of the radiation impedance on the theoretical predictions in open line cases is negligible. The use of $Z_L = 0$ rather than the radiation impedance resulted in an insignificant increase in the gain.

5. The Modified LRCG model, which is formed by adding the full frequency dependent expression for the

conductance to the MCLRC model, was seen to predict lower
attenuation than the Constant LRCG model at low frequency.
The resultant increase in the gain varied from as much as
6 dB for the small diameter line to less than 1 dB for the
large diameter line.   The change was negligible at high
frequency.

VI. Recommendations

1. Automated data processing equipment currently on order should be utilized to increase accuracy, facilitate low frequency measurements and significantly reduce the time required to collect and correlate experimental data. With automated experimental equipment a large data base could be easily built up and more time would be available for analytical work.

2. Efforts should be made to extend the range of experimental results, particularly into the low frequency region. Digital wave analyzers teamed with automated data processing equipment would hopefully allow low frequency measurements with current line configurations and at least would greatly improve data collection capability.

Appendix A: <u>Comparison</u> <u>of</u> <u>Experimental</u>

<u>and</u> <u>Theoretical</u> <u>Results</u>

<u>Case</u> <u>Number</u> <u>Explanation</u>

Case ABxxx

A - line diameter

    1 = 0.041 in.

    2 = 0.119 in.

    3 = 0.196 in.

B - line termination

    0 = blocked

    1 = 0.0135 in. diameter orifice

    2 = 0.016 in. diameter orifice

    3 = open

xxx = Nominal Reynolds number in hundreds
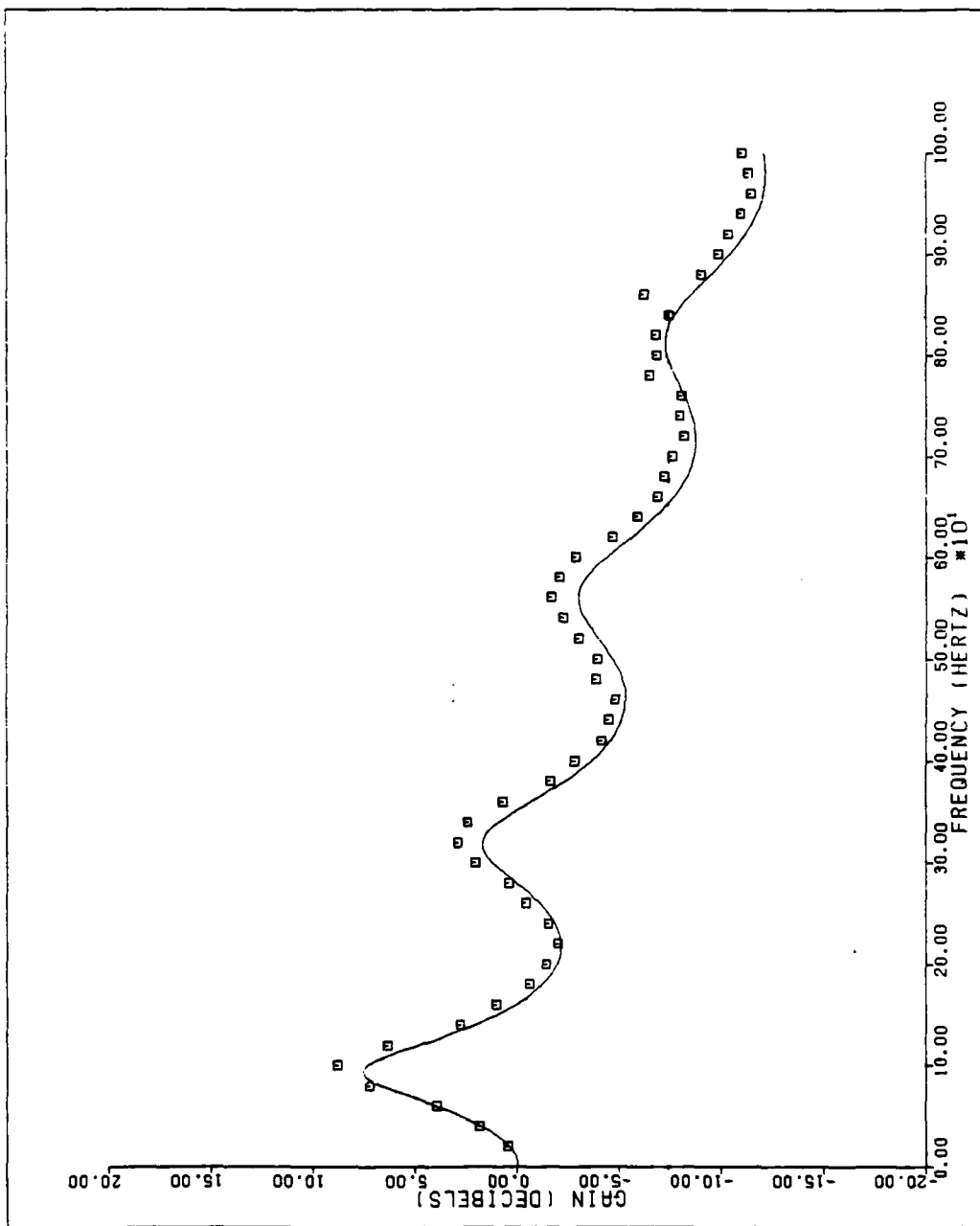
Fig. 15. Theoretical and Experimental Gain--Case 10000 -- Laminar Theory
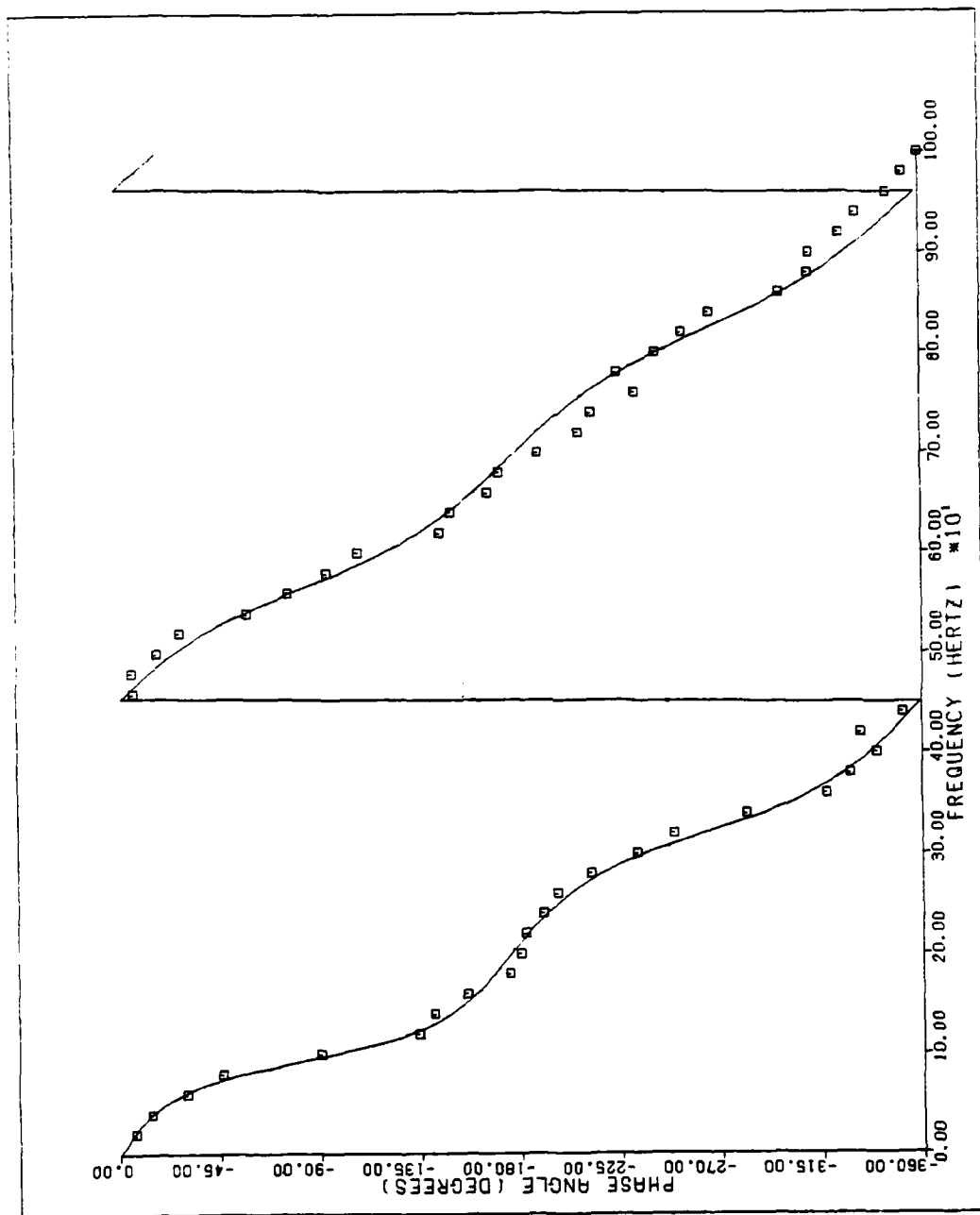
Fig. 16. Theoretical and Experimental Phase Shift--Case 10000--Laminar Theory

68
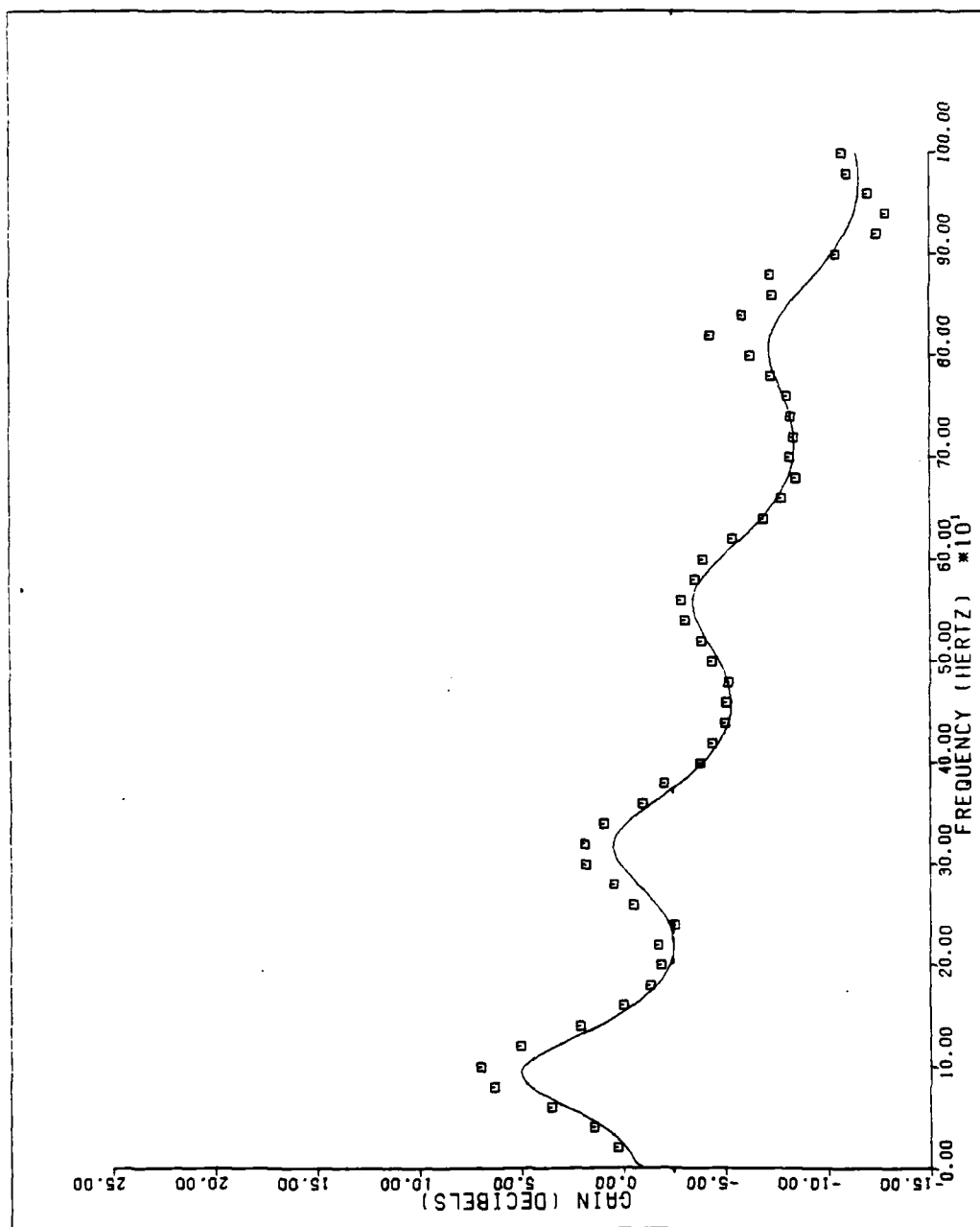
Fig. 17. Theoretical and Experimental Gain—Case 11006—Laminar Theory

69
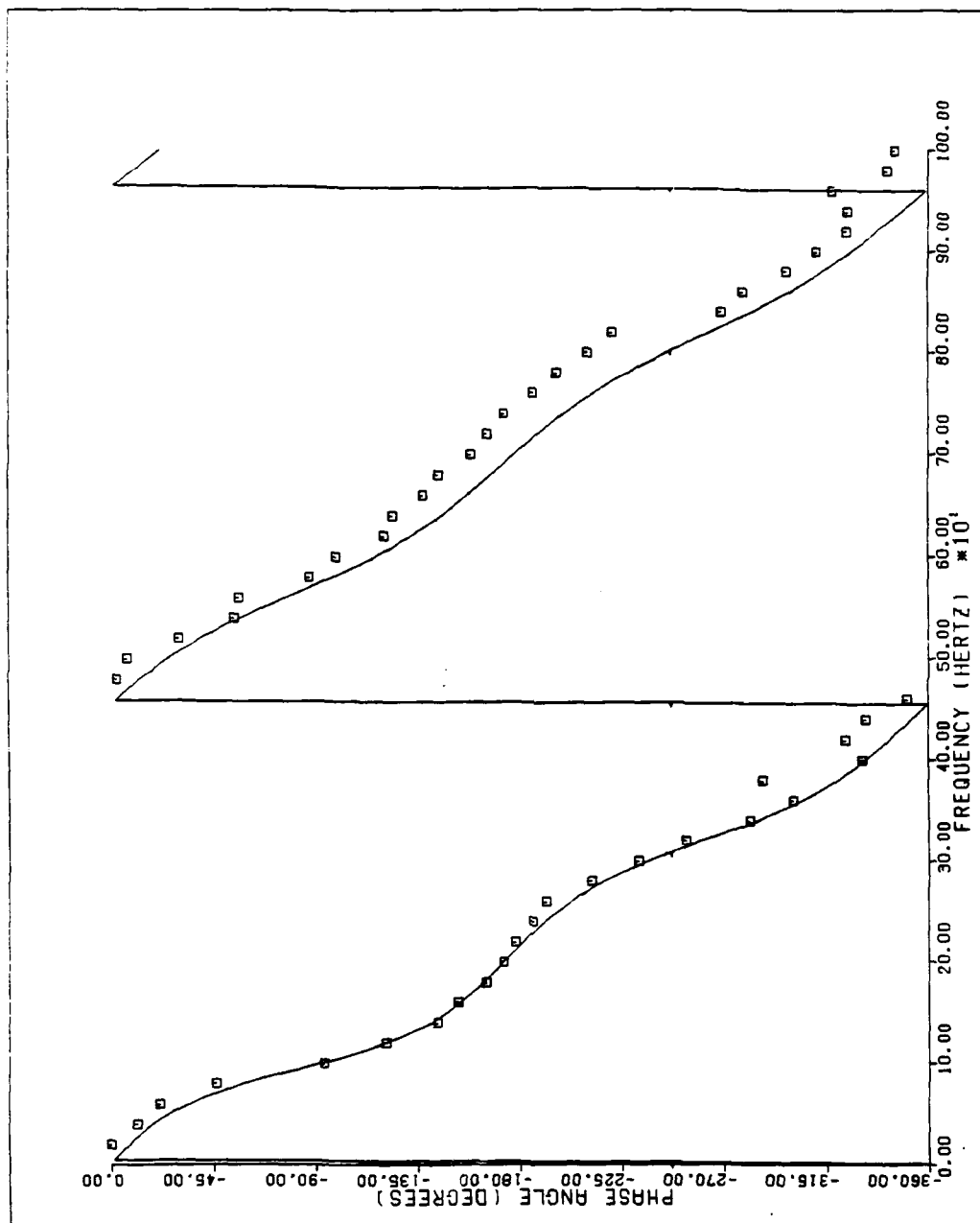
Fig. 18. Theoretical and Experimental Phase Shift--Case 11006--Laminar Theory
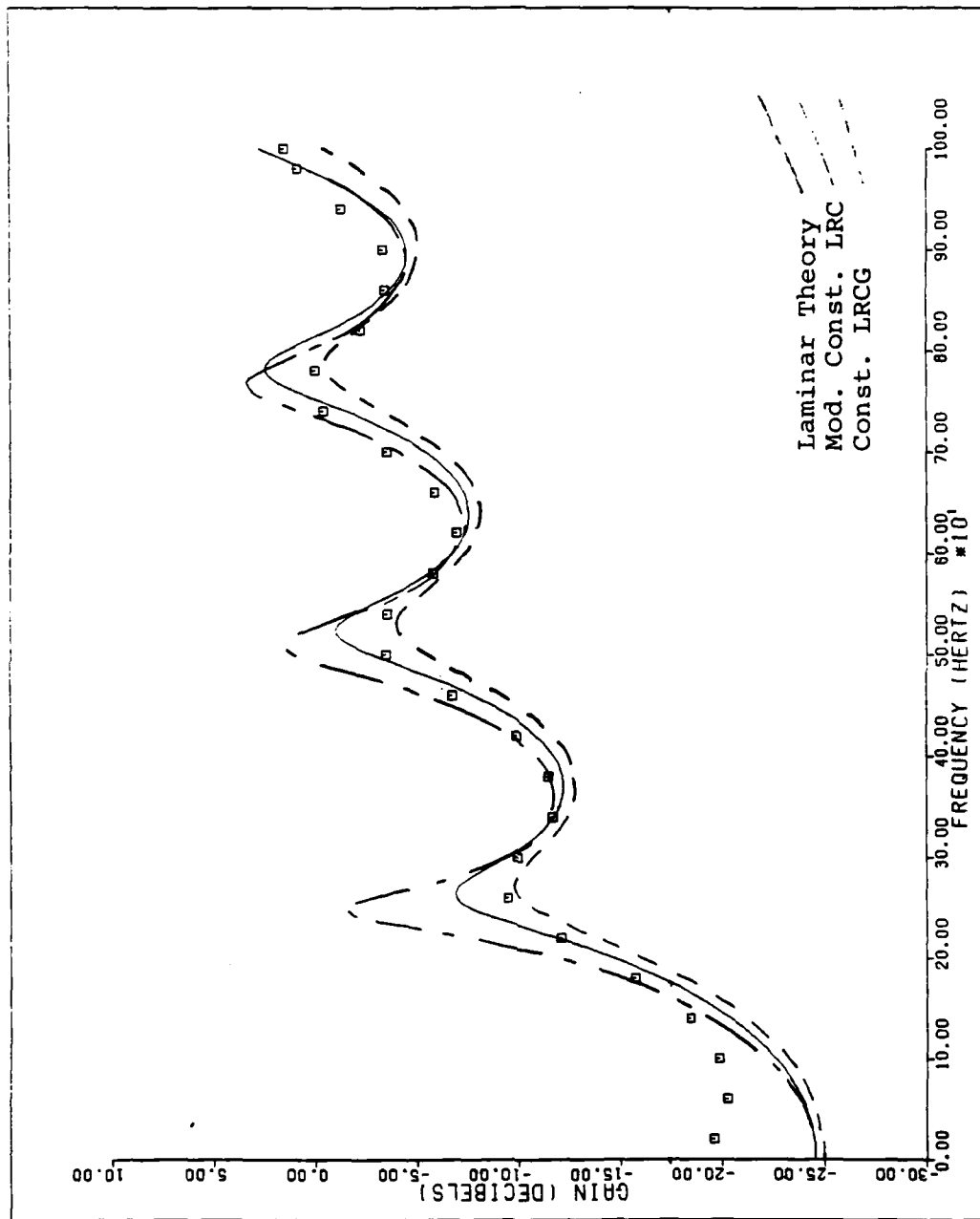
Fig. 19. Theoretical and Experimental Gain--Case 23090
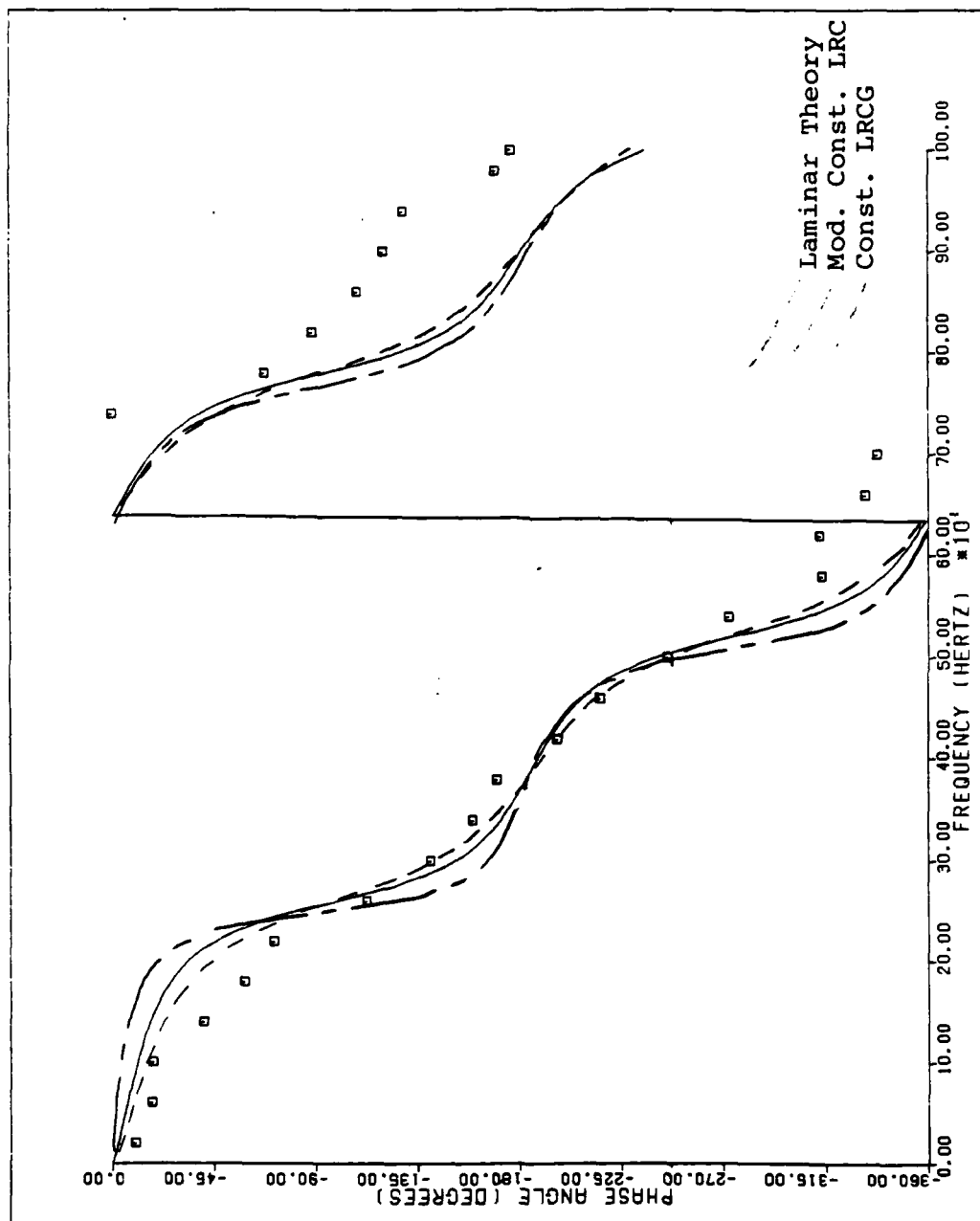
Fig. 20. Theoretical and Experimental Phase Shift--Case 23090
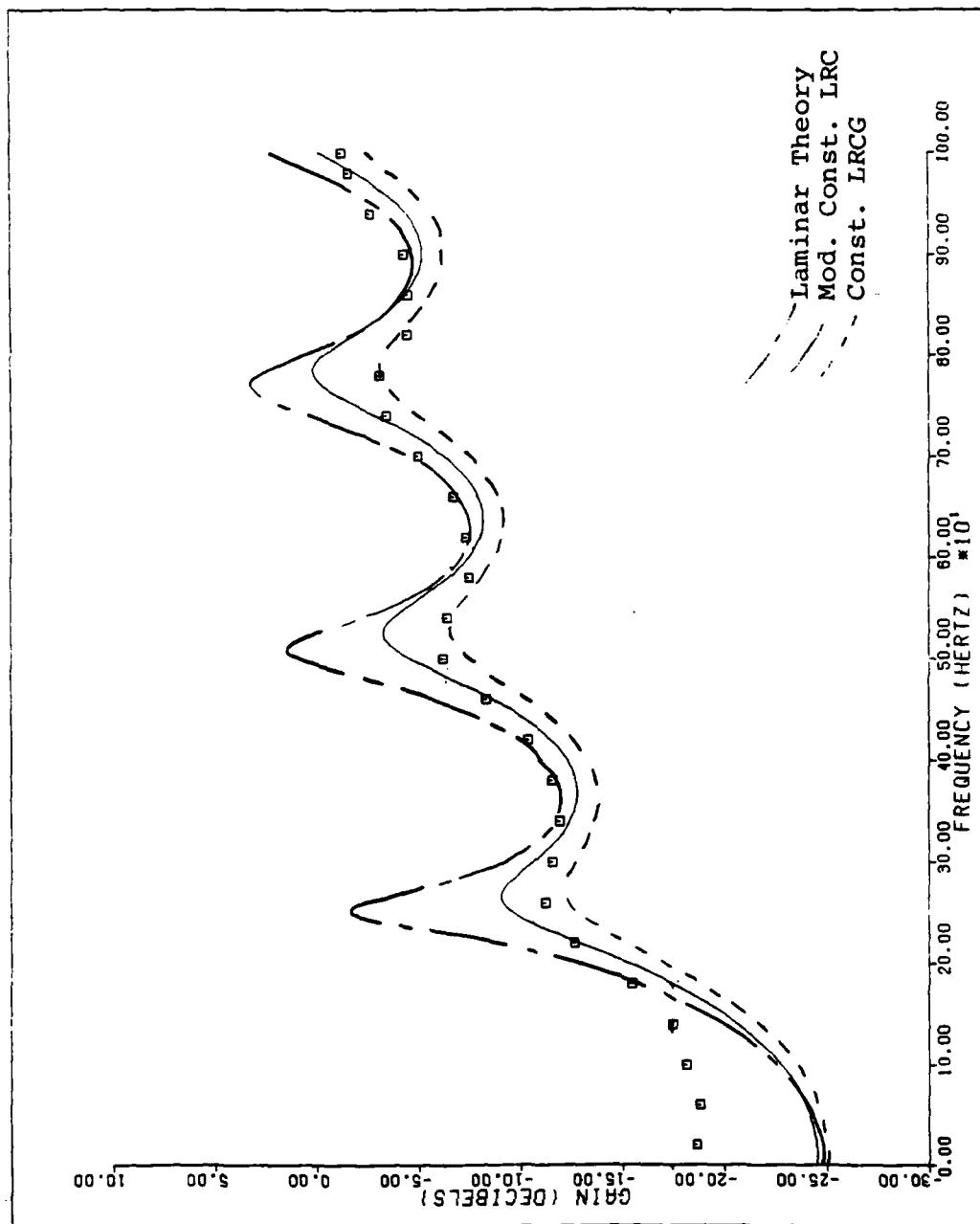
Fig. 21. Theoretical and Experimental Gain—Case 23129

73
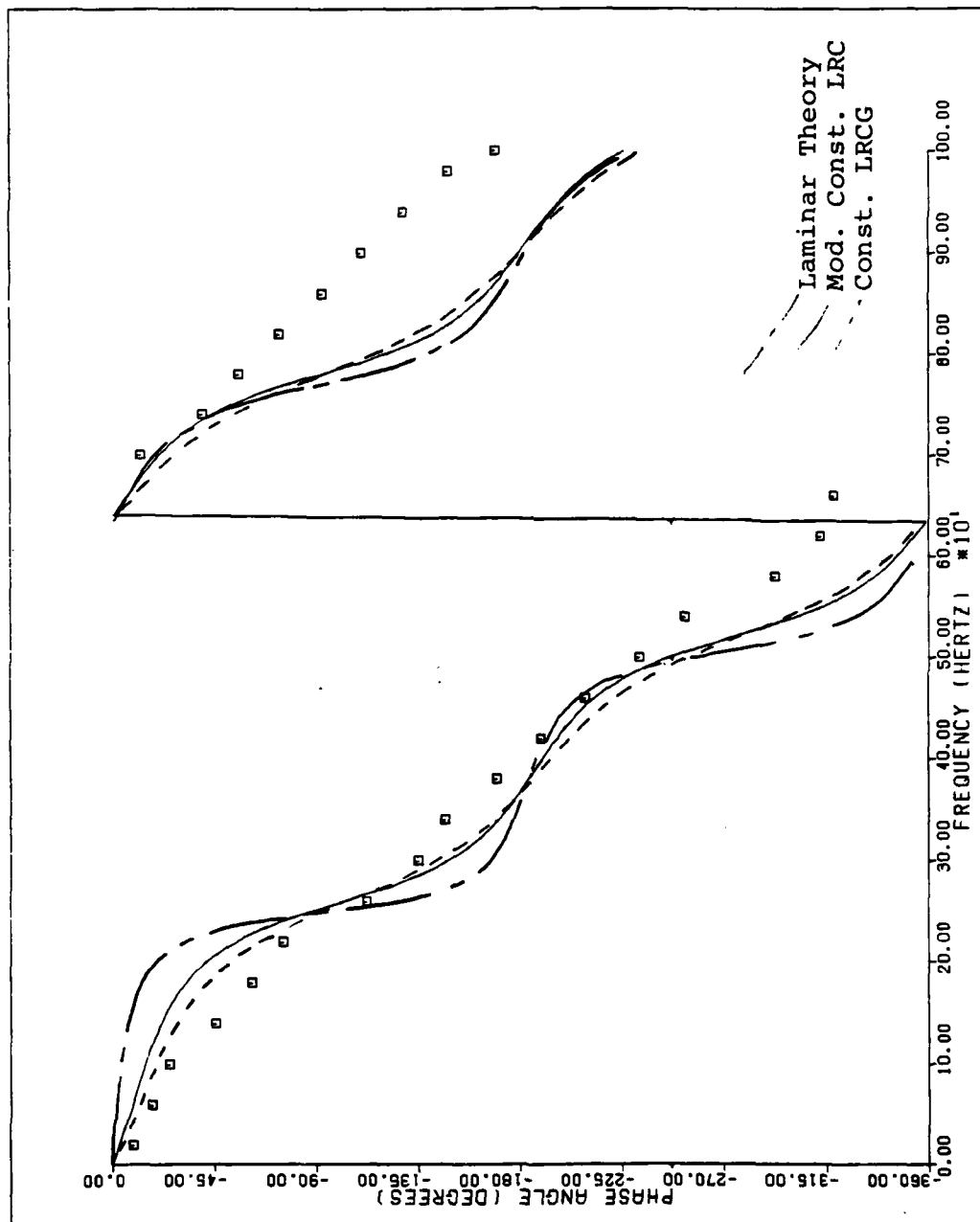
Fig. 22. Theoretical and Experimental Phase Shift--Case 23129

74
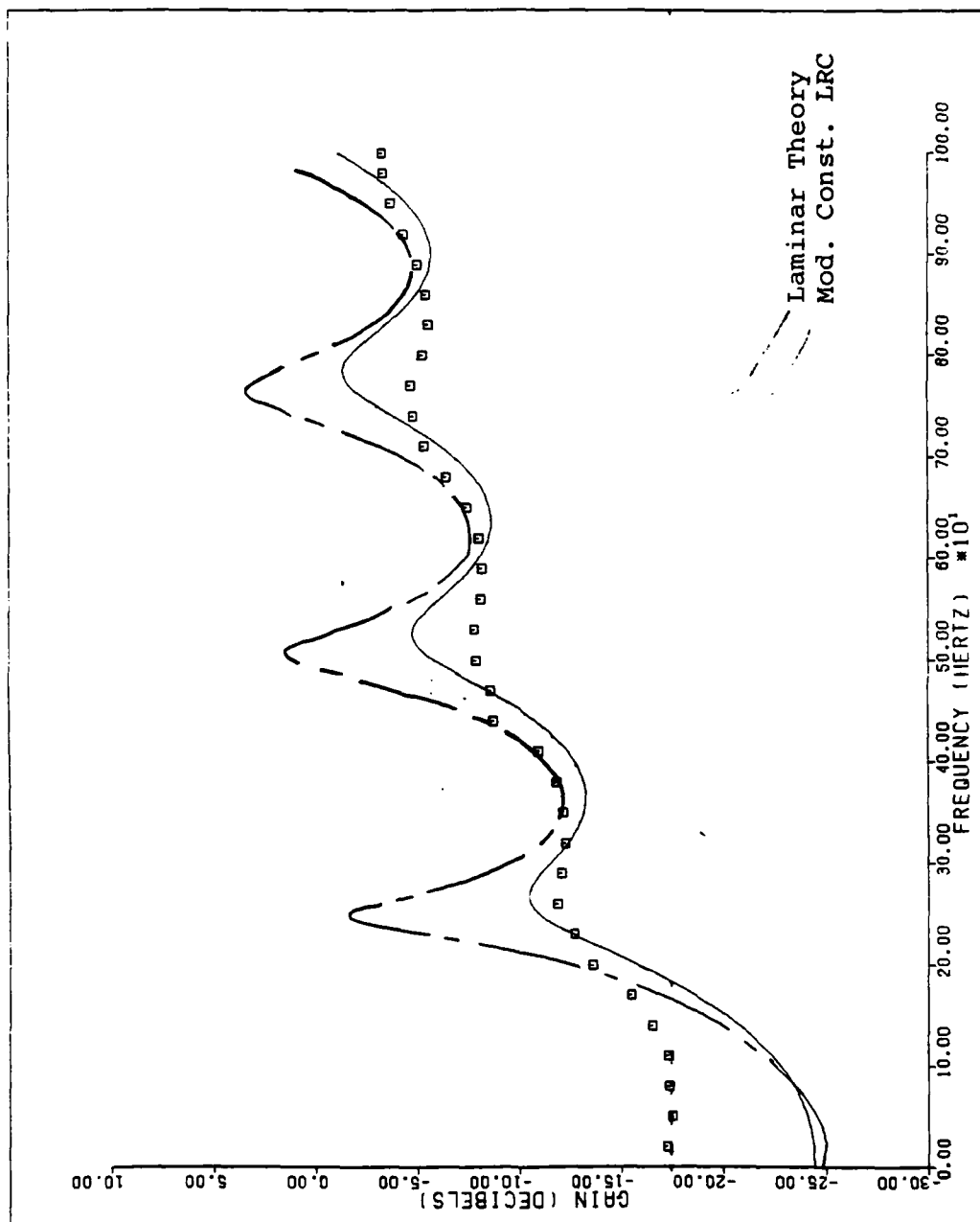
Fig. 23. Theoretical and Experimental Gain--Case 23165

75
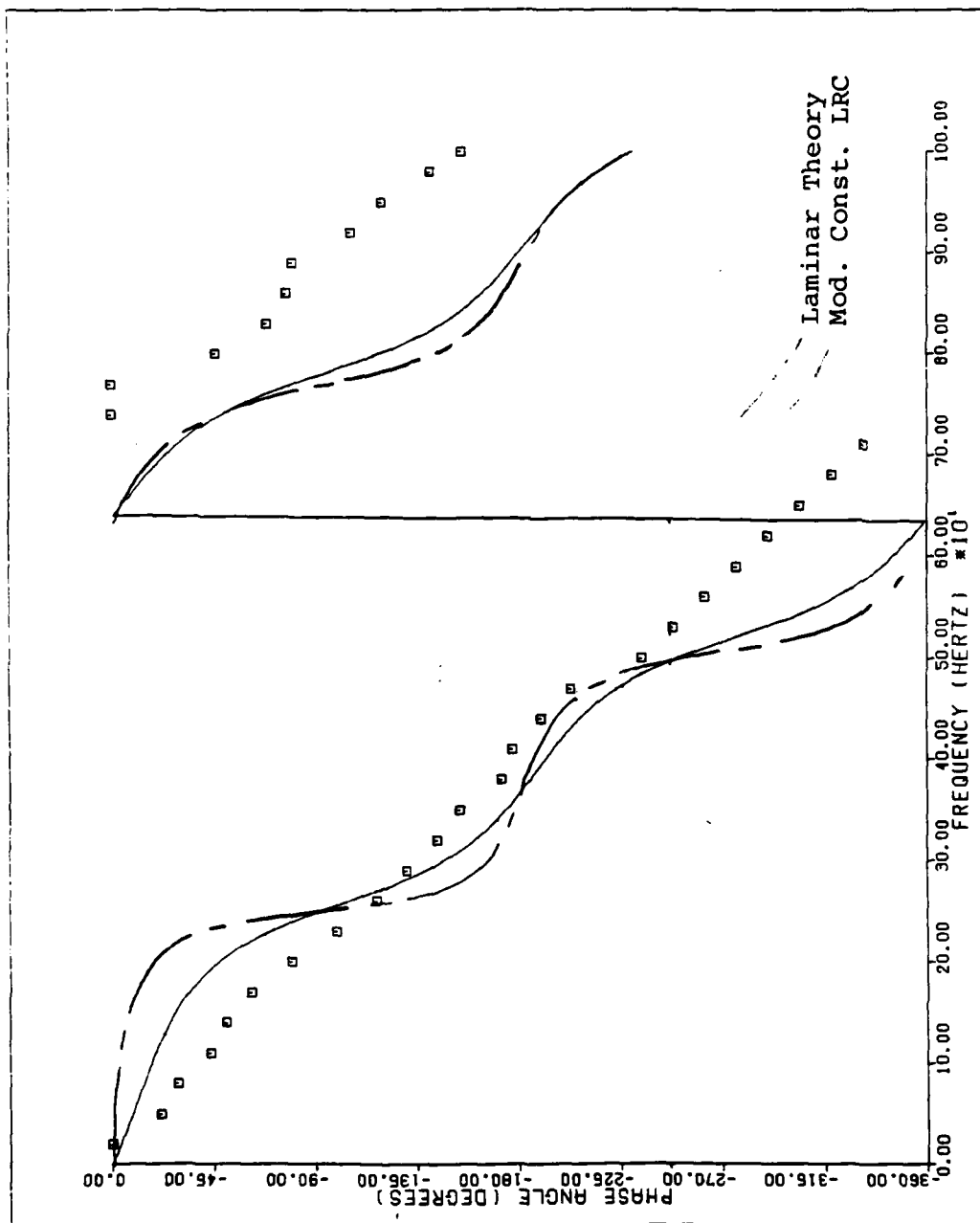
Fig. 24. Theoretical and Experimental Phase Shift--Case 23165

Fig. 25. Theoretical and Experimental Gain--Case 23165

Laminar Theory
Const. LRCG

77
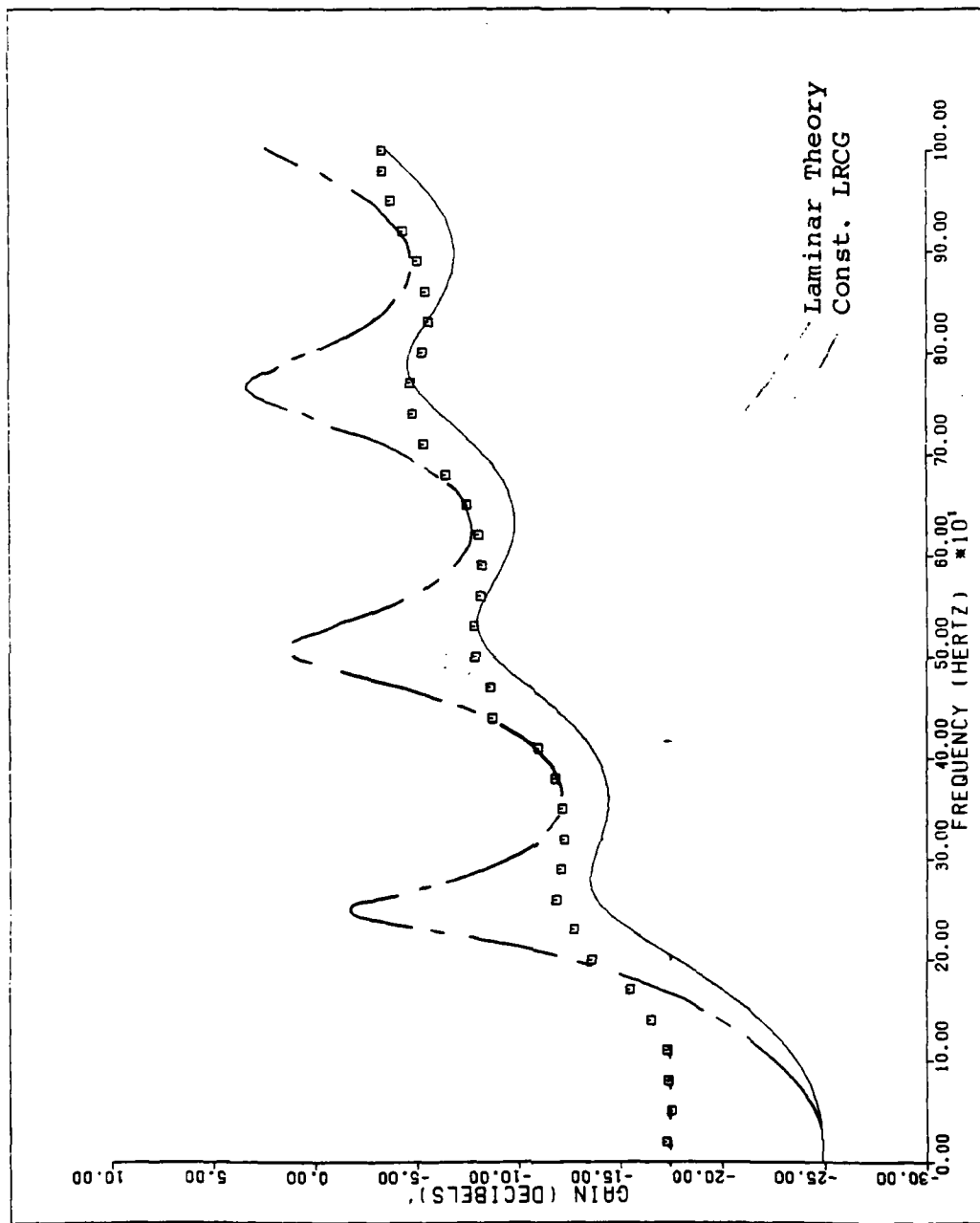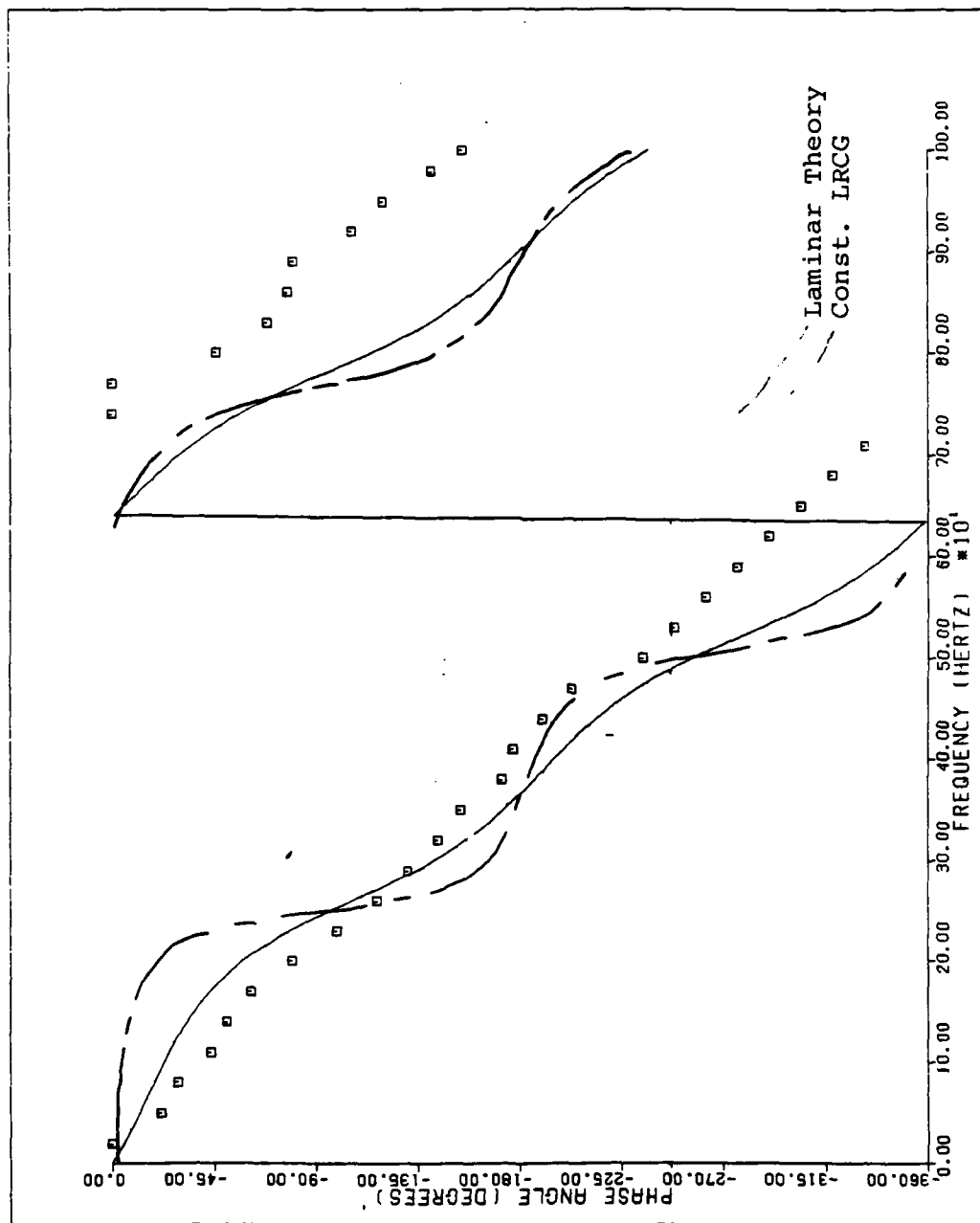
Fig. 26. Theoretical and Experimental Phase Shift--Case 23165
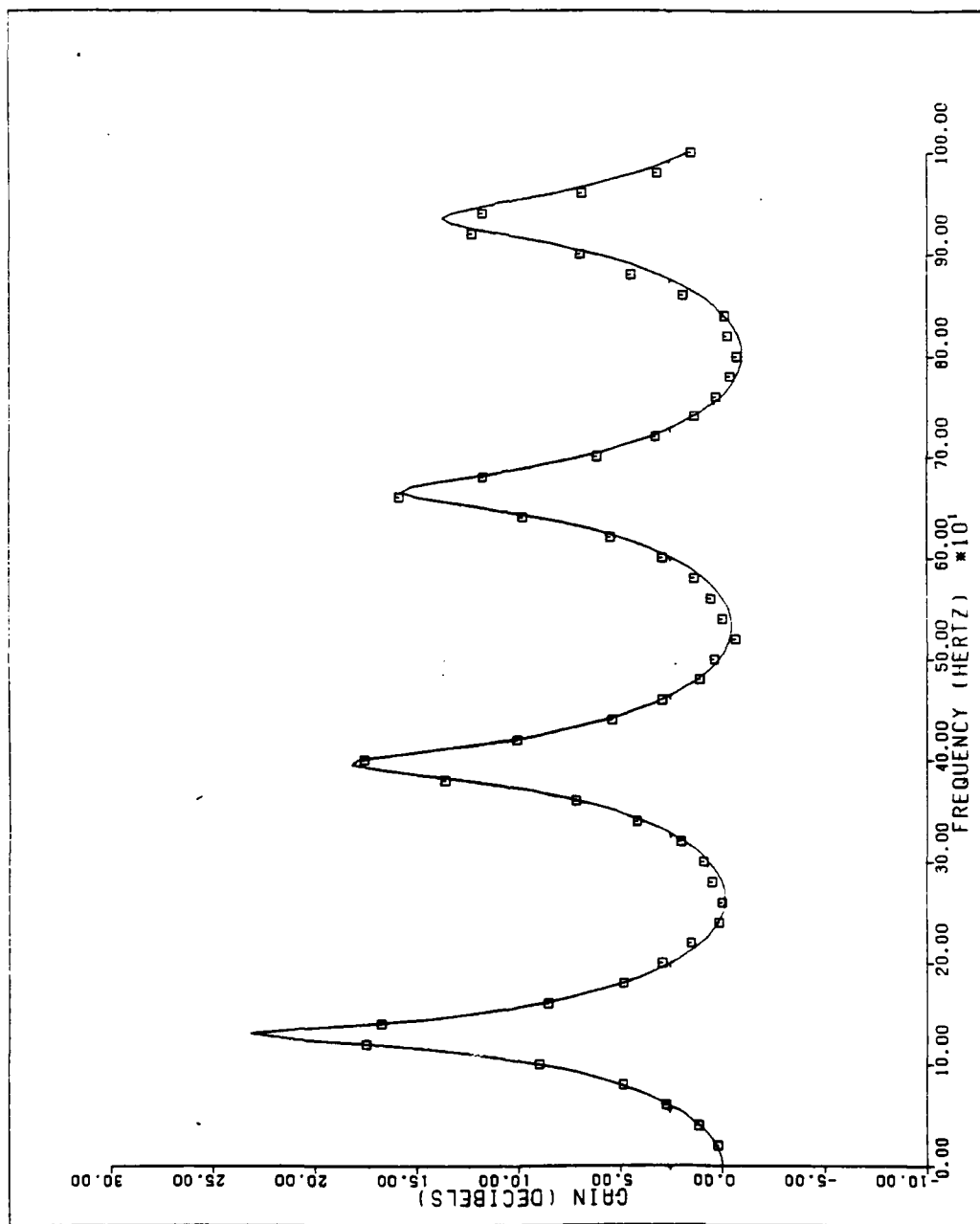
Fig. 27. Theoretical and Experimental Gain--Case 30000--Laminar Theory

79
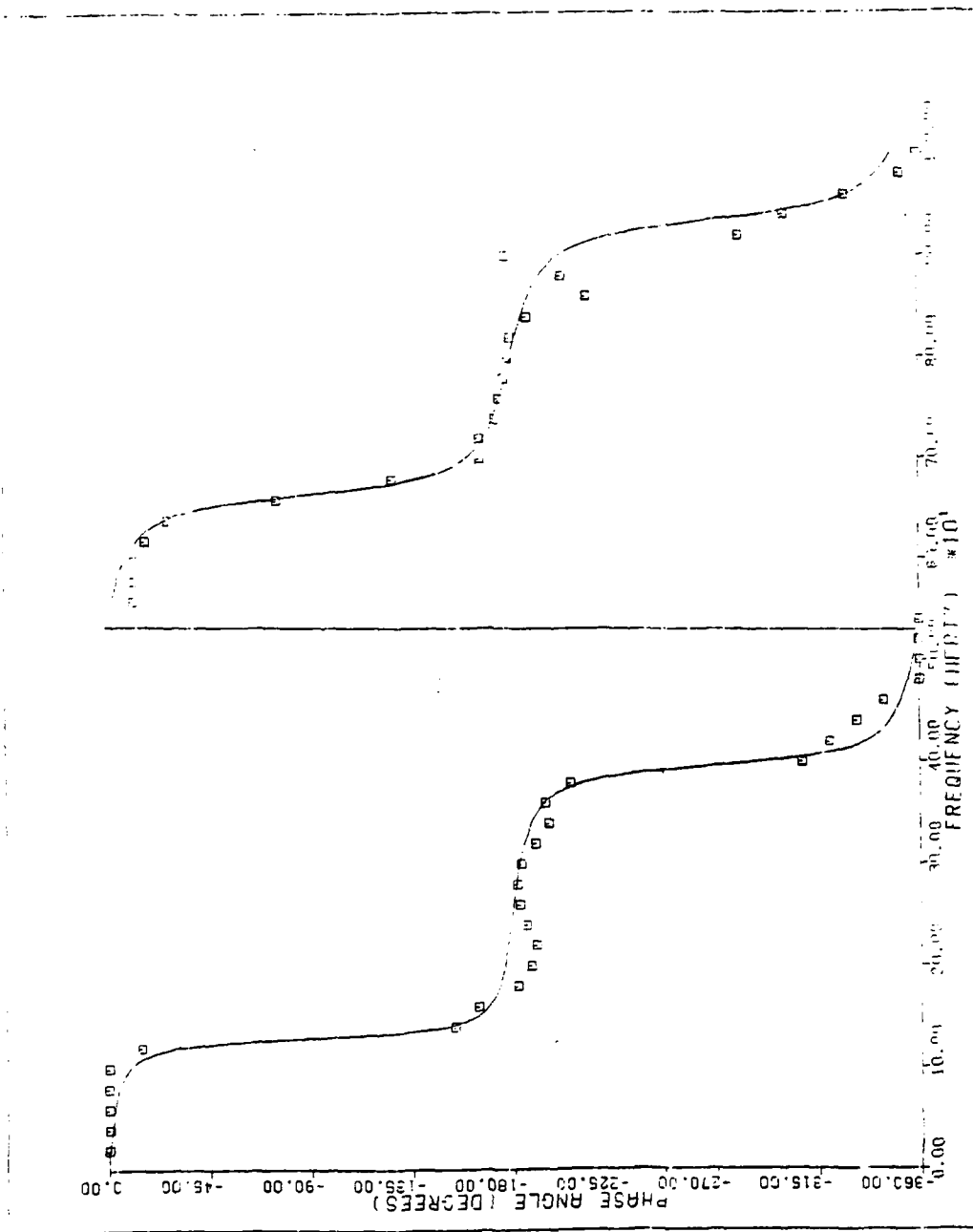
Fig. 28. Theoretical and Experimental Phase Shift--Case 30000--Laminar Theory
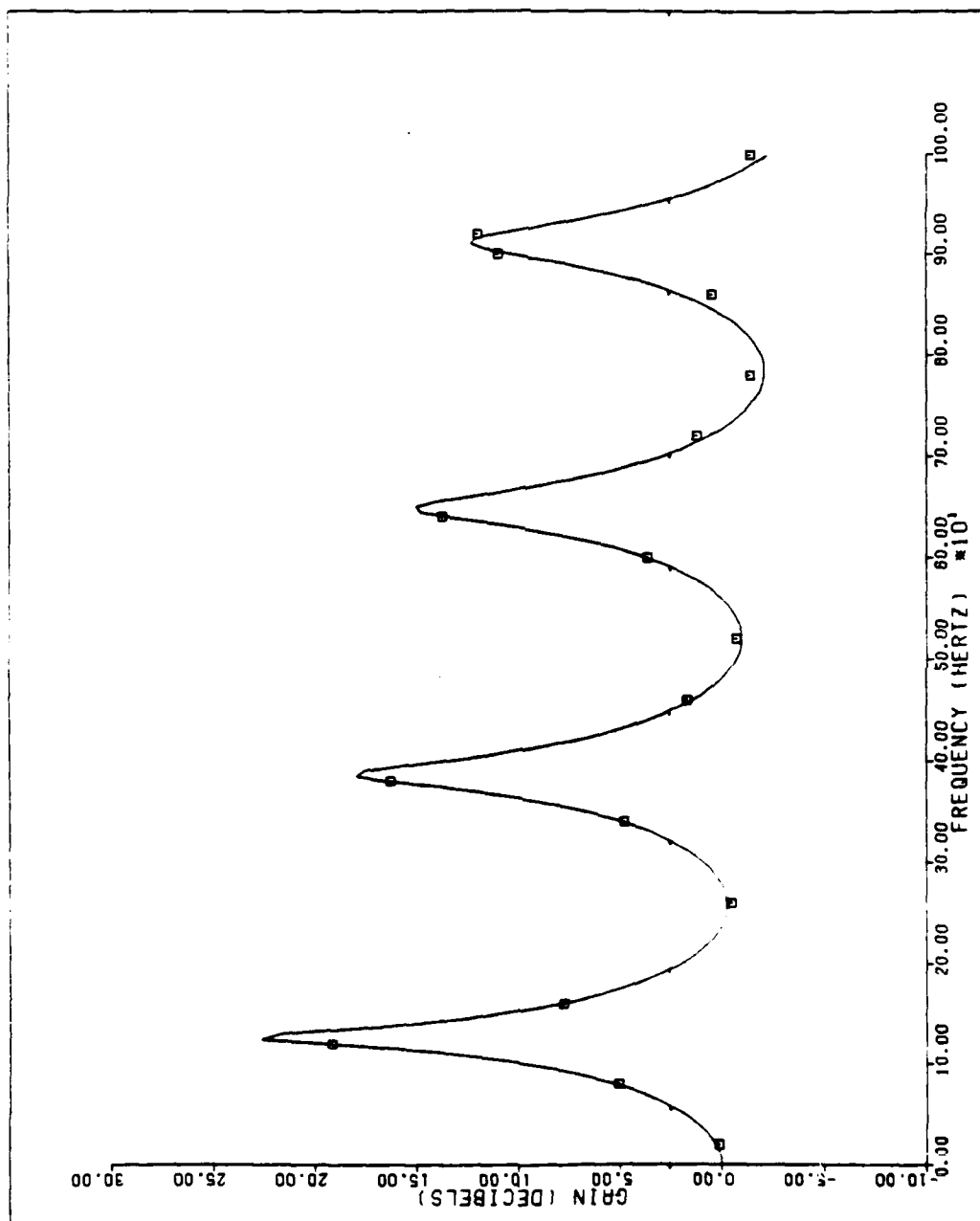
Fig. 29. Theoretical and Experimental Gain--Gase 31003b--Laminar Theory

81
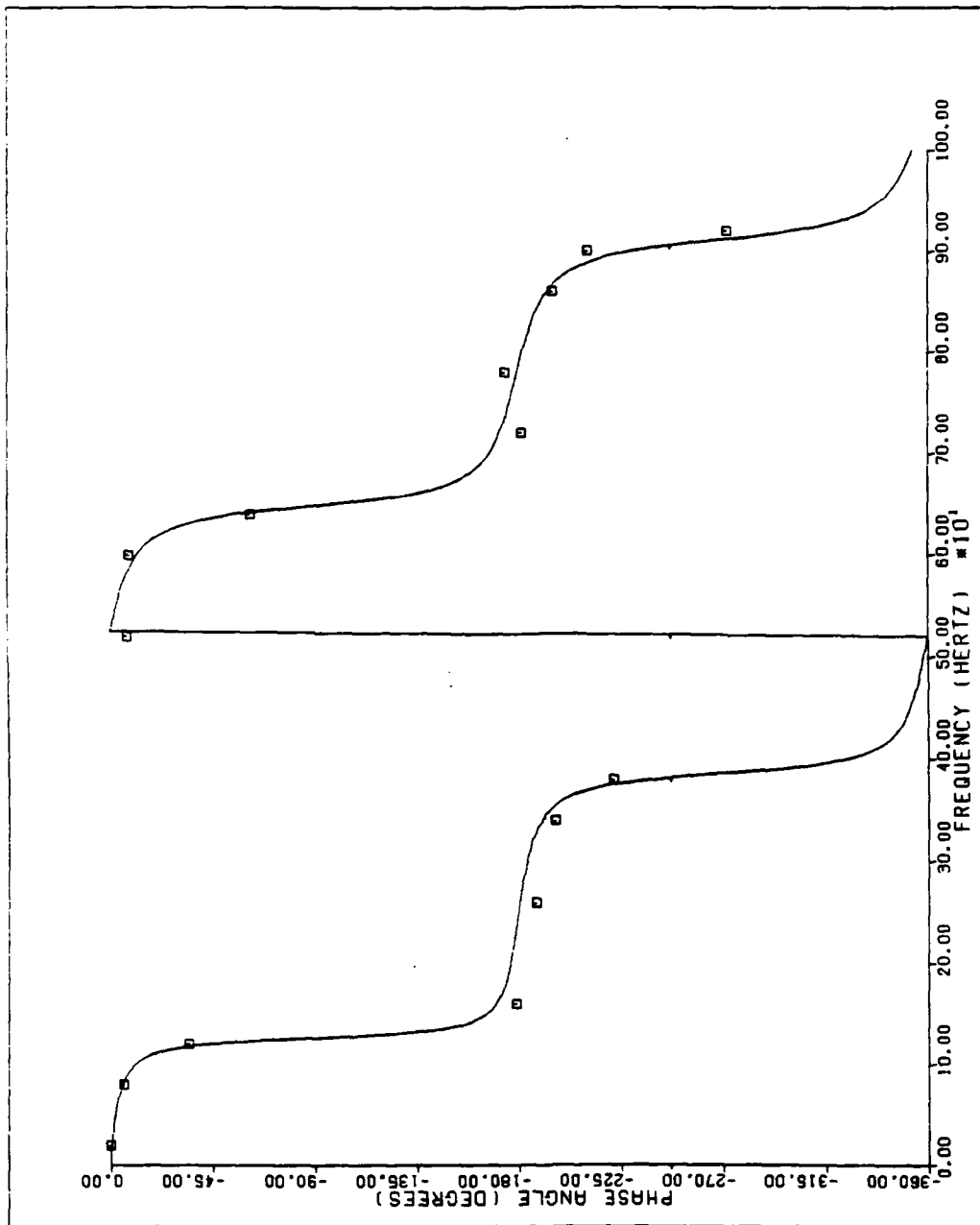
Fig. 30. Theoretical and Experimental Phase Shift--Case 31003b--Laminar Theory

82
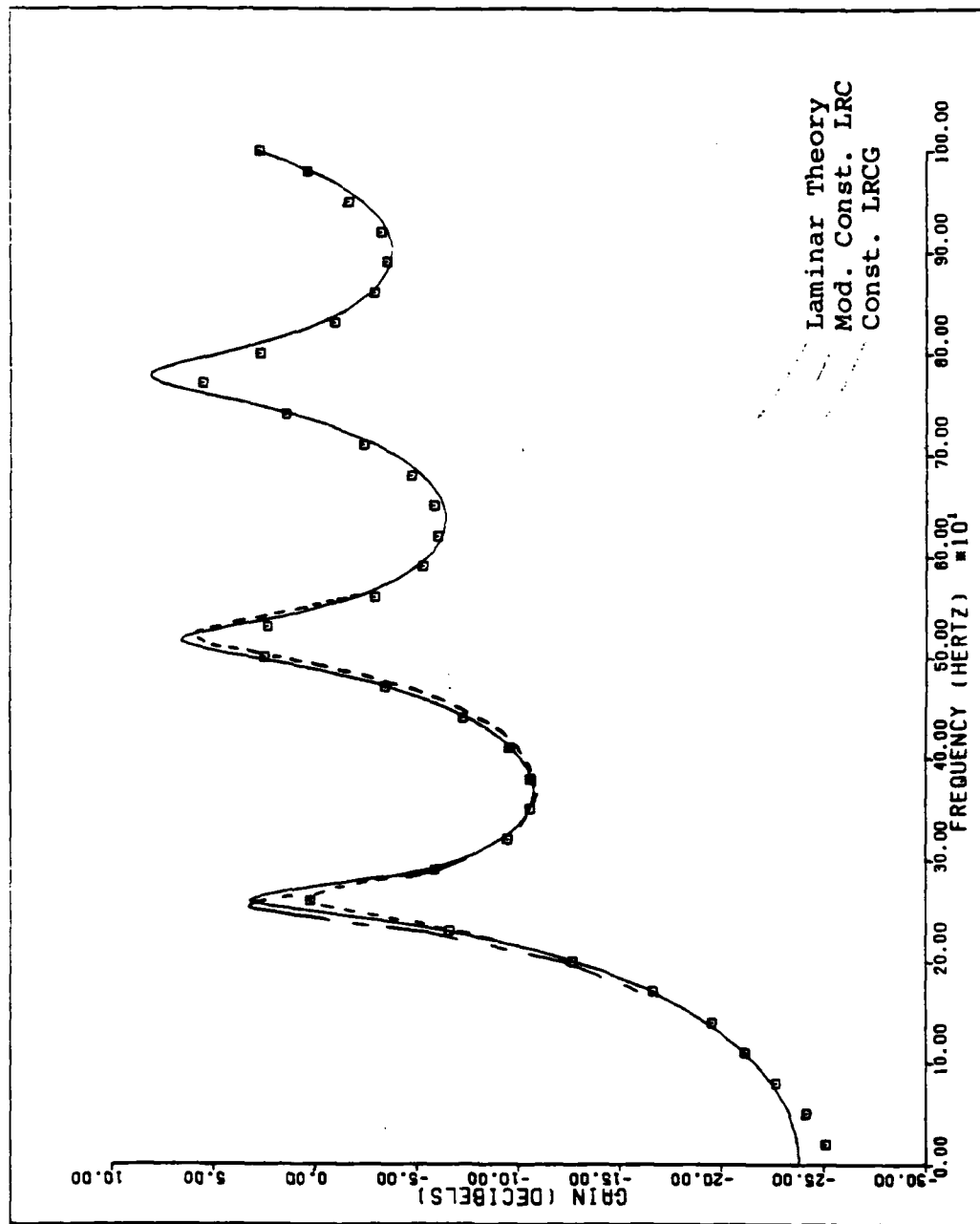
Fig. 31. Theoretical and Experimental Gain--Case 33079

83
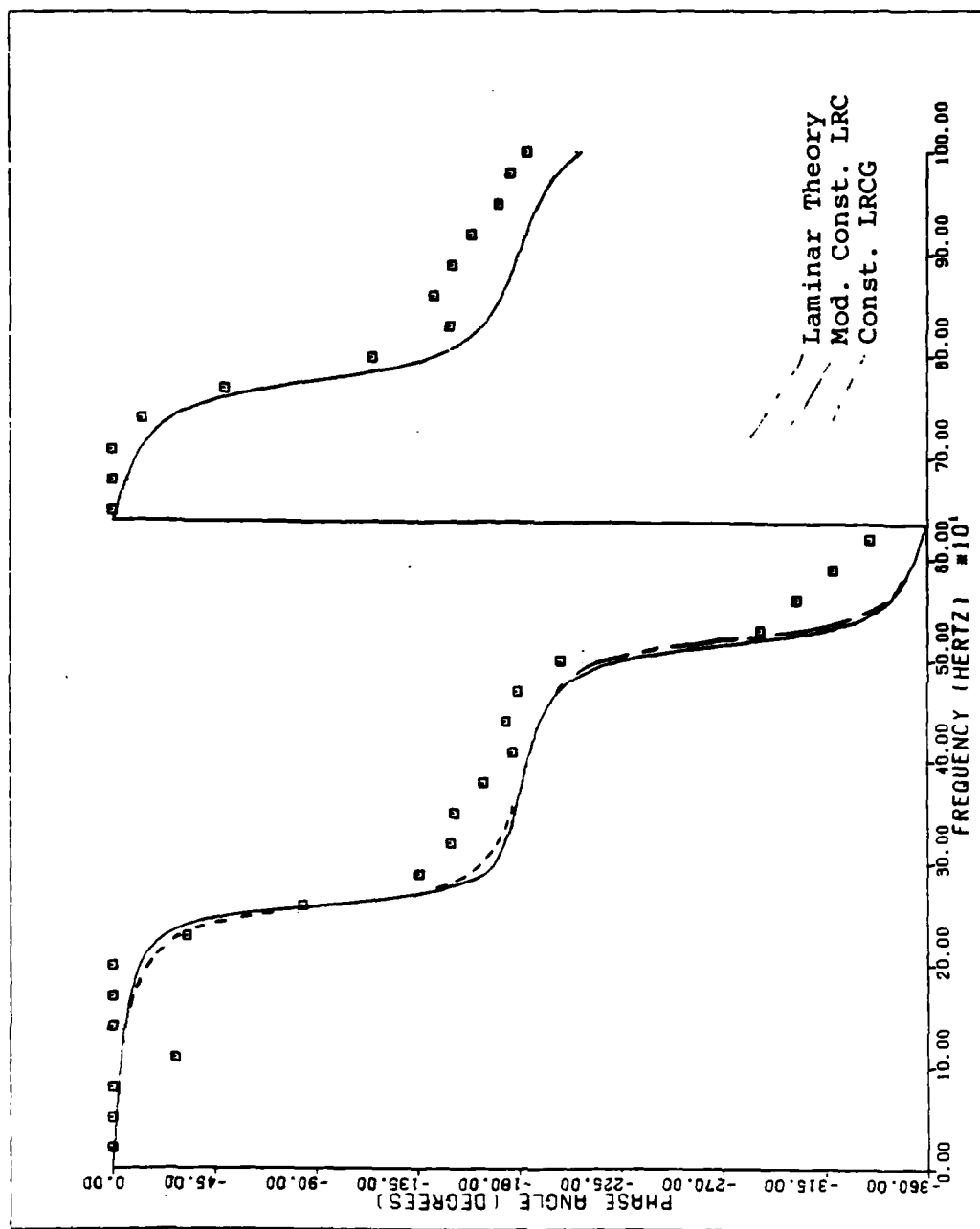
Fig. 32. Theoretical and Experimental Phase Shift--Case 33079

84
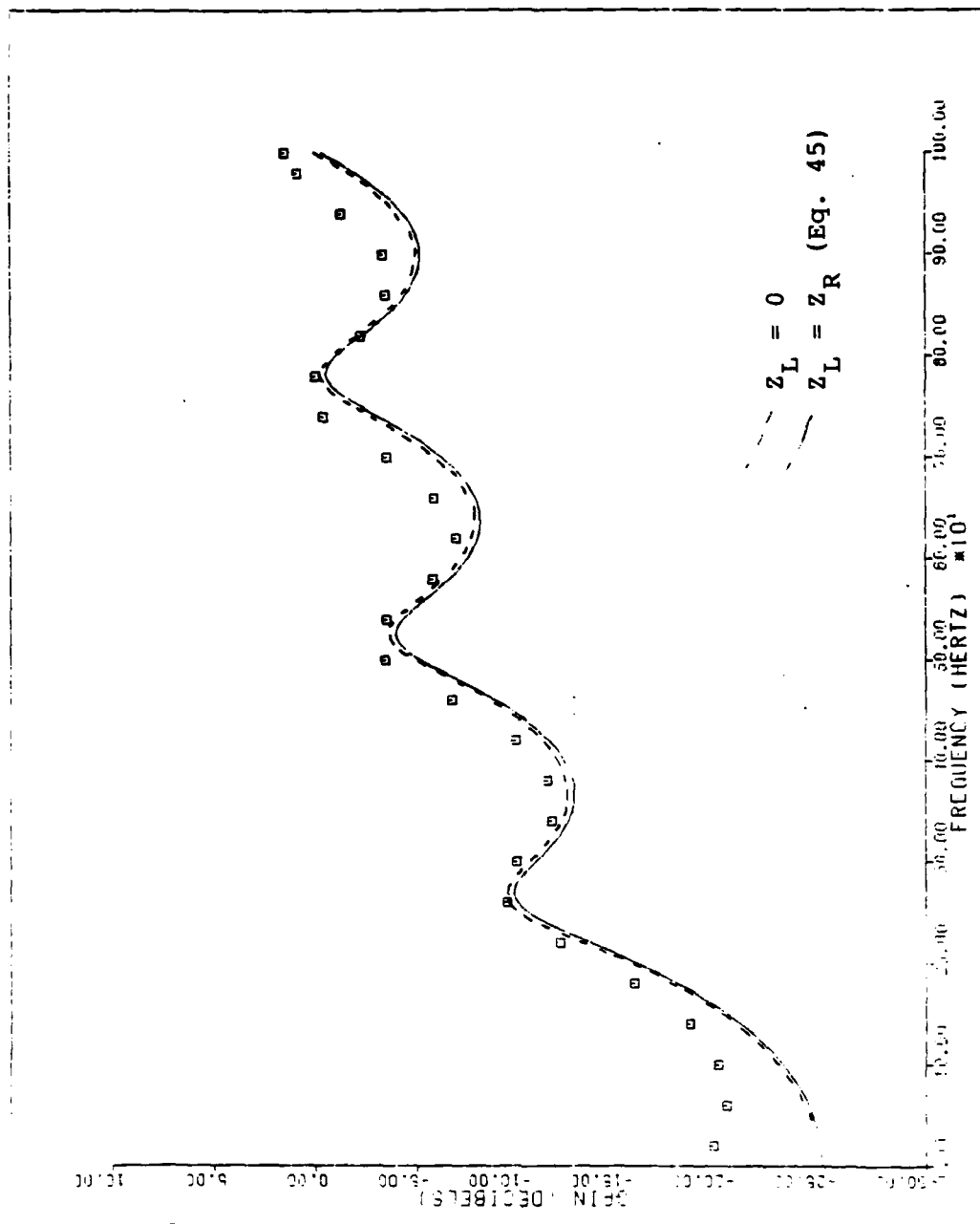
Fig. 33. Effect of Radiation Impedance on Theoretical Gain—Case 23090—Constant LRCG

85
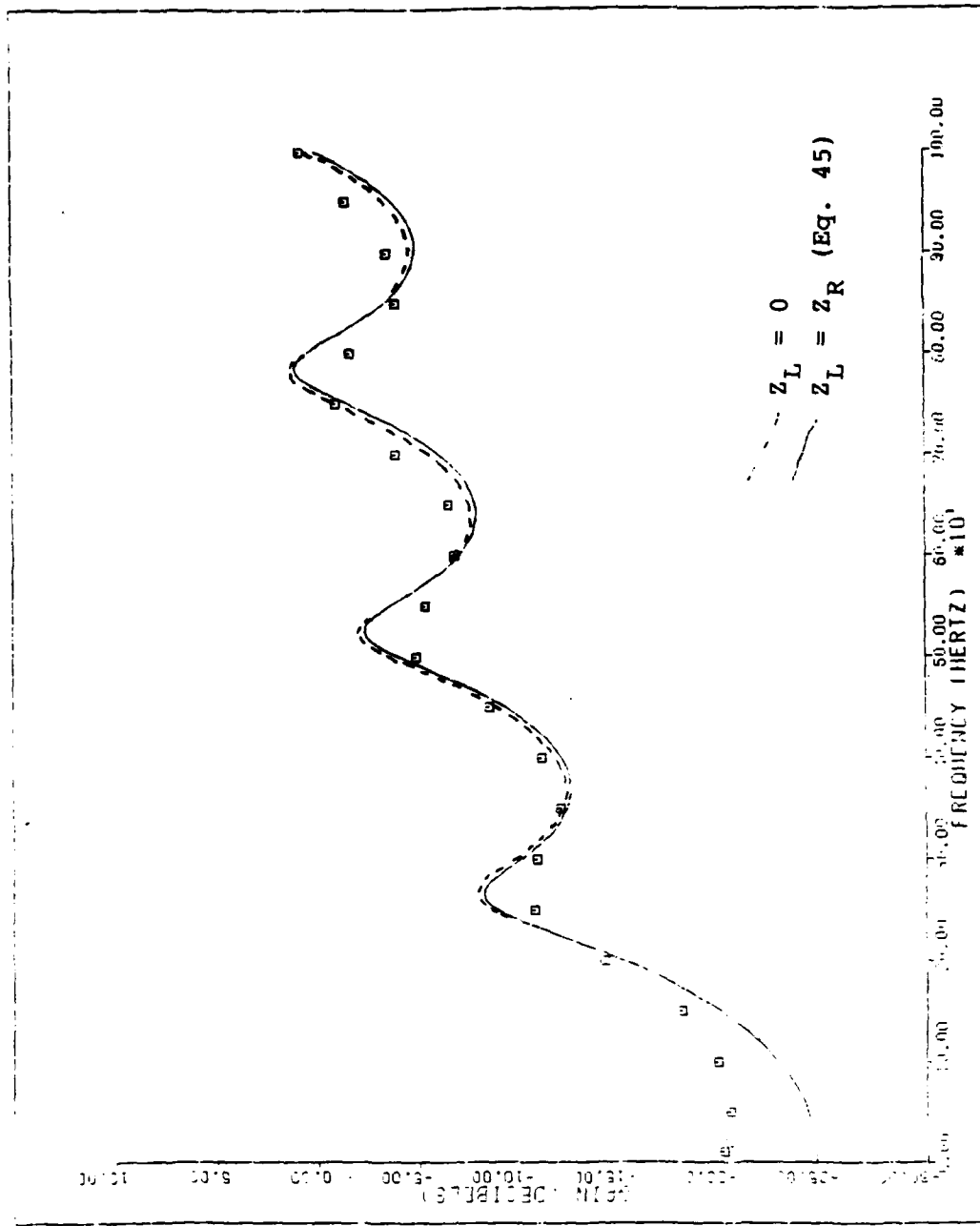
Fig. 34. Effect of Radiation Impedance on Theoretical Gain--Case 23107--Mod. Const. LRC
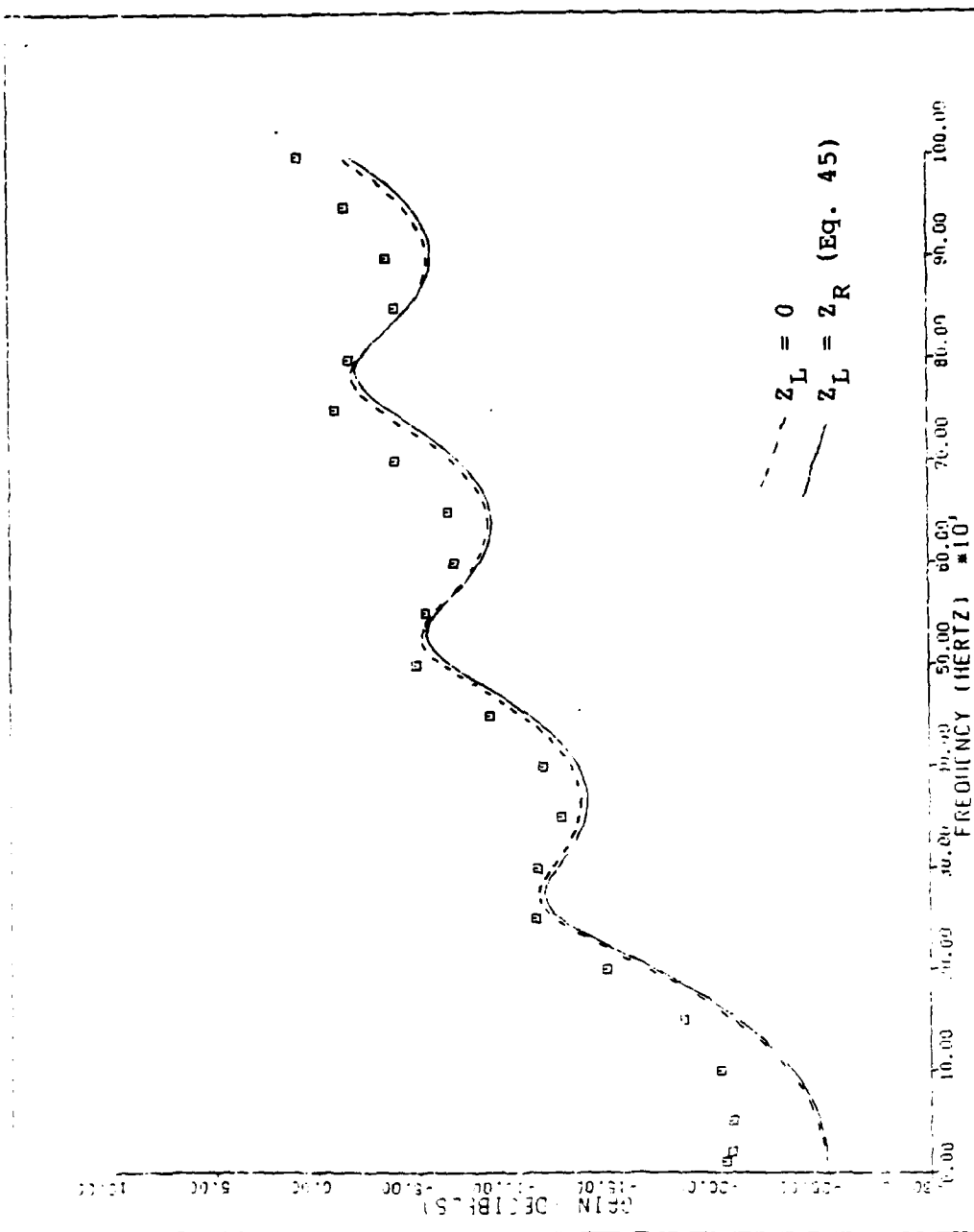
Fig. 35. Effect of Radiation Impedance on Theoretical Gain--Case 23107--Constant LRCG
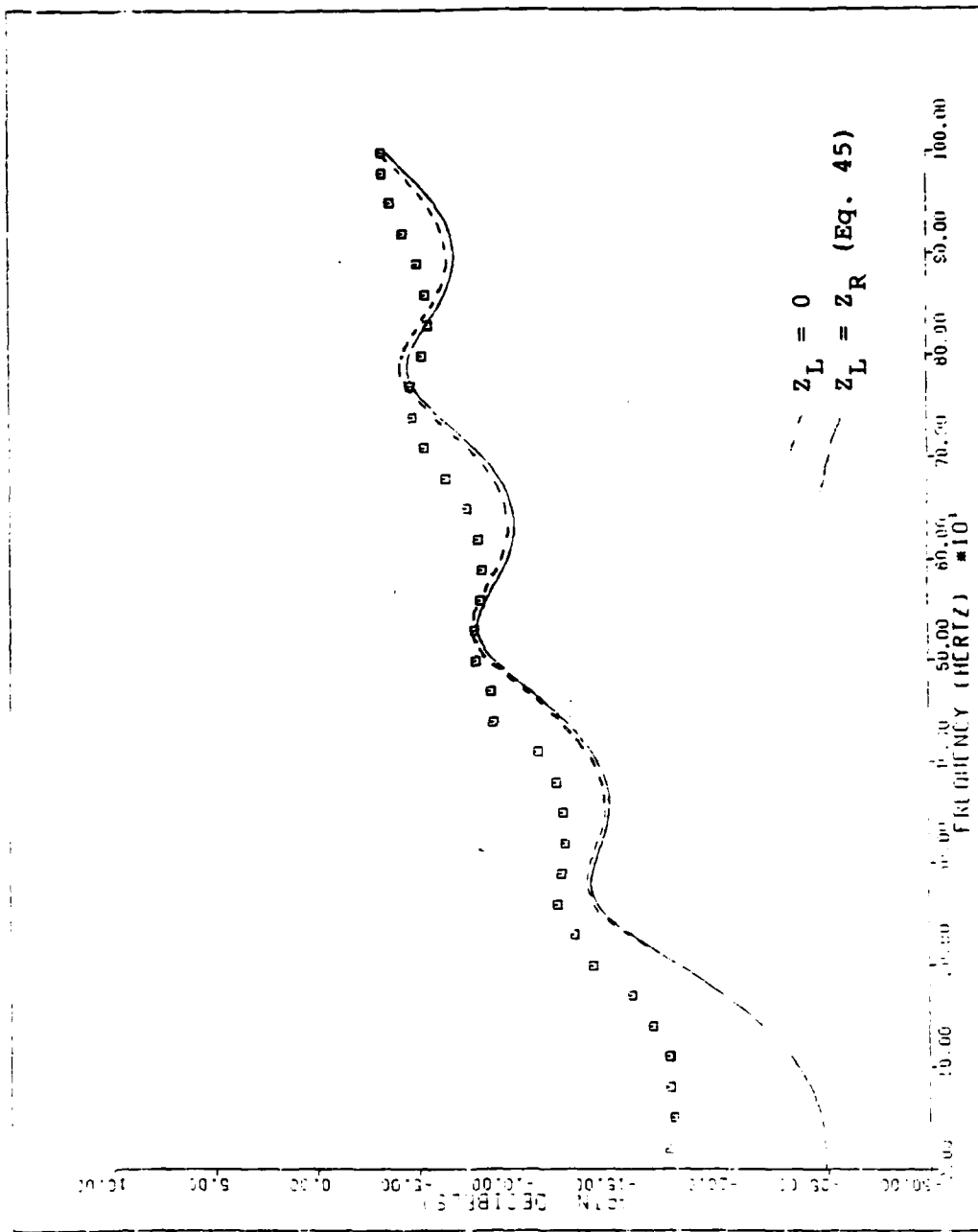
Fig. 36. Effect of Radiation Impedance on Theoretical Gain--Case 23165--Constant LRCG
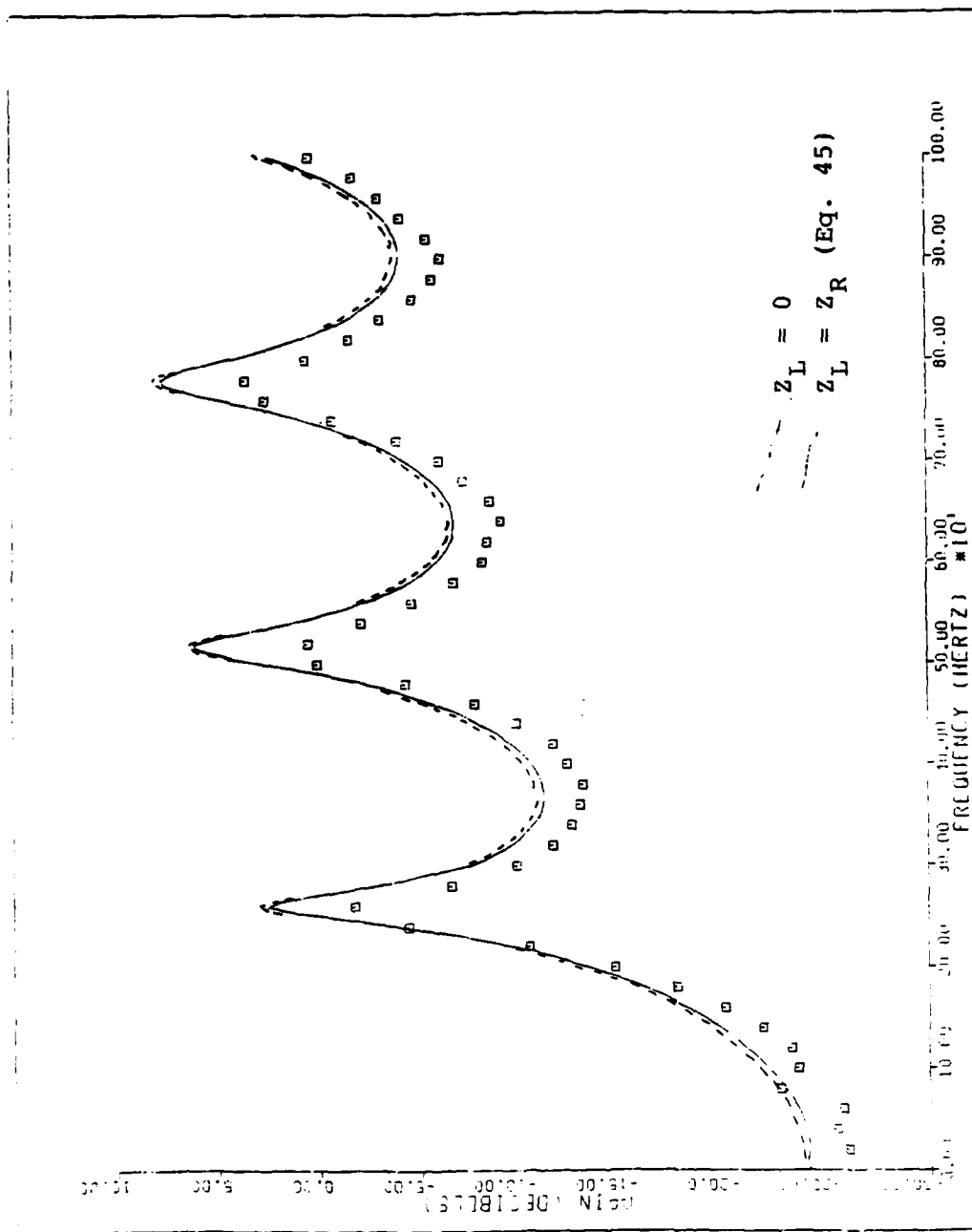
Fig. 37. Effect of Radiation Impedance on Theoretical Gain--Case 33052--Constant LRCG
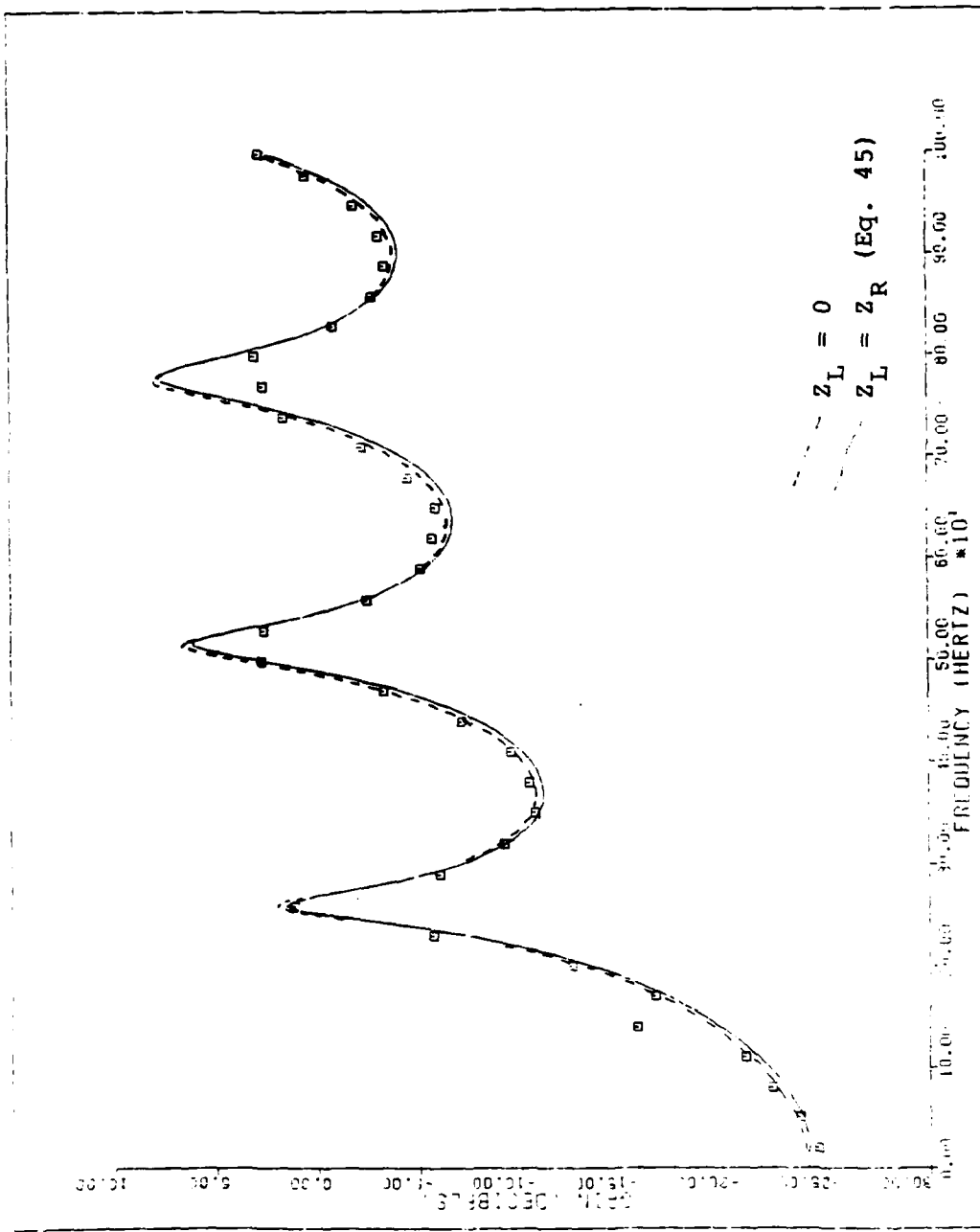
Fig. 38. Effect of Radiation Impedance on Theoretical Gain--Case 33060--Constant LRCG
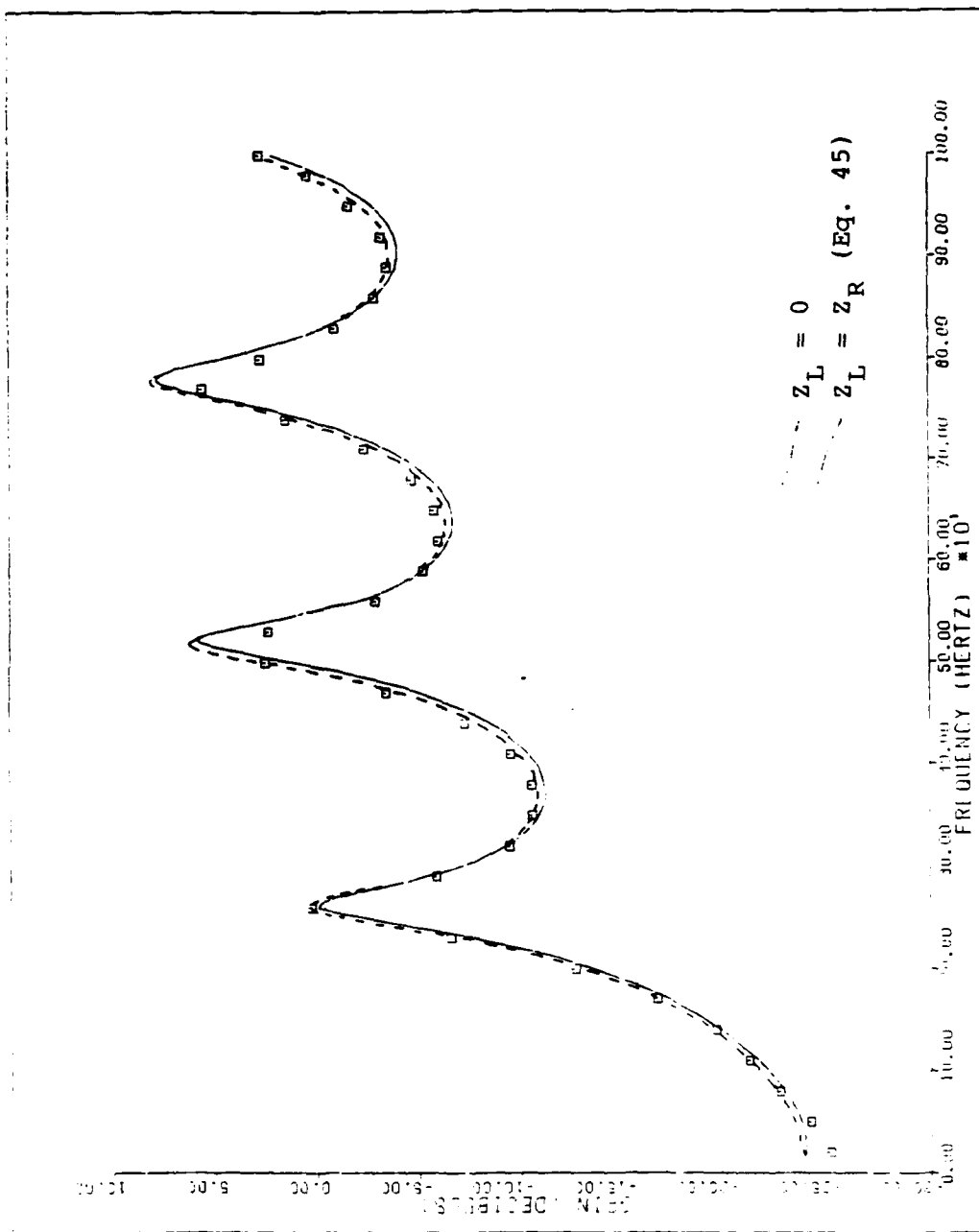
Fig. 39. Effect of Radiation Impedance on Theoretical Gain--Case 33079--Constant LRCG
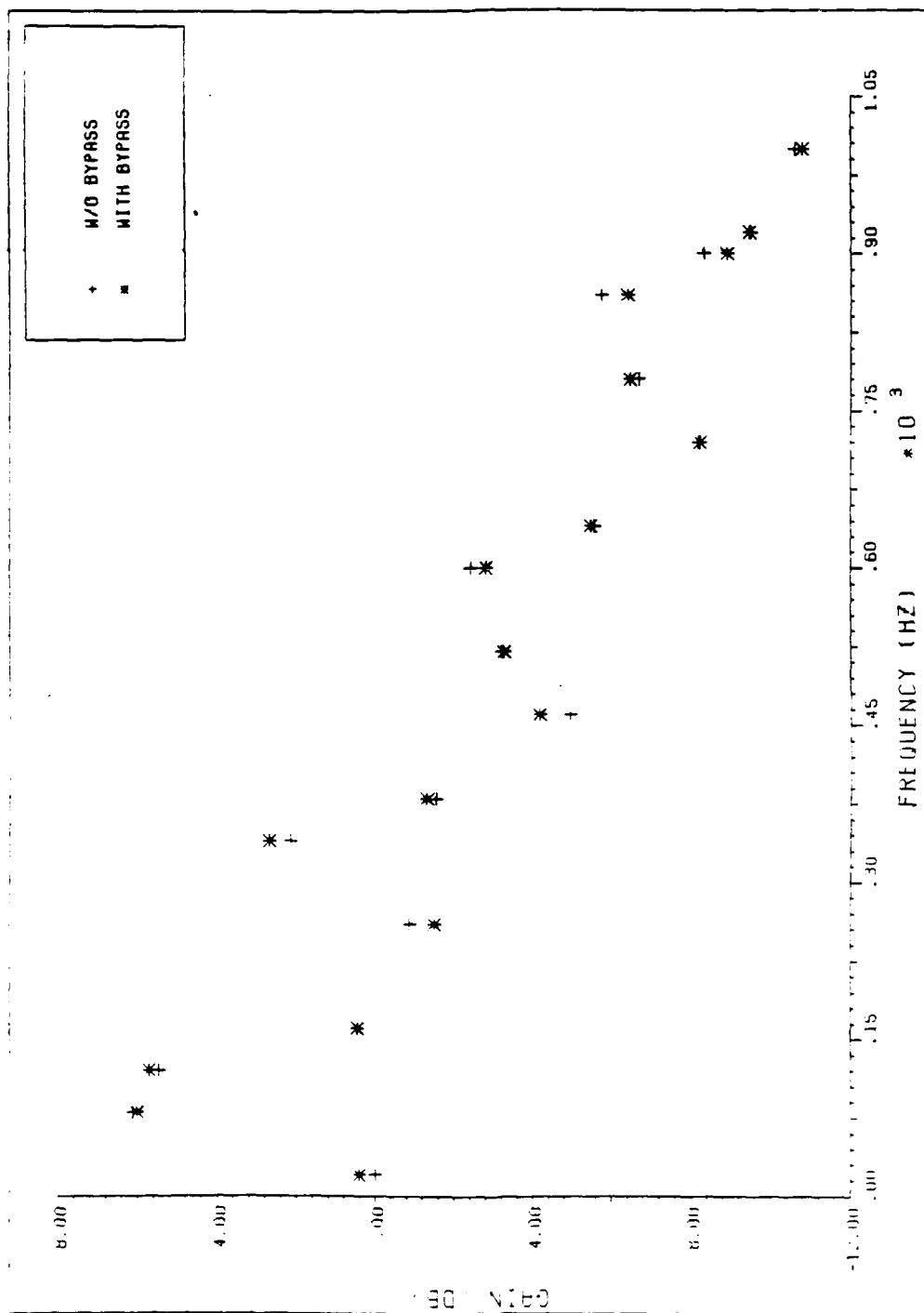
Fig. 40. Effect of Upstream Conditions on Experimental Gain--Case 11012

92
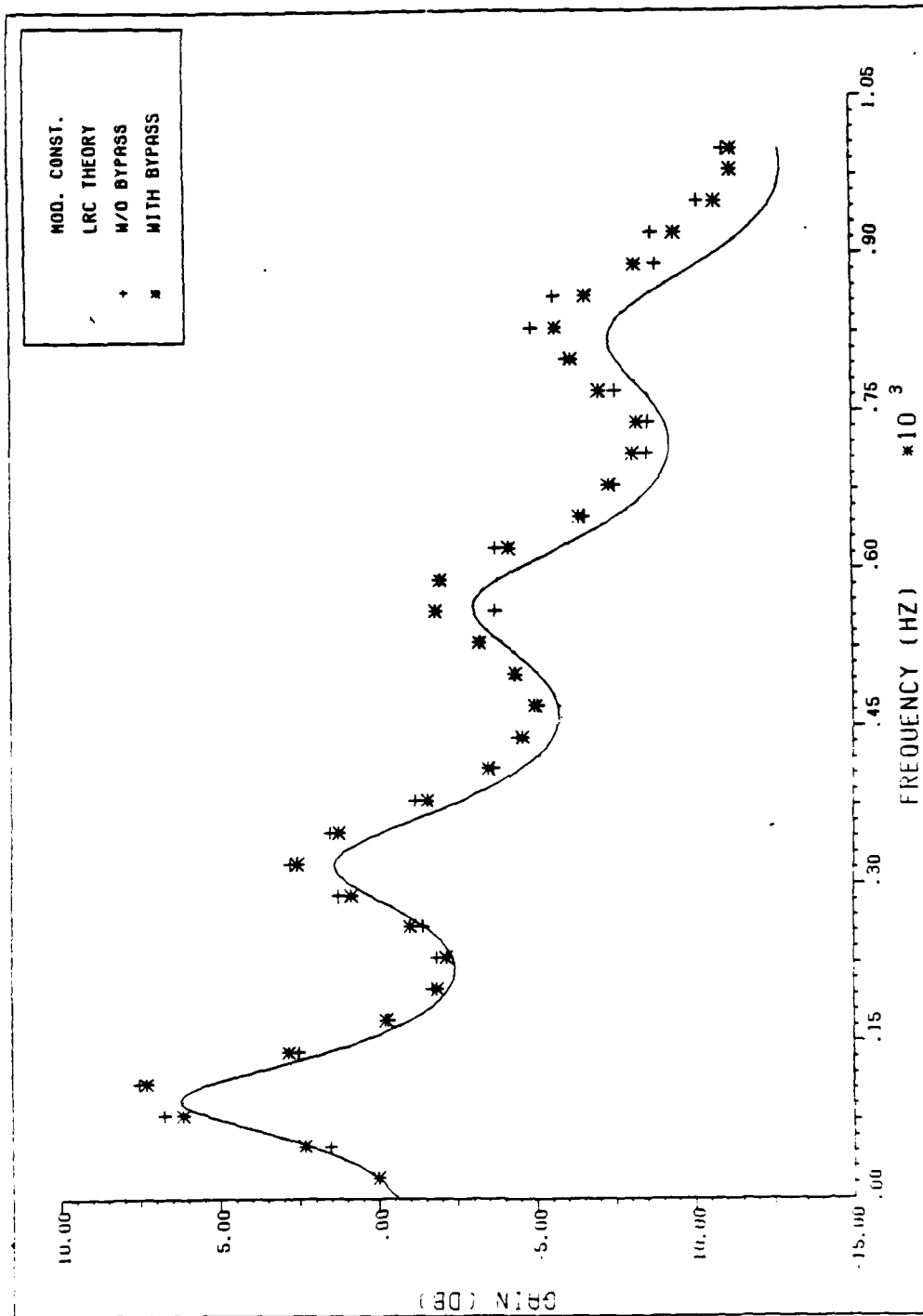
Fig. 41. Effect of Upstream Conditions on Experimental Gain--Case 11014n
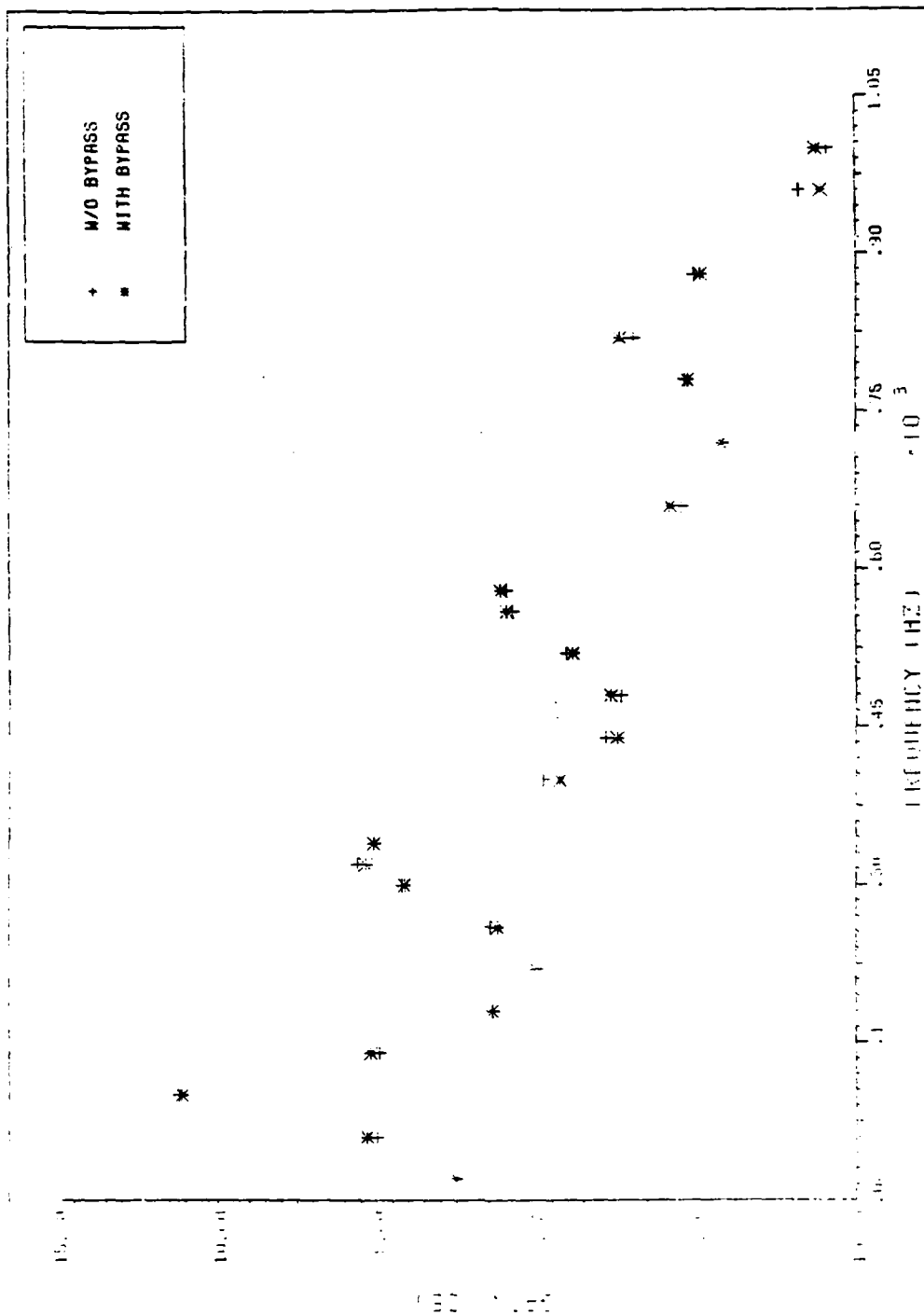
Fig. 42. Effect of Upstream Conditions on Experimental Gain--Case 11020
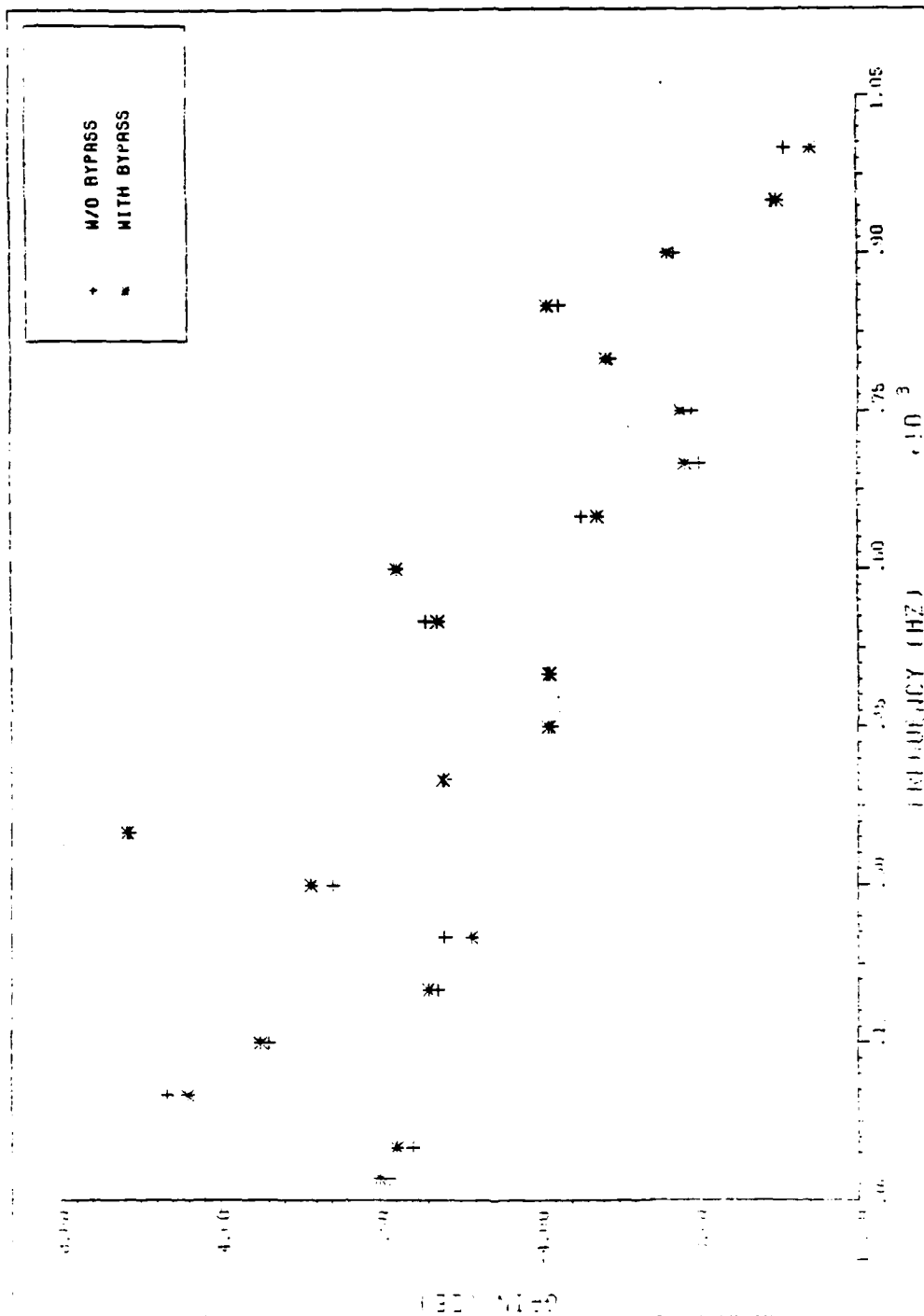
Fig. 43. Effect of Upstream Conditions on Experimental Gain--Case 11033
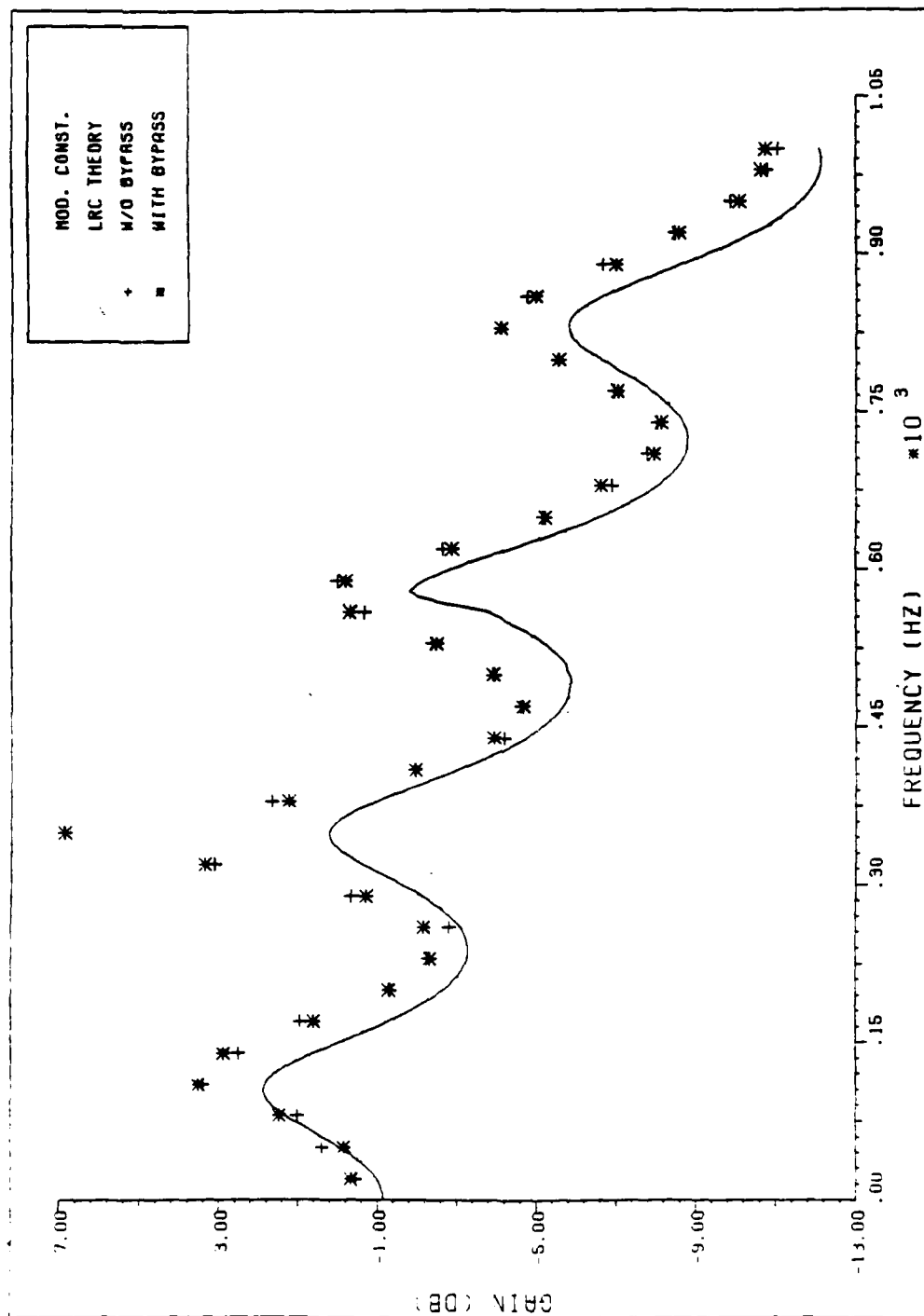
Fig. 44. Effect of Upstream Conditions on Experimental Gain—Case 12034n
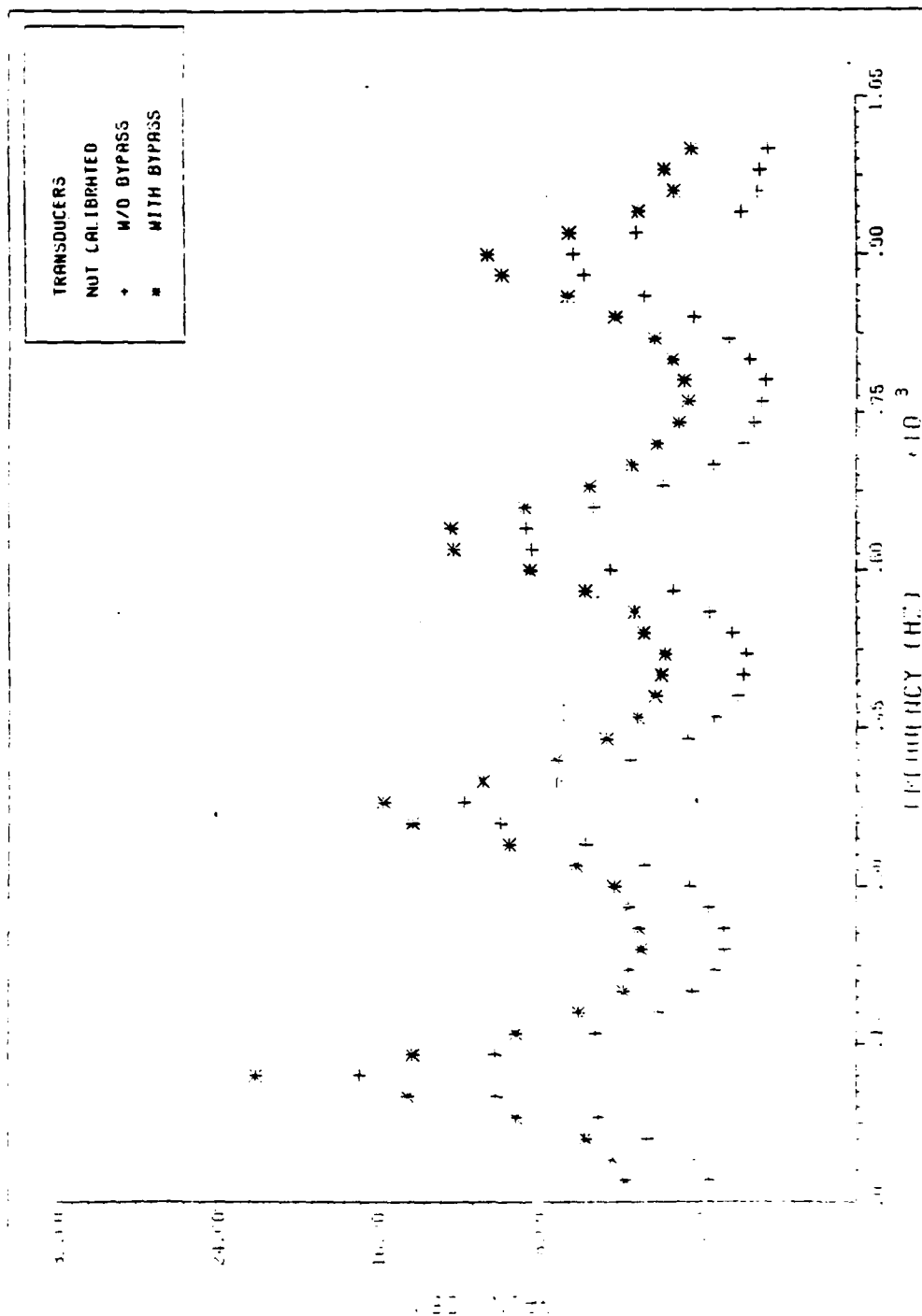
Fig. 45. Effect of Upstream Conditions on Experimental Gain--Case 21004

97
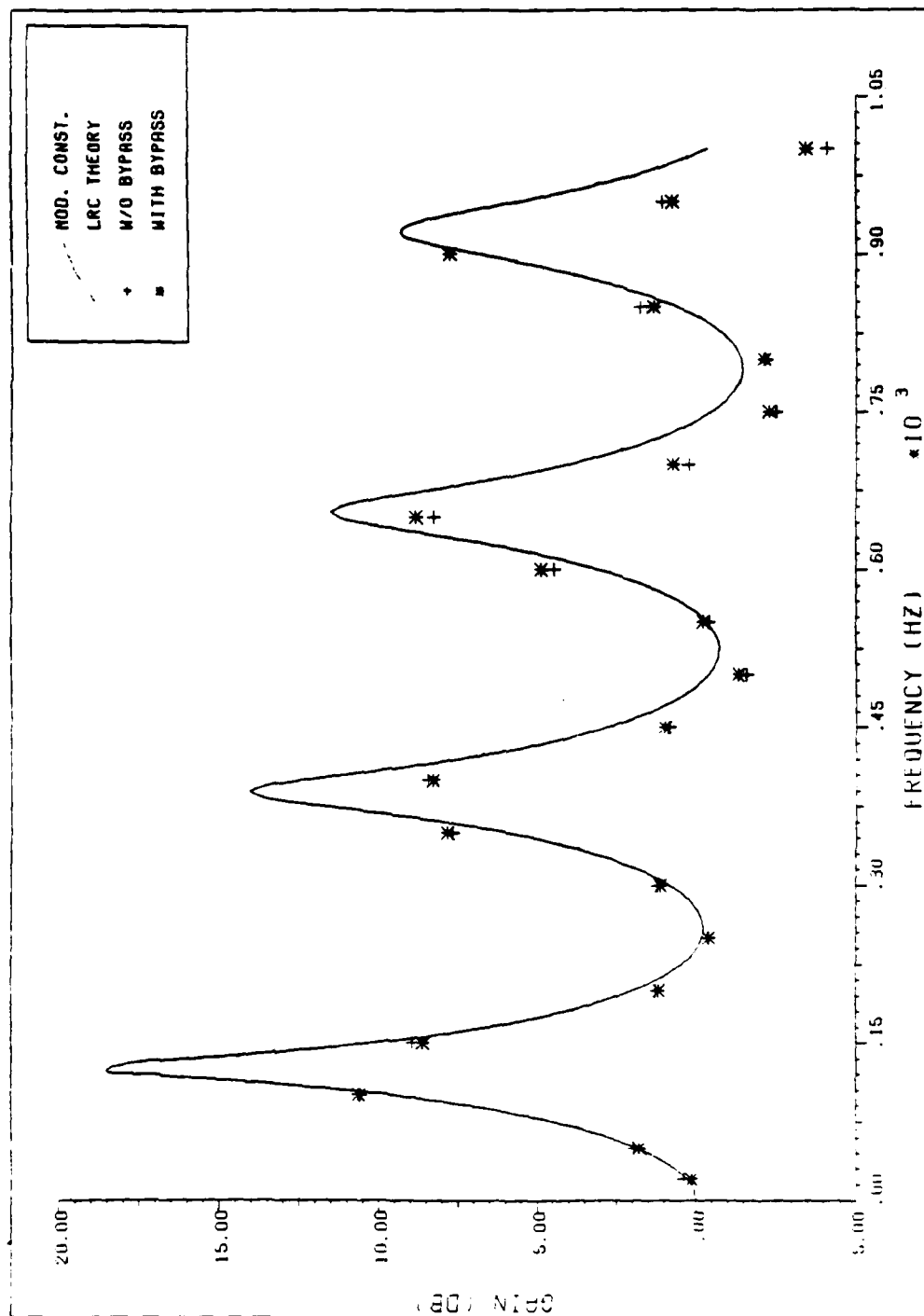
Fig. 46. Effect of Upstream Conditions on Experimental Gain--Case 21007
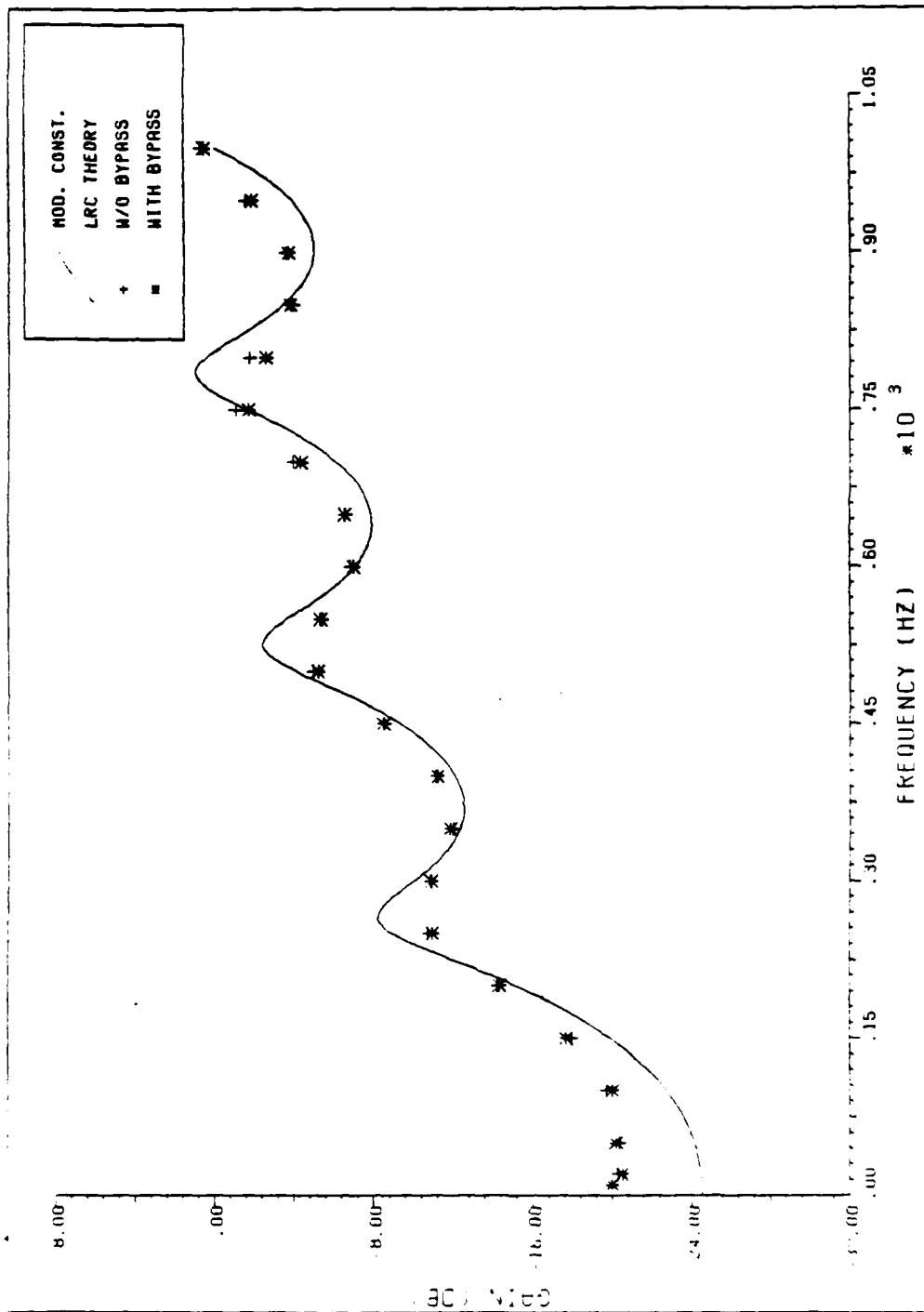
Fig. 47. Effect of Upstream Conditions on Experimental Gain--Case 23107

99
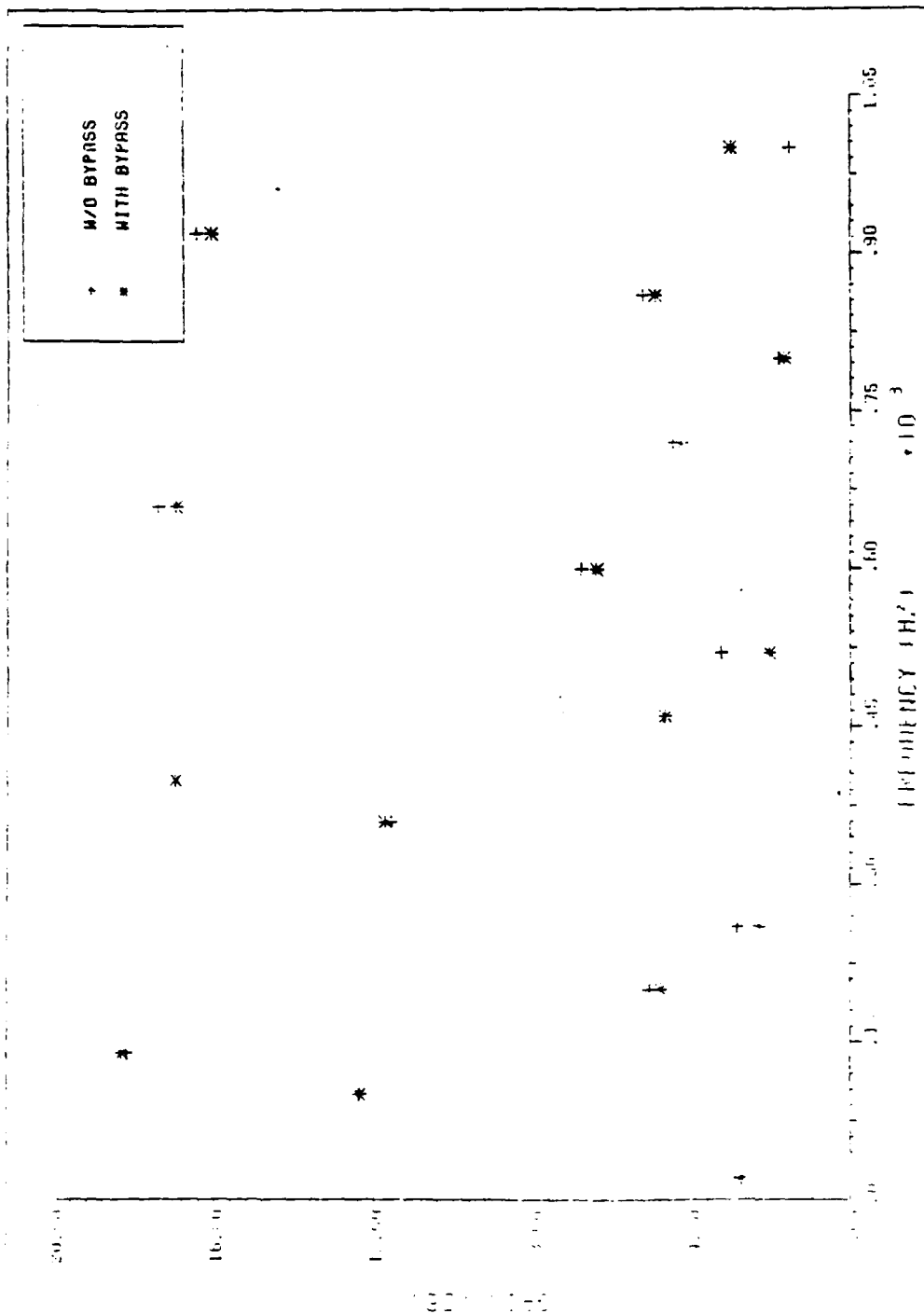
Fig. 48. Effect of Upstream Conditions on Experimental Gain--Case 31009
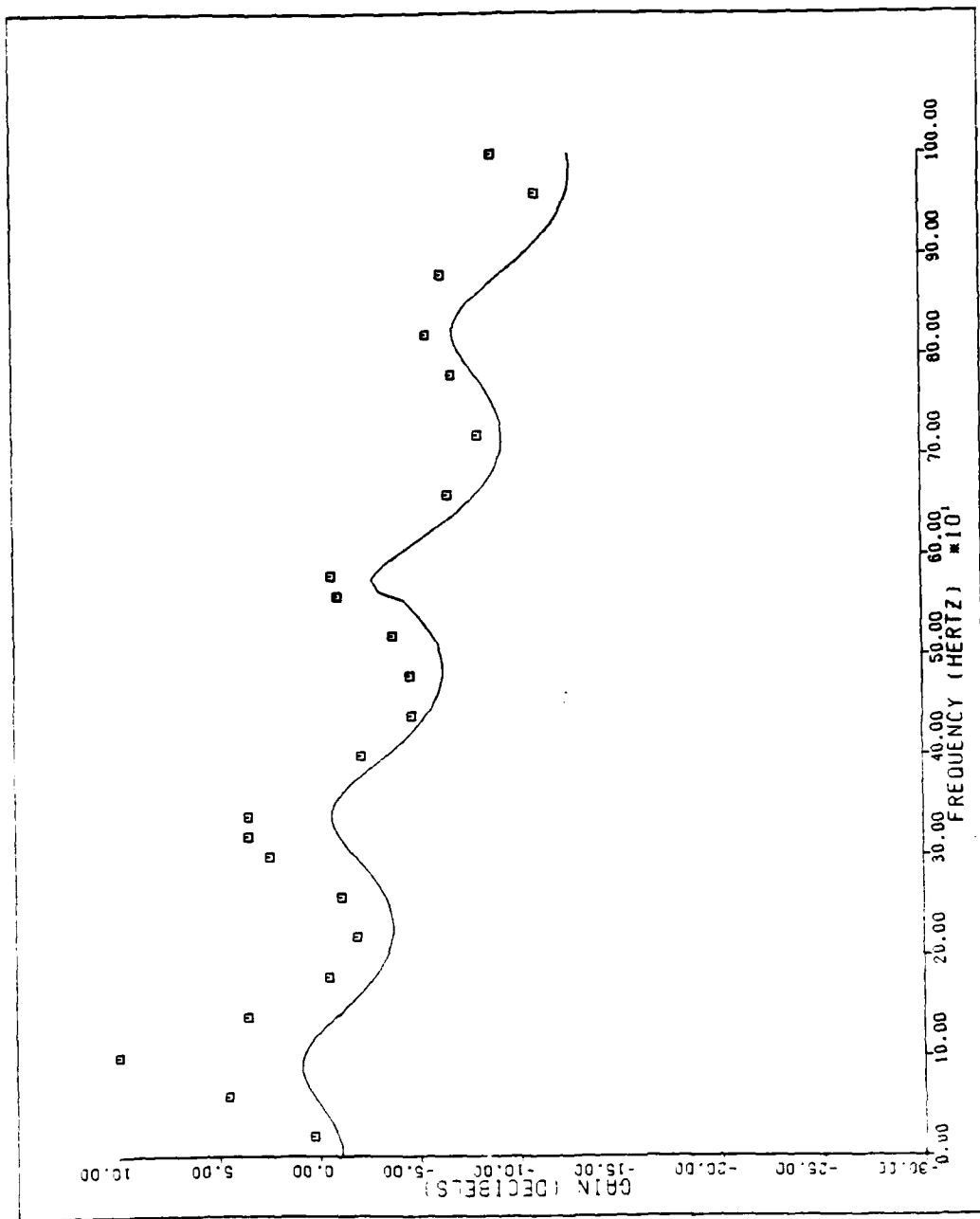
Fig. 49. Theoretical and Experimental Gain--Case 11030n--Mod. Const. LRC

101
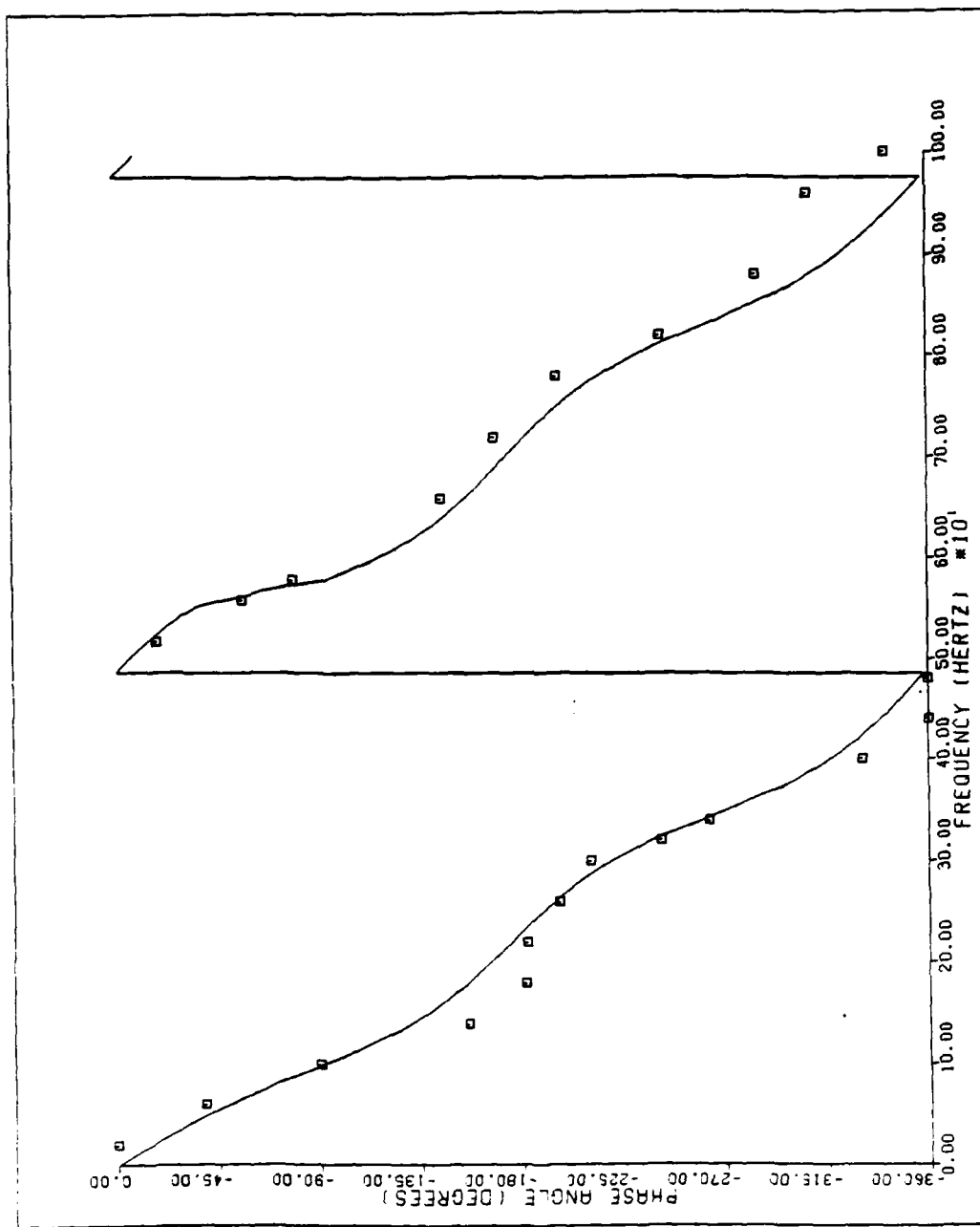
Fig. 50. Theoretical and Experimental Phase Shift--Case 11030n--Mod. Const. LRC
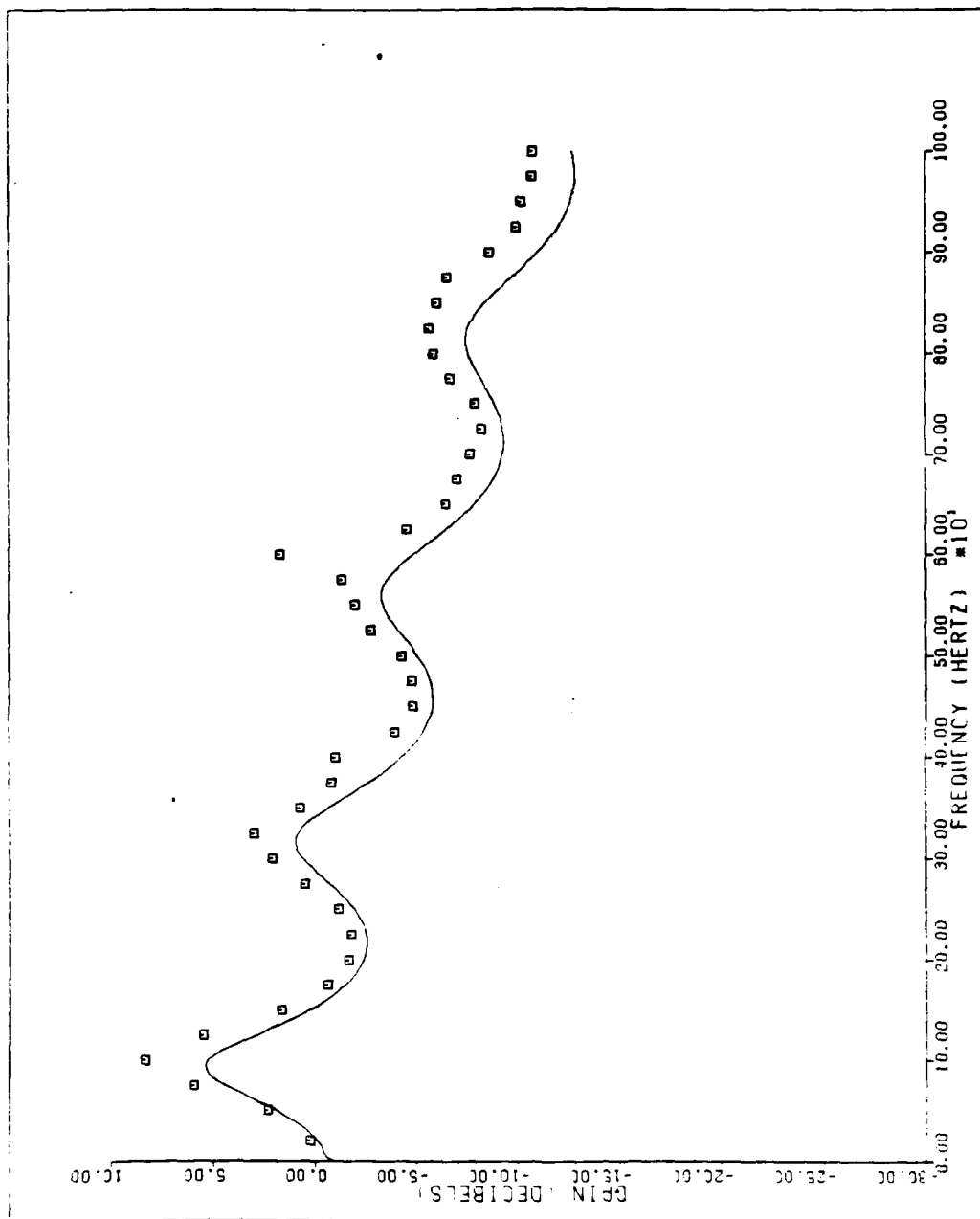
Fig. 51. Theoretical and Experimental Gain--Case 12018n--Laminar Theory

103
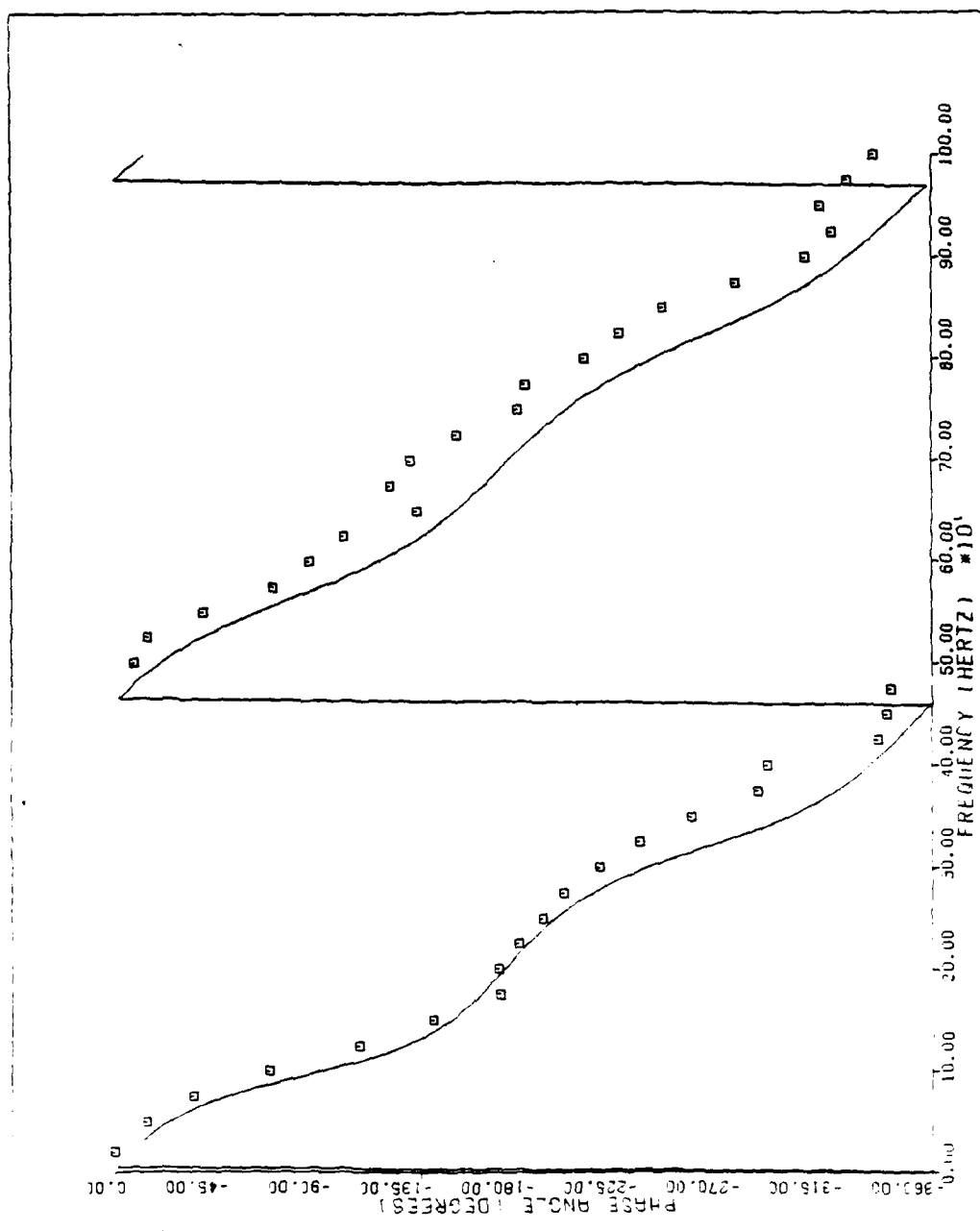
Fig. 52. Theoretical and Experimental Phase Shift--Case 12018n--Laminar Theory
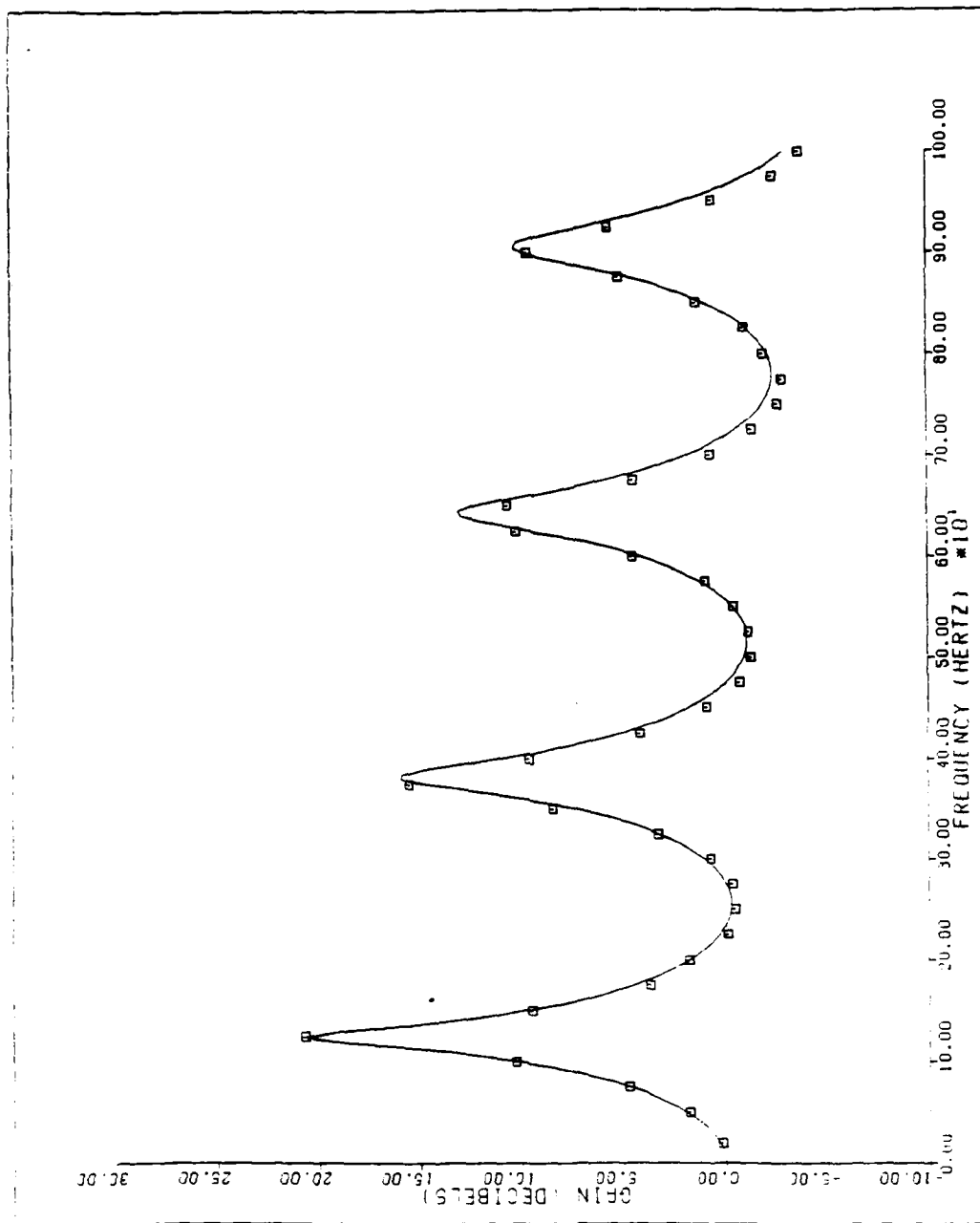
Fig. 53. Theoretical and Experimental Gain--Case 21015n--Laminar Theory
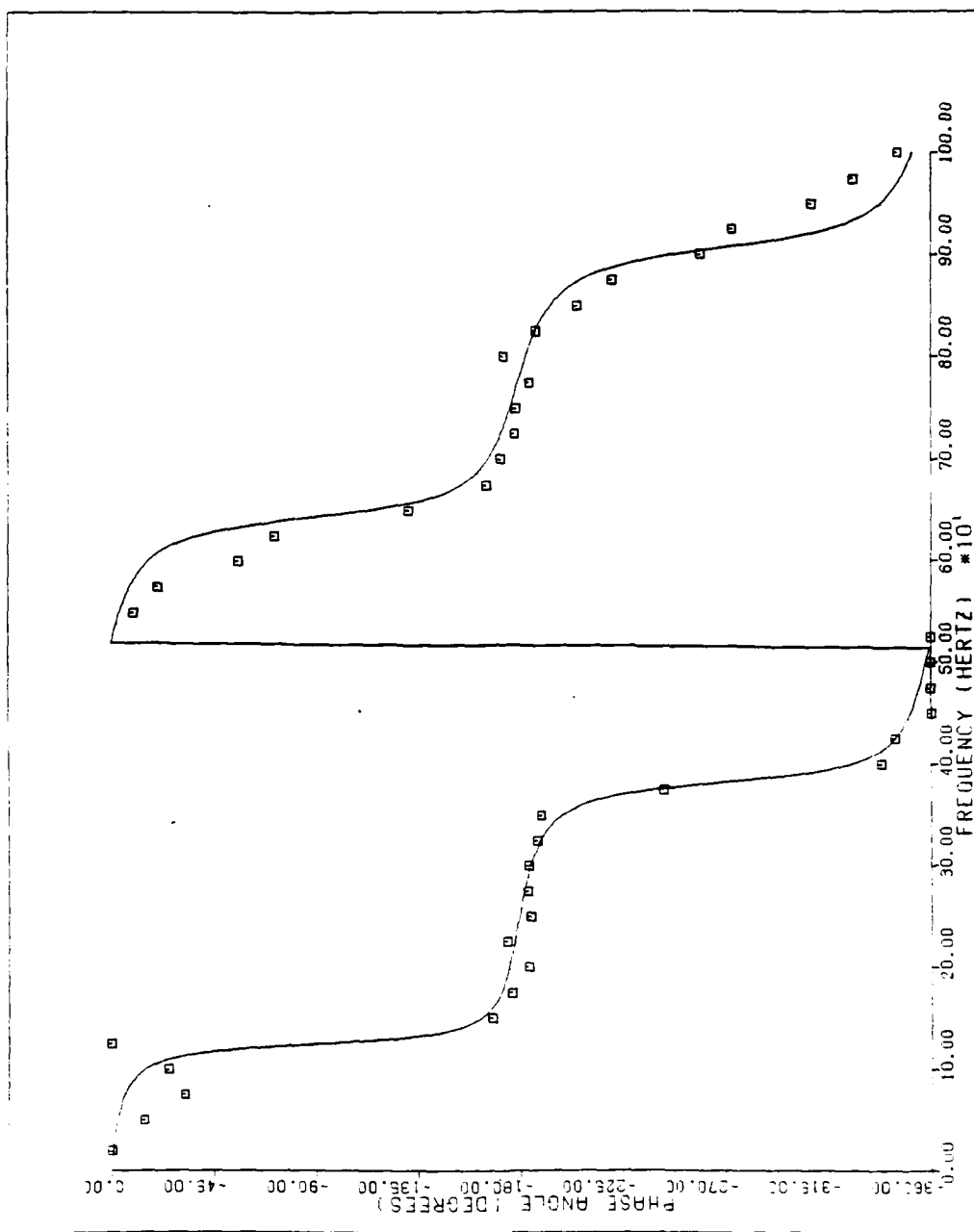
Fig. 54. Theoretical and Experimental Phase Shift—Case 21015n—Laminar Theory

106
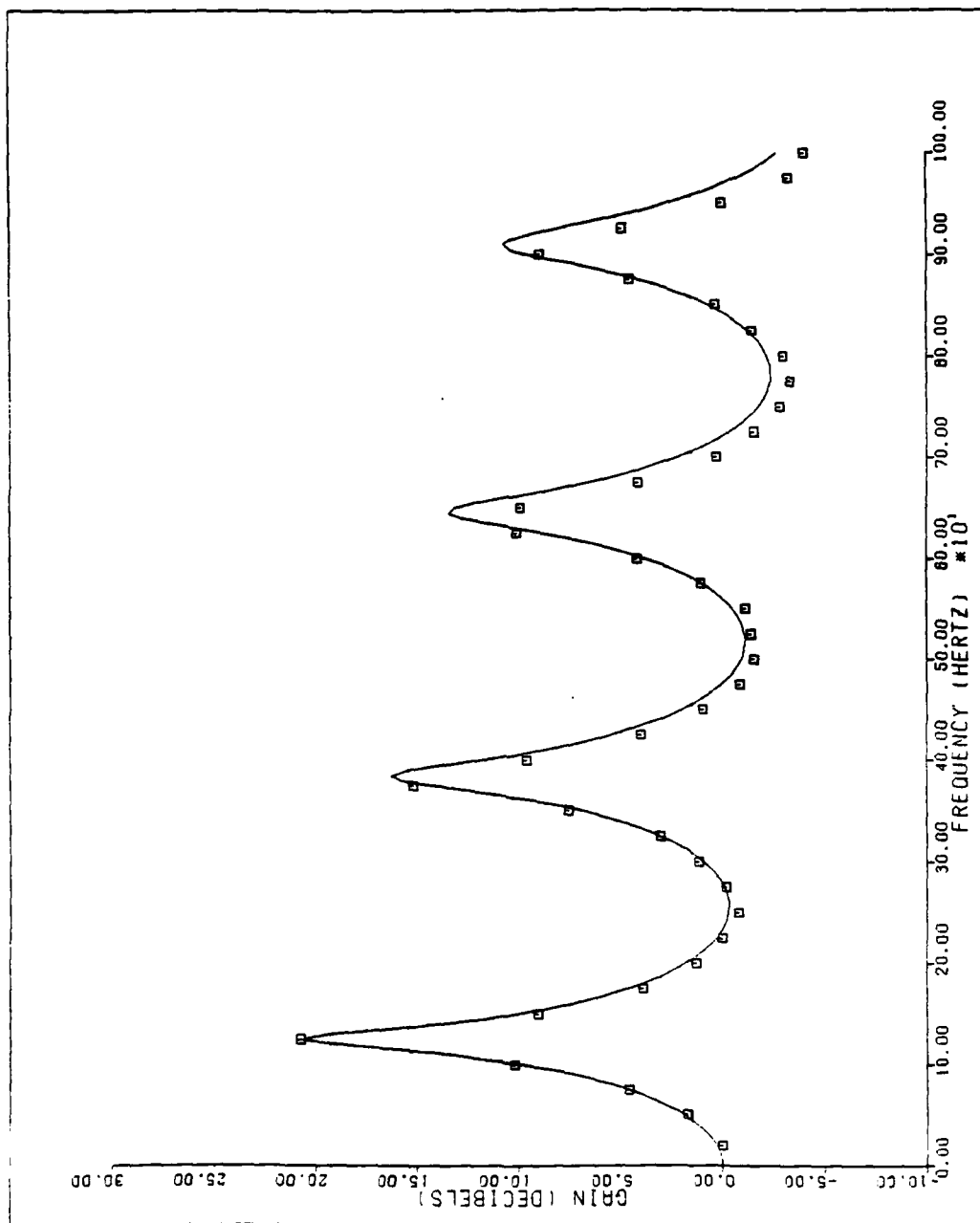
Fig. 55. Theoretical and Experimental Gain--Case 22020n--Laminar Theory

107
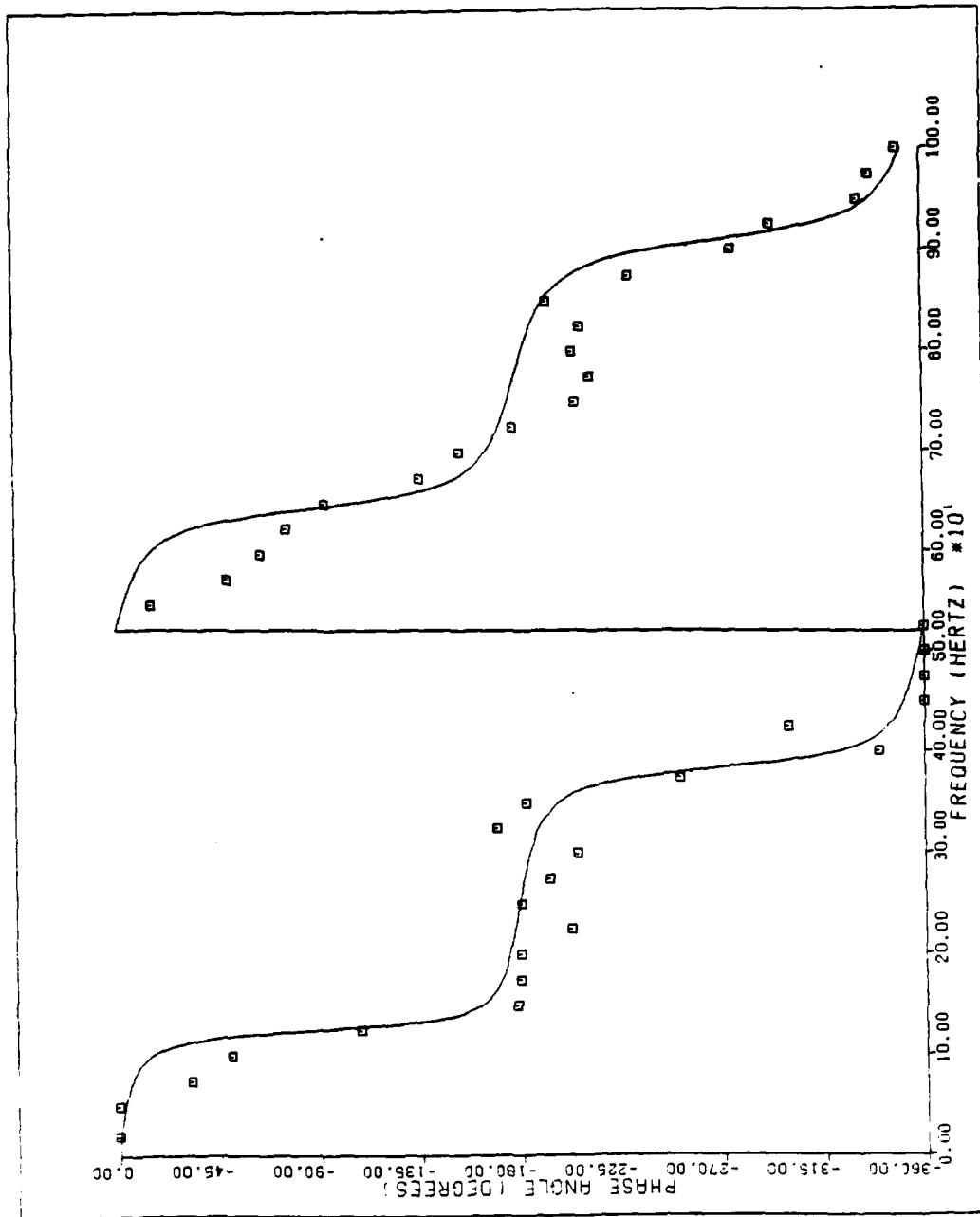
Fig. 56. Theoretical and Experimental Phase Shift--Case 22020n--Laminar Theory
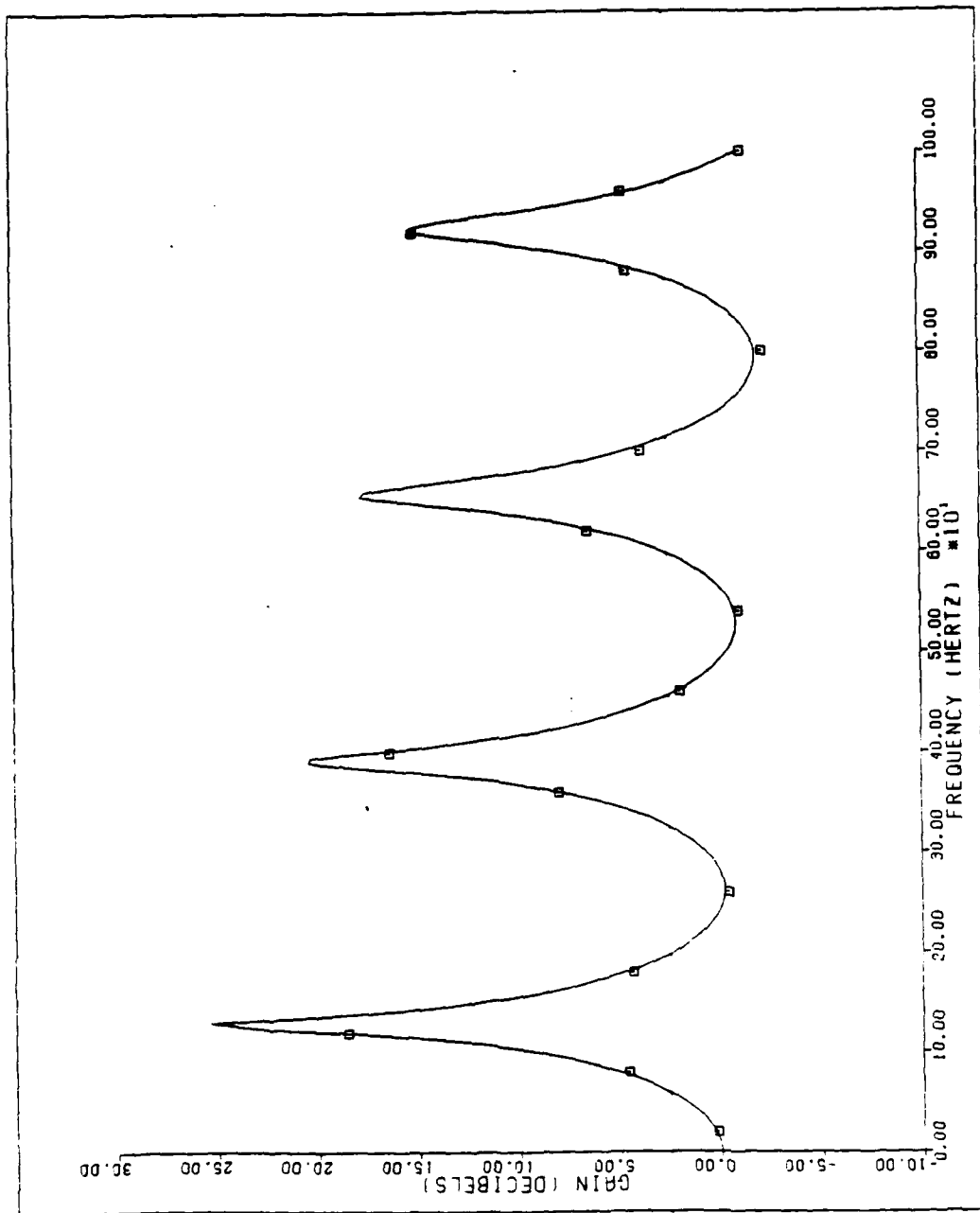
Fig. 57. Theoretical and Experimental Gain--Case 31009n--Laminar Theory
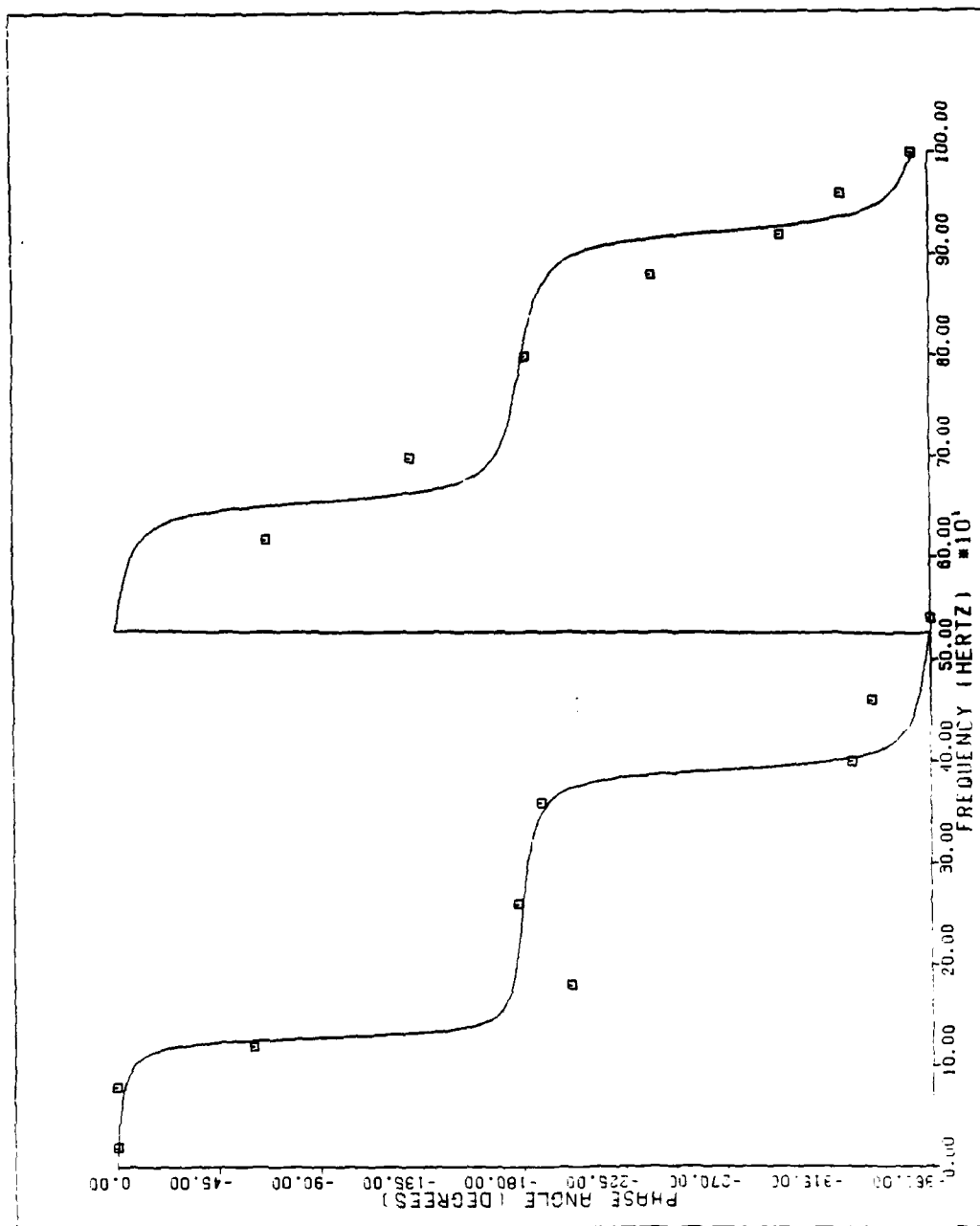
Fig. 58. Theoretical and Experimental Phase Shift--Case 31009n--Laminar Theory

110
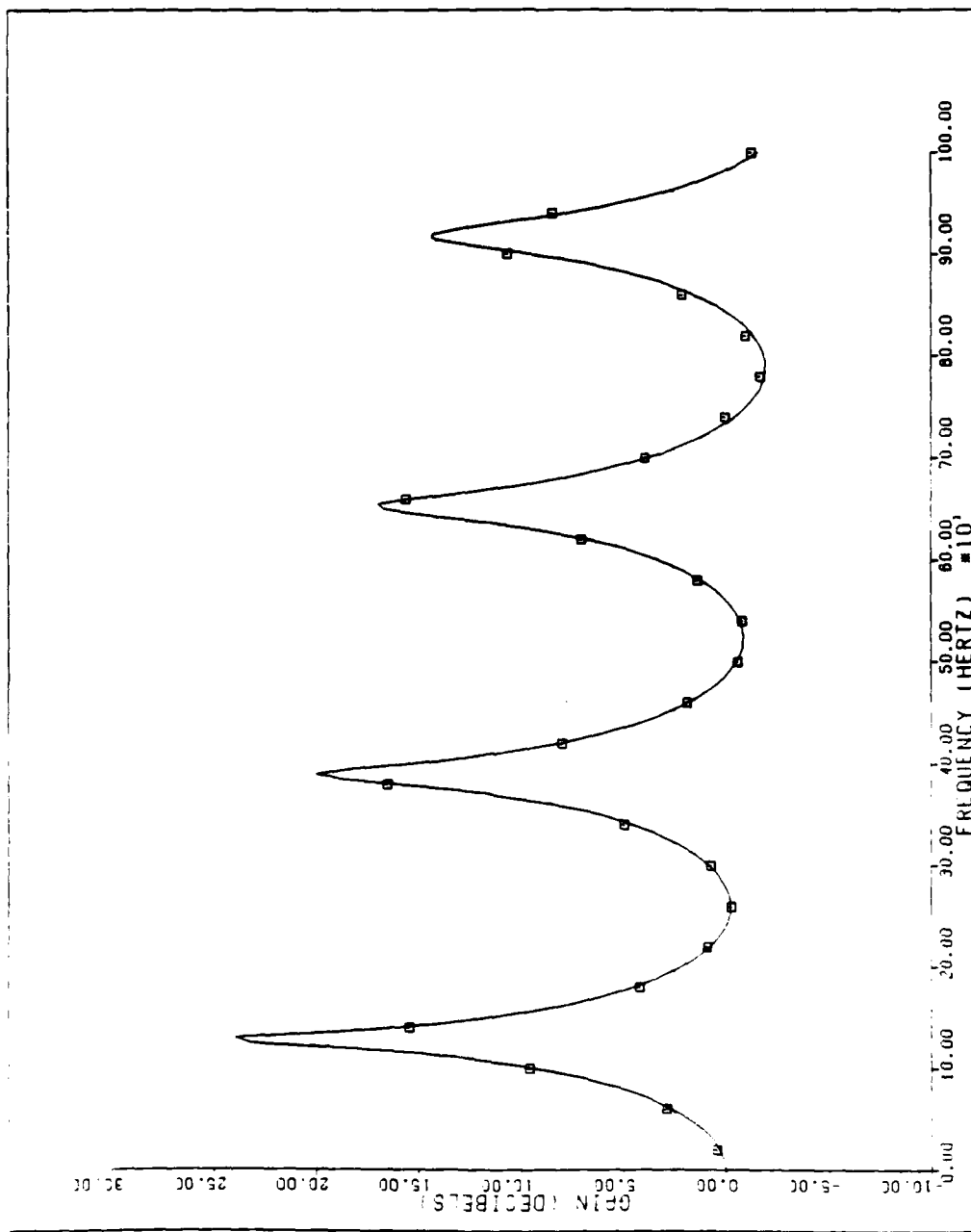
Fig. 59. Theoretical and Experimental Gain--Case 32010n--Laminar Theory

111
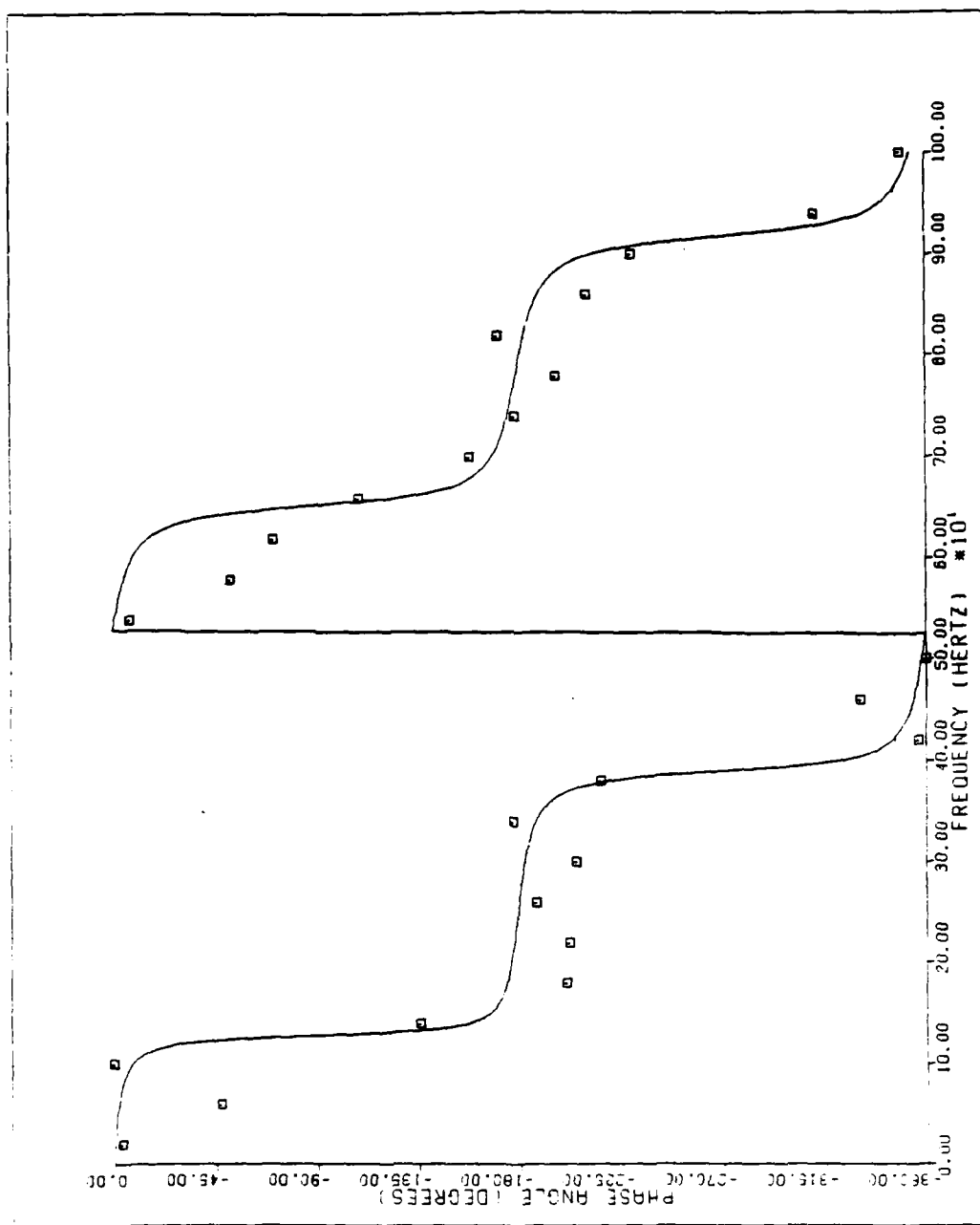
Fig. 60. Theoretical and Experimental Phase Shift--Case 32010n--Laminar Theory

112
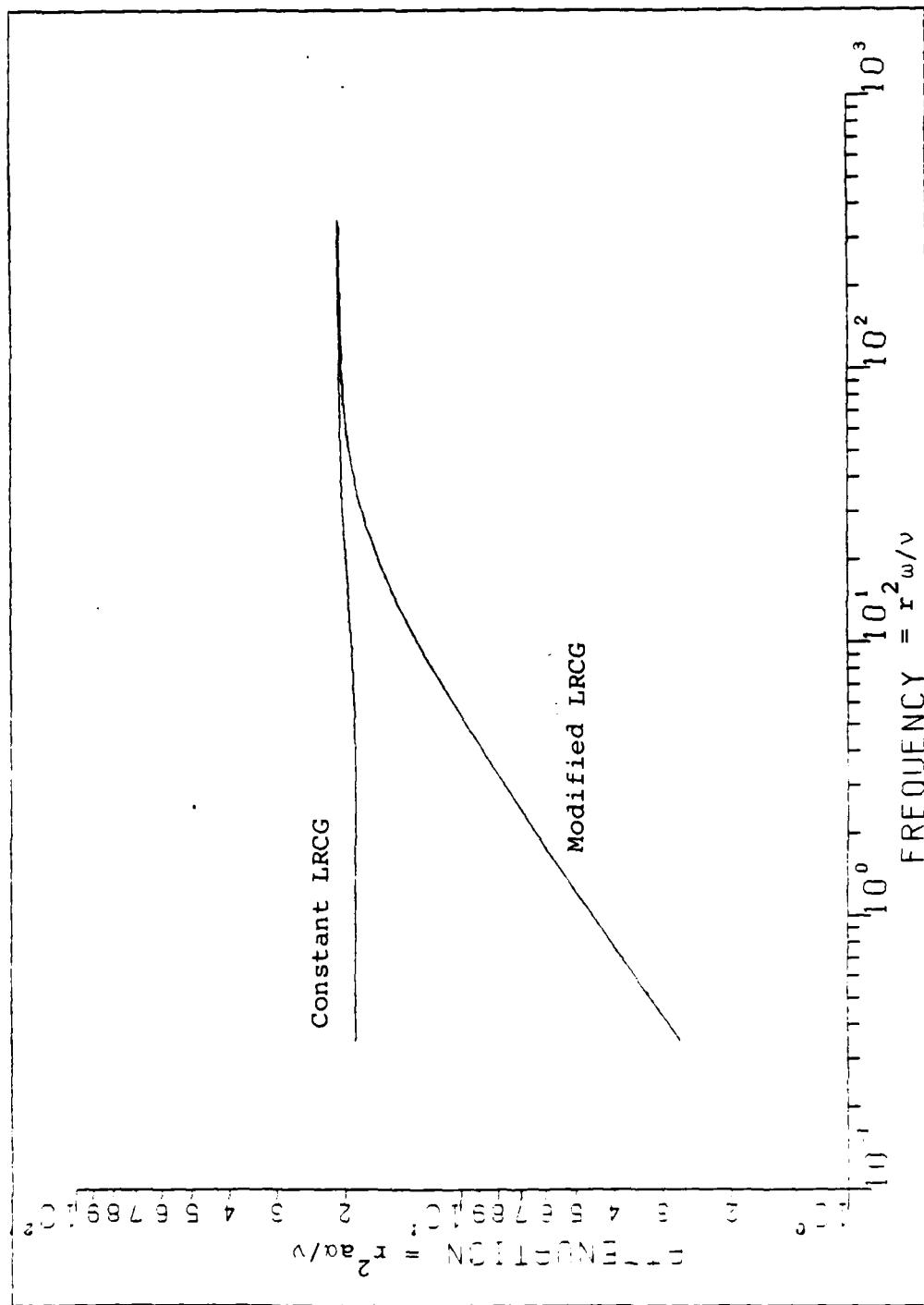
Fig. 61. Nondimensional Behavior--Constant LRCG vs. Modified LRCG--Case 11033

113
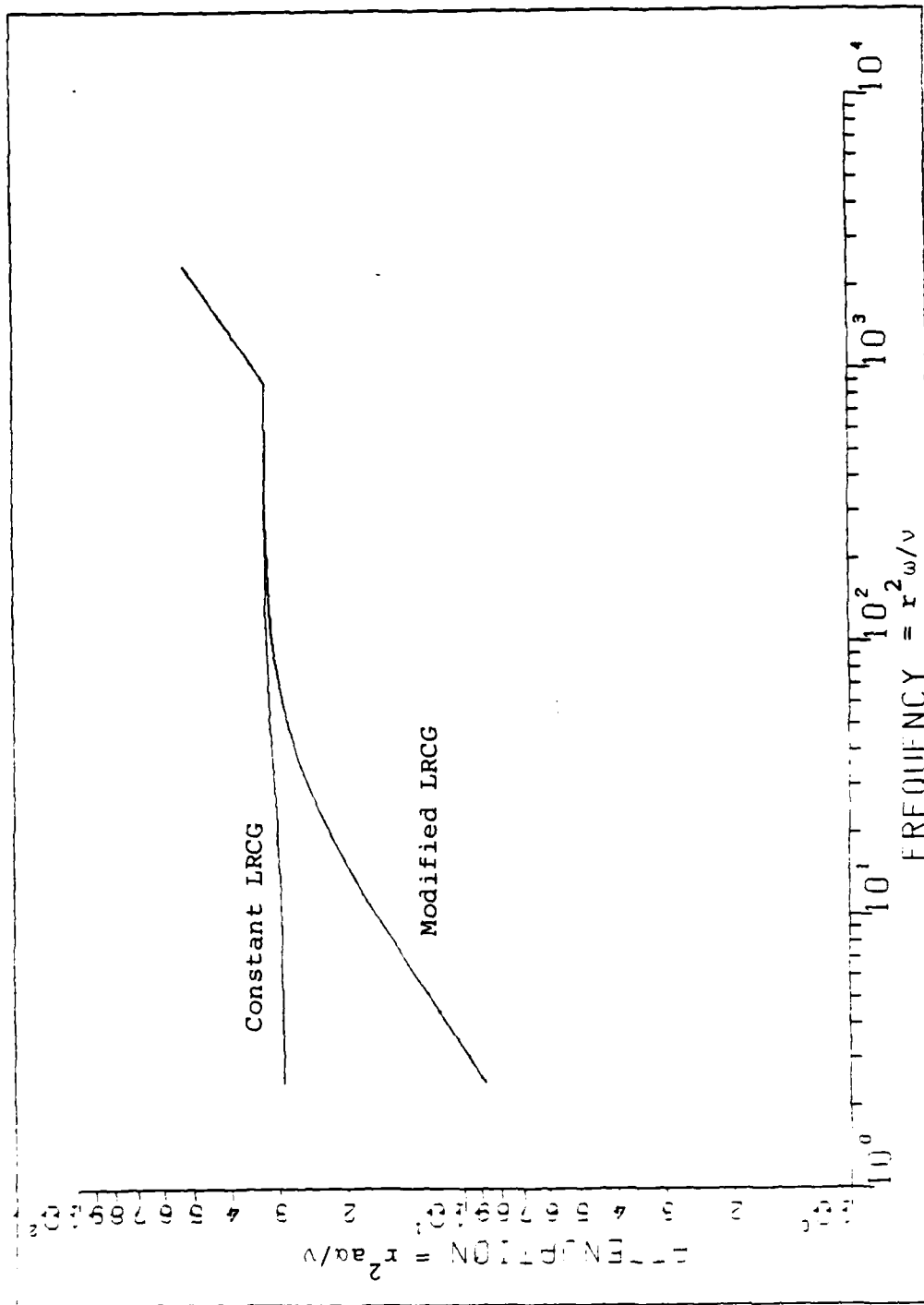
Fig. 62. Nondimensional Behavior--Constant LRCG vs. Modified LRCG--Case 33060

114
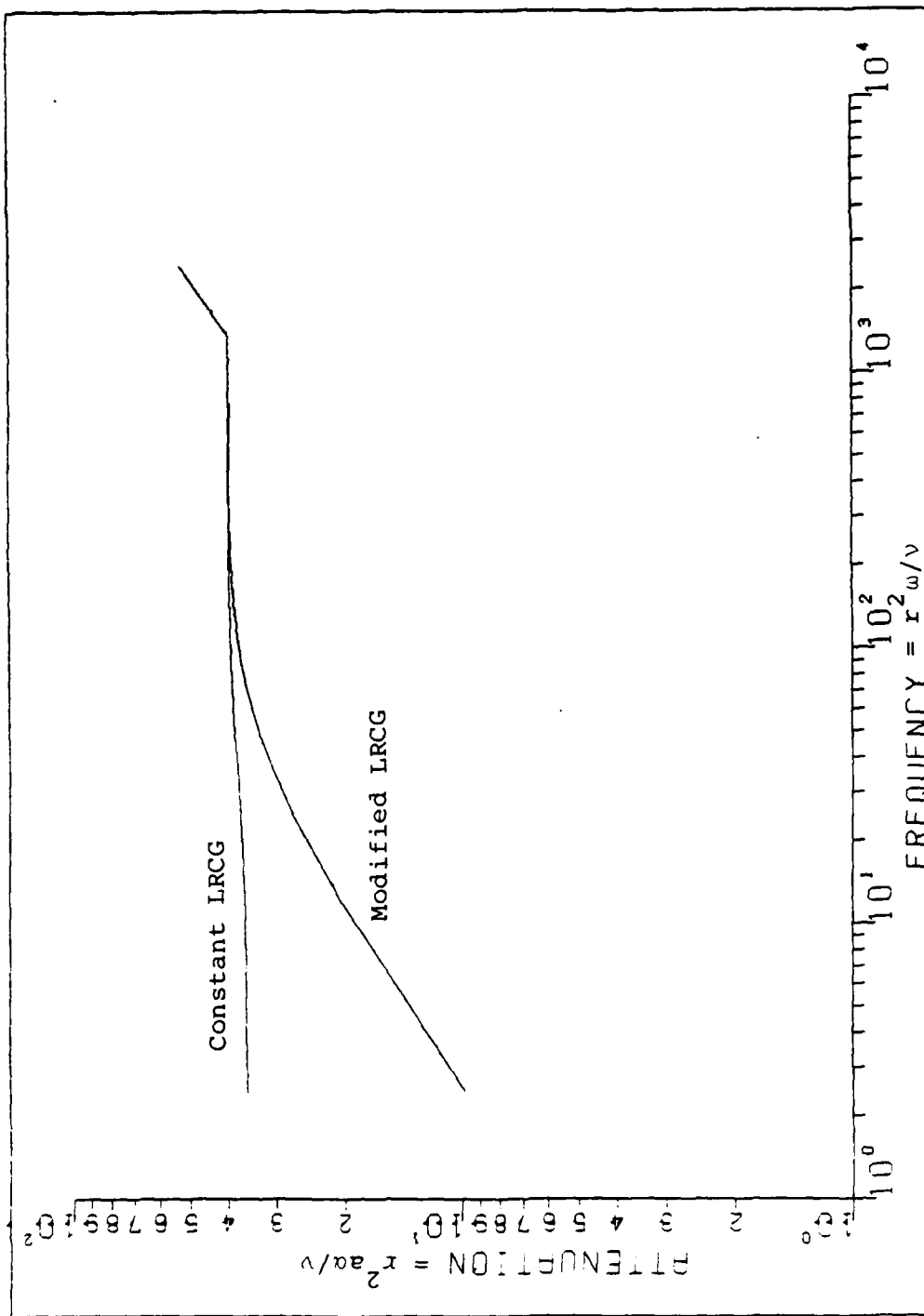
Fig. 63. Nondimensional Behavior--Constant LRCG vs. Modified LRCG--Case 33079

115
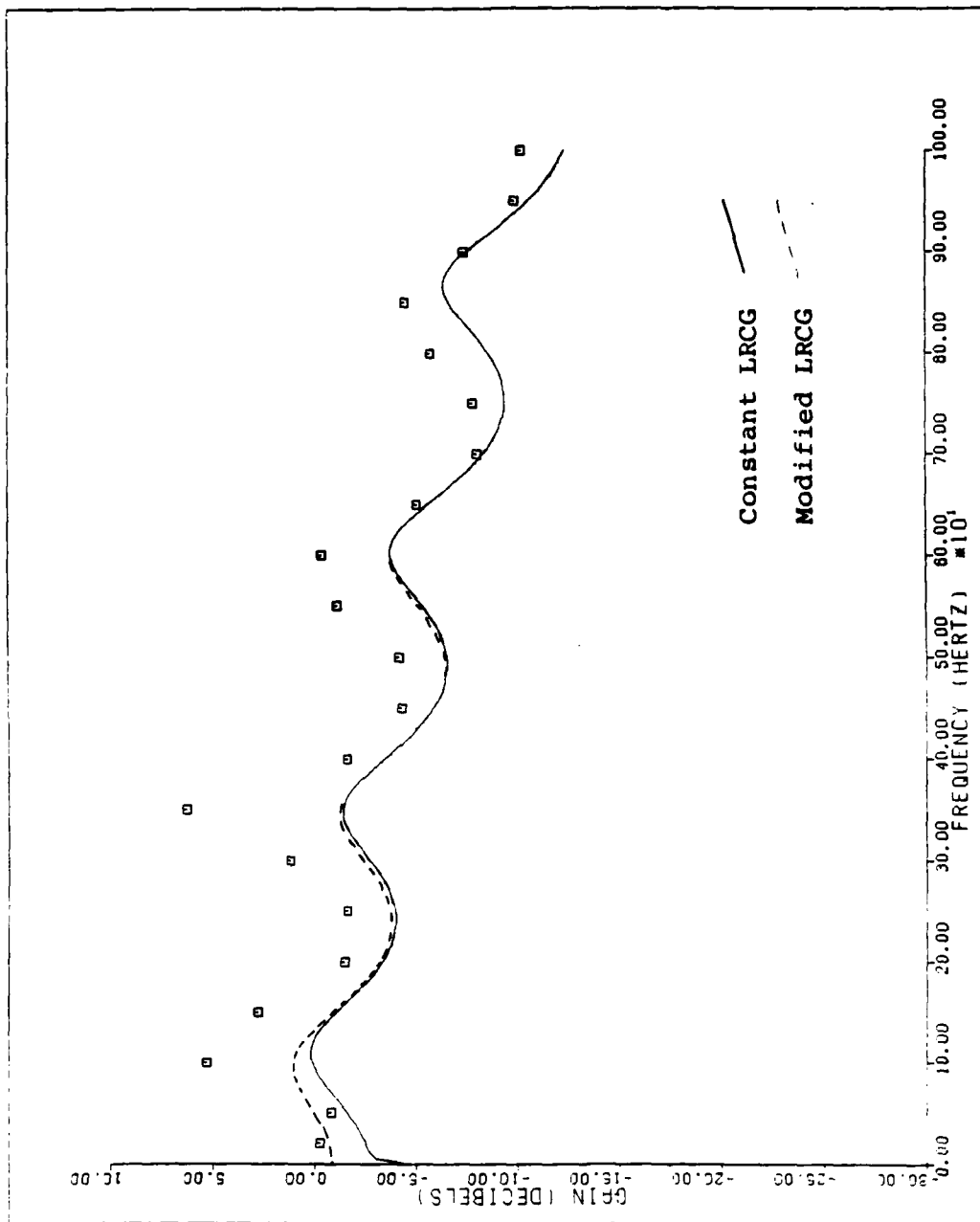
Fig. 64. Effect of Modified LRCG on Theoretical Gain--Case 11033

116
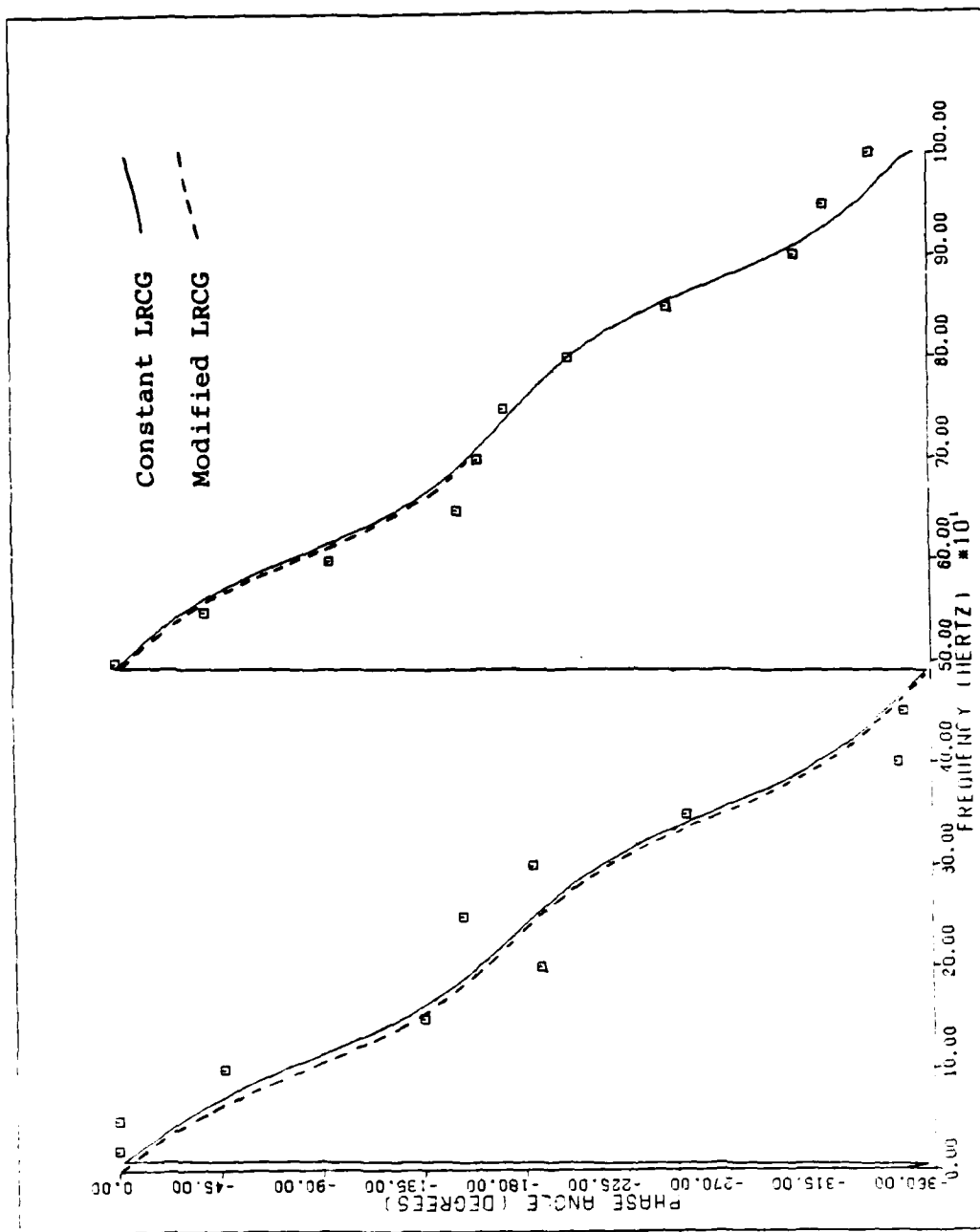
Fig. 65. Effect of Modified LRCG on Theoretical Phase Shift--Case 11033
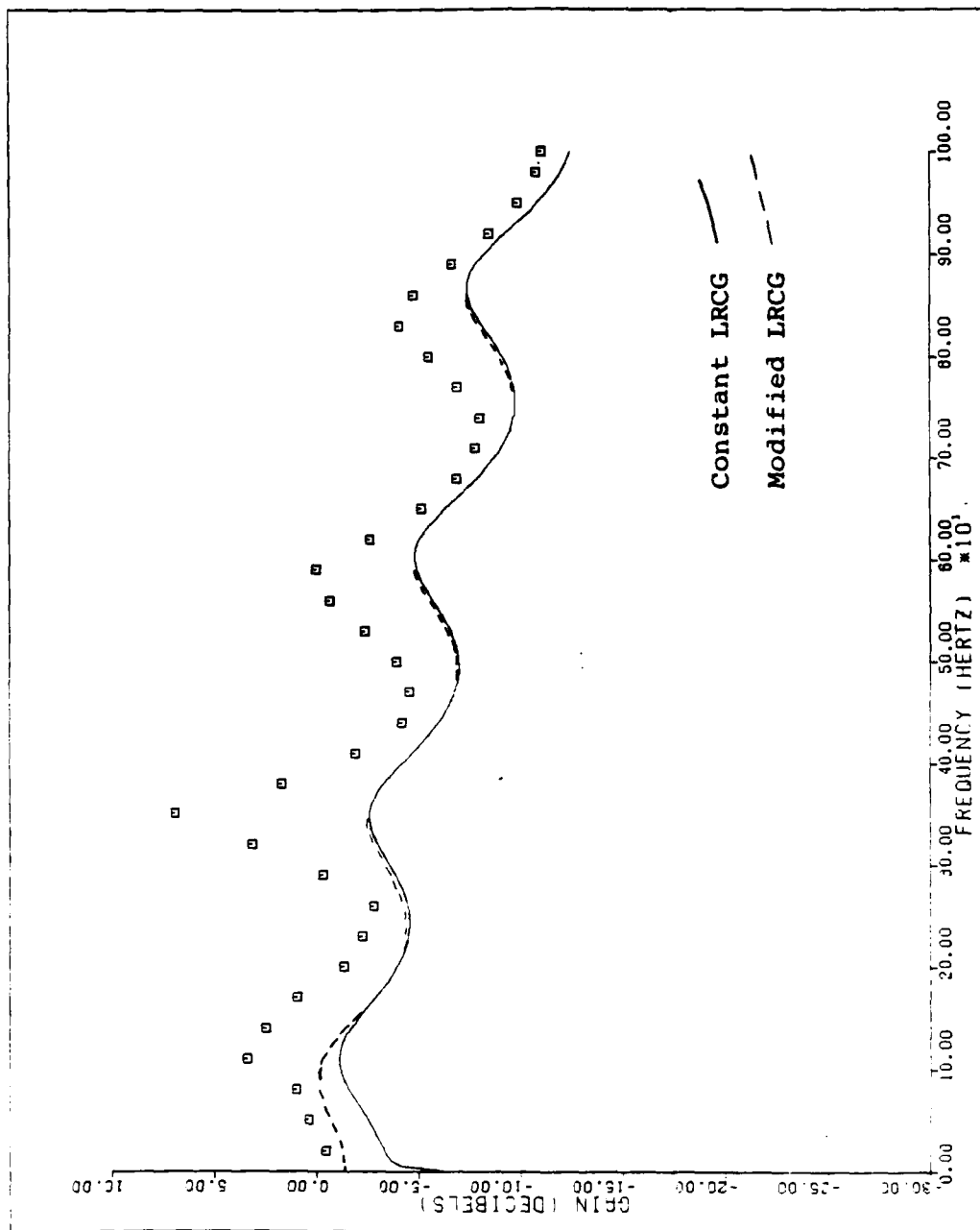
Fig. 66. Effect of Modified LRCG on Theoretical Gain--Case 12034
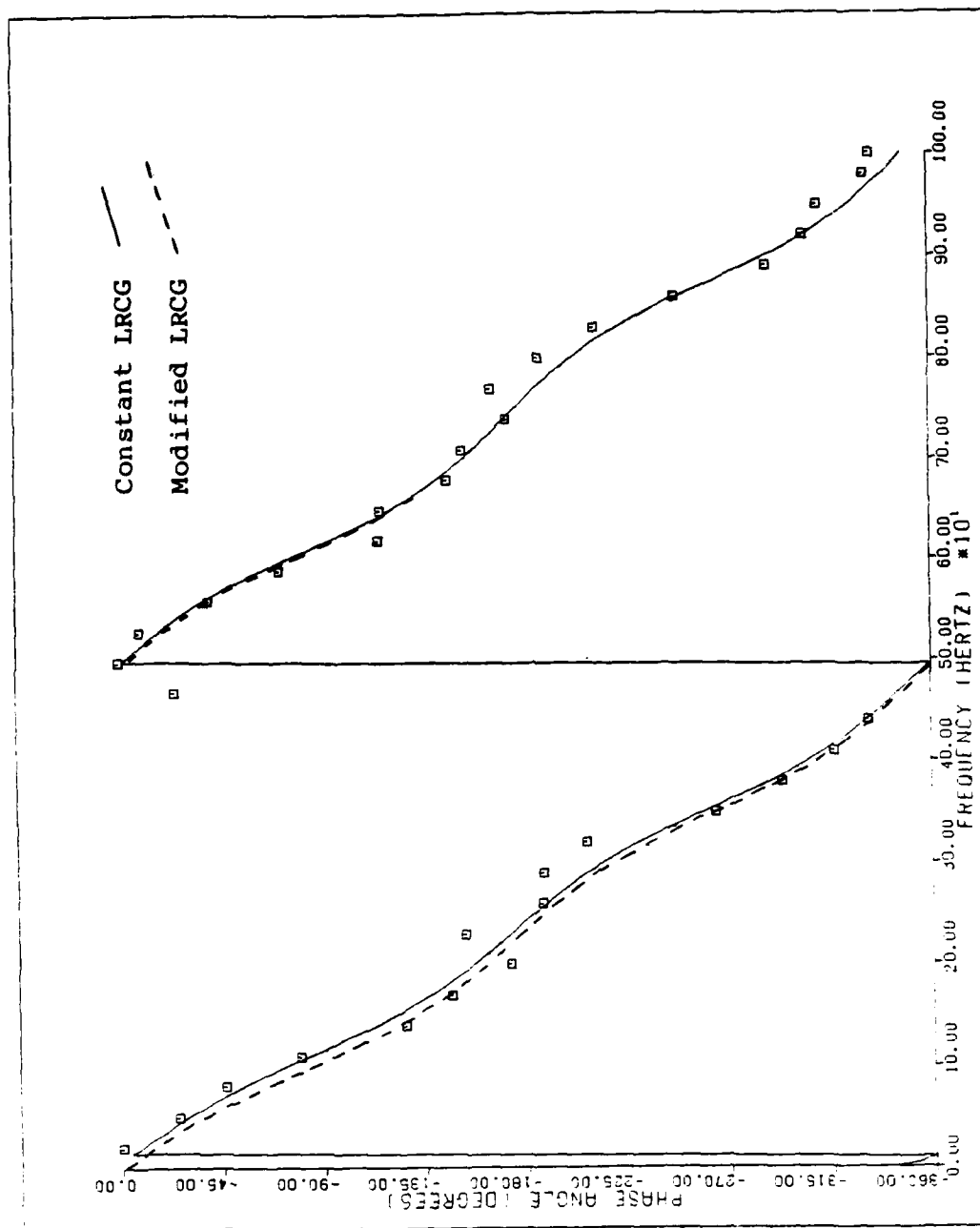
Fig. 67. Effect of Modified LRCG on Theoretical Phase Shift--Case 12034
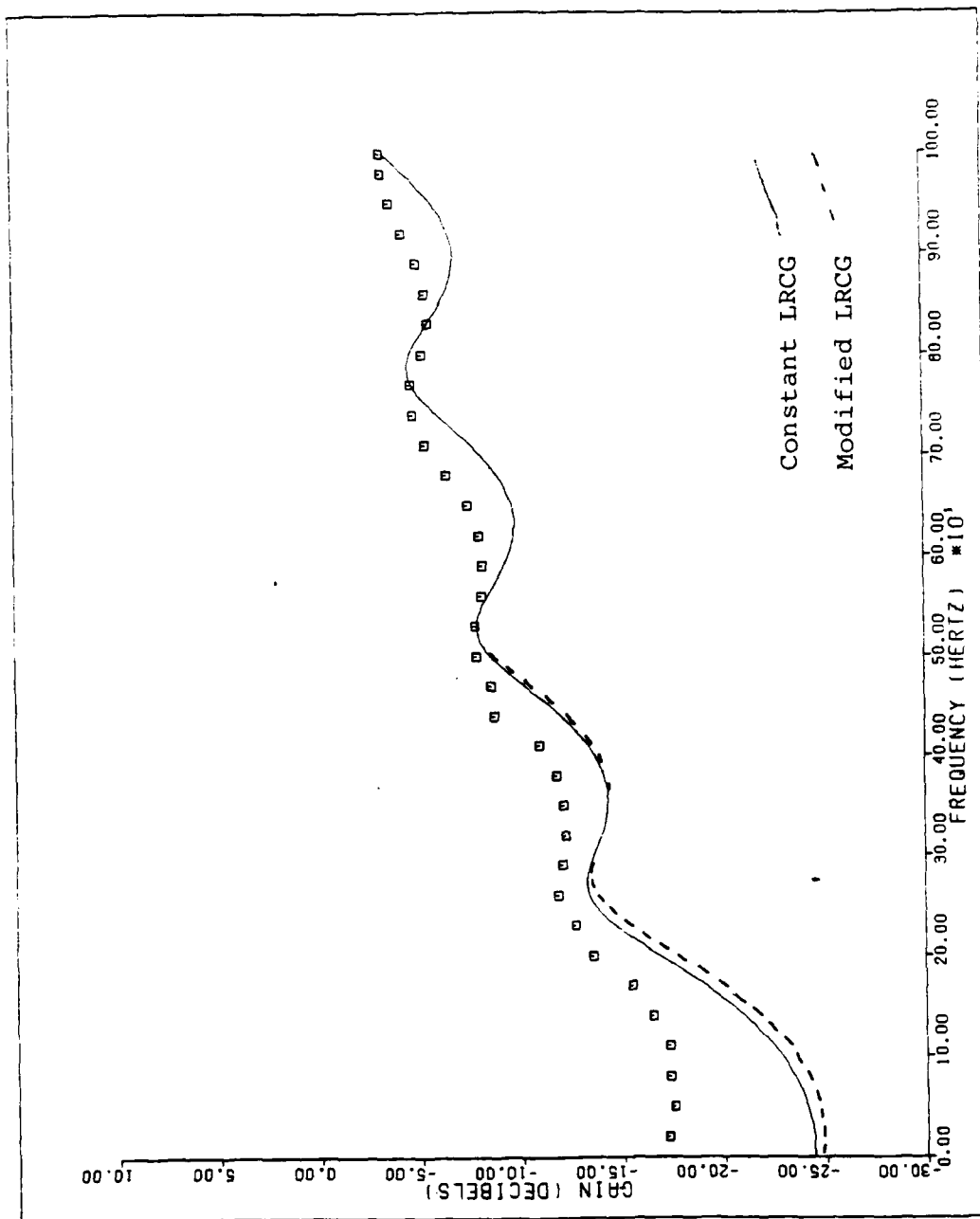
Fig. 68. Effect of Modified LRCG on Theoretical Gain--Case 23165
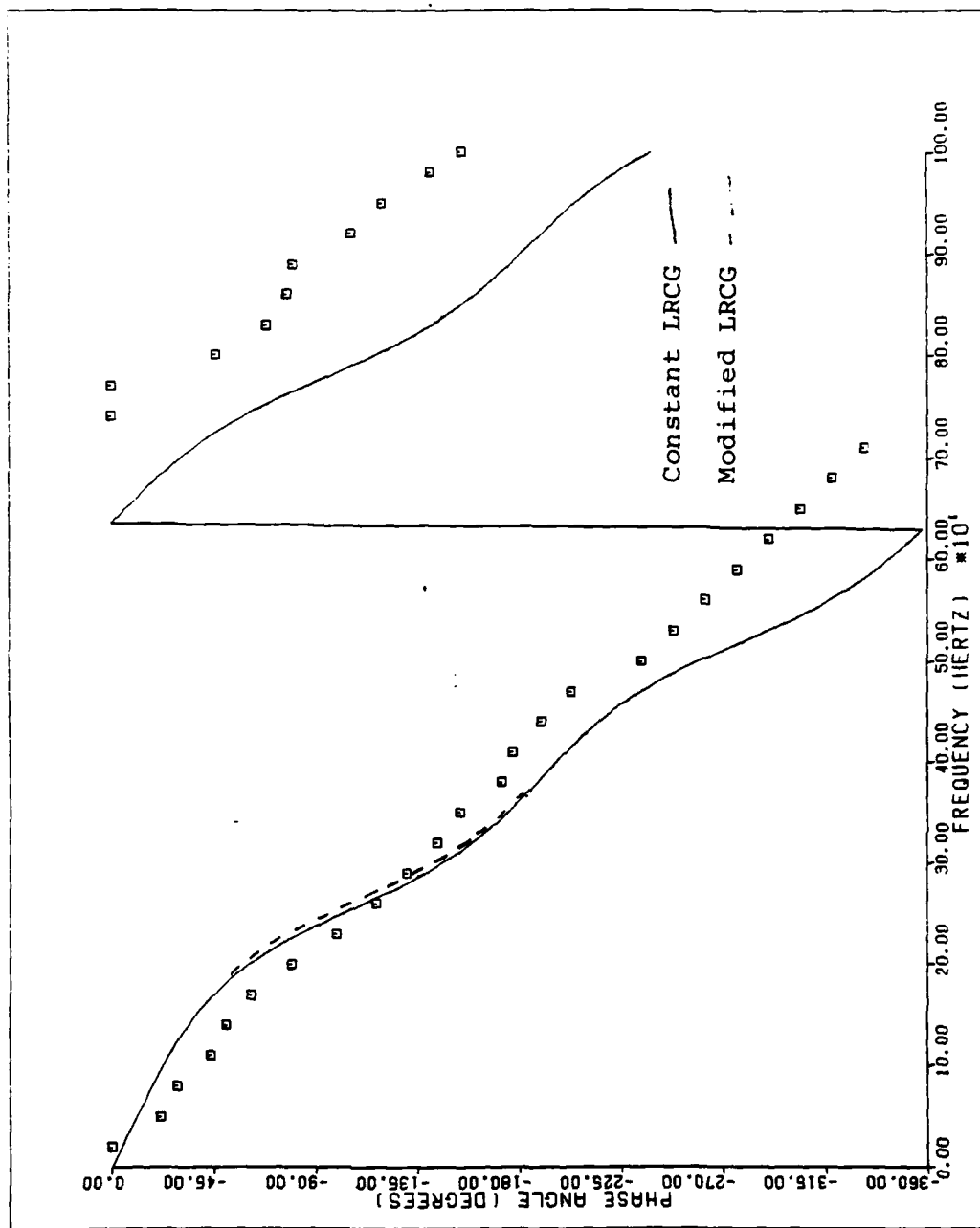
Fig. 69. Effect of Modified LRCG on Theoretical Phase Shift--Case 23165

121
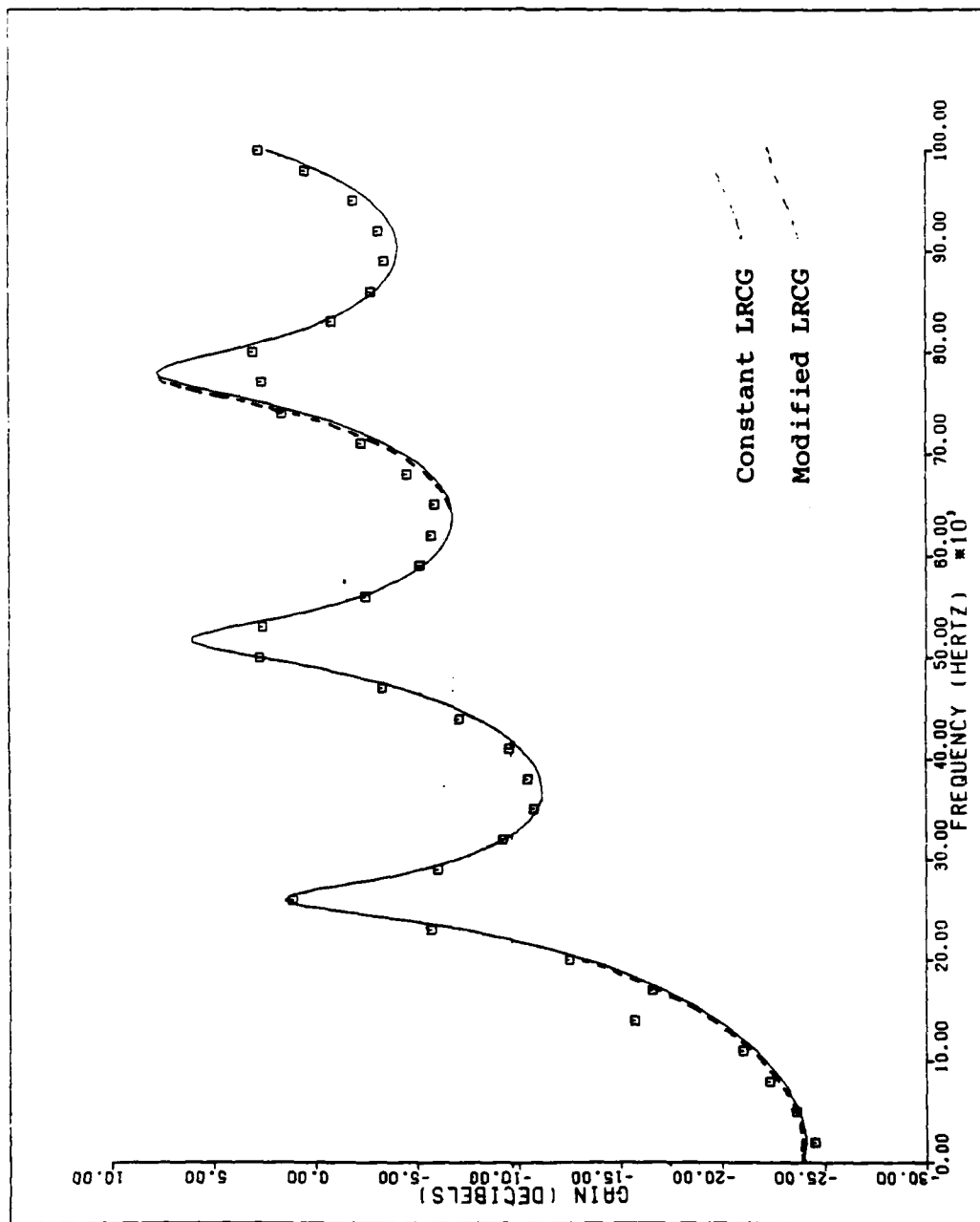
Fig. 70. Effect of Modified LRCG on Theoretical Gain--Case 33060
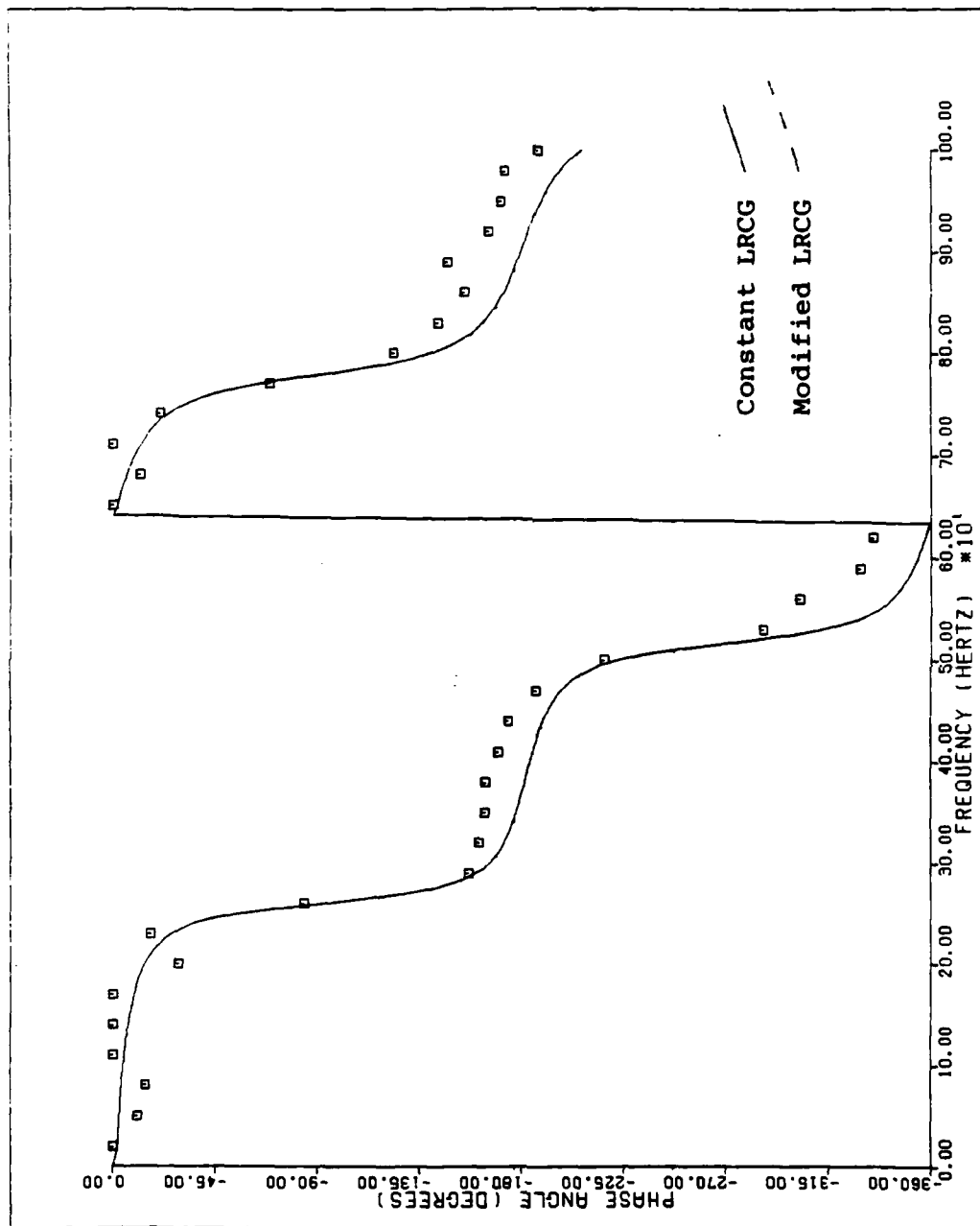
Fig. 71. Effect of Modified LRCG on Theoretical Phase Shift--Case 33060

123
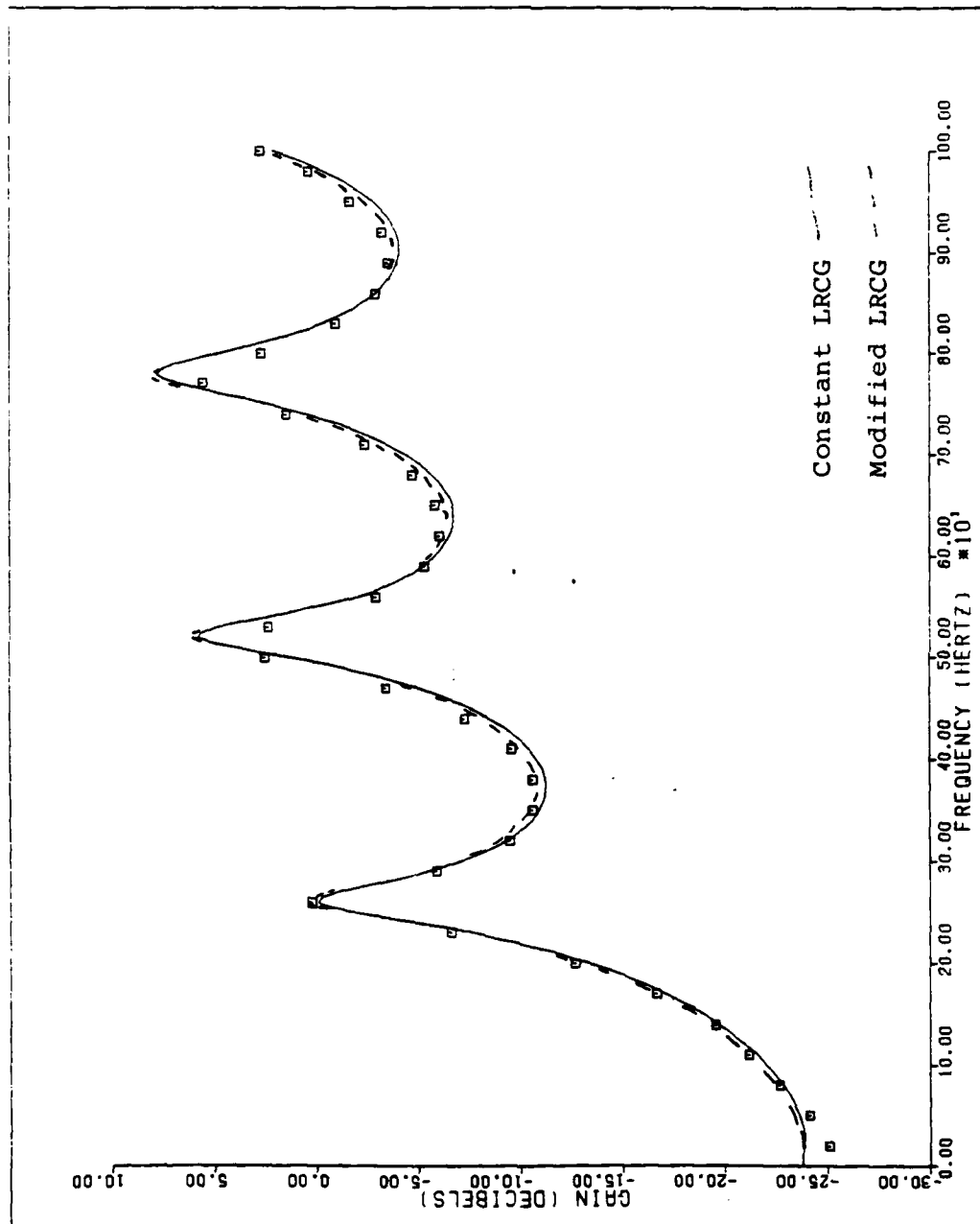
Fig. 72. Effect of Modified LRCG on Theoretical Gain--Case 33079

124
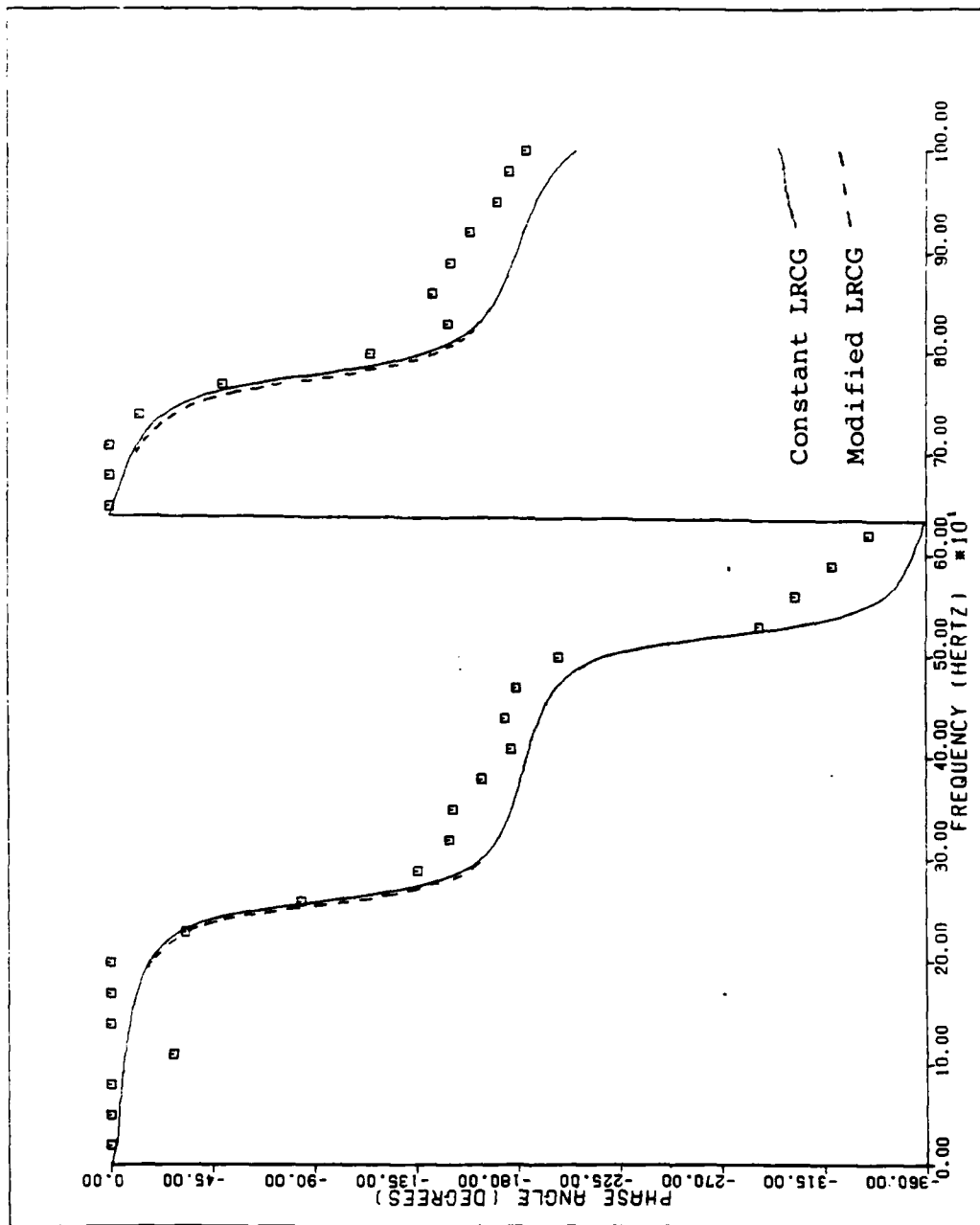
Fig. 73. Effect of Modified LRCG on Theoretical Phase Shift--Case 33079
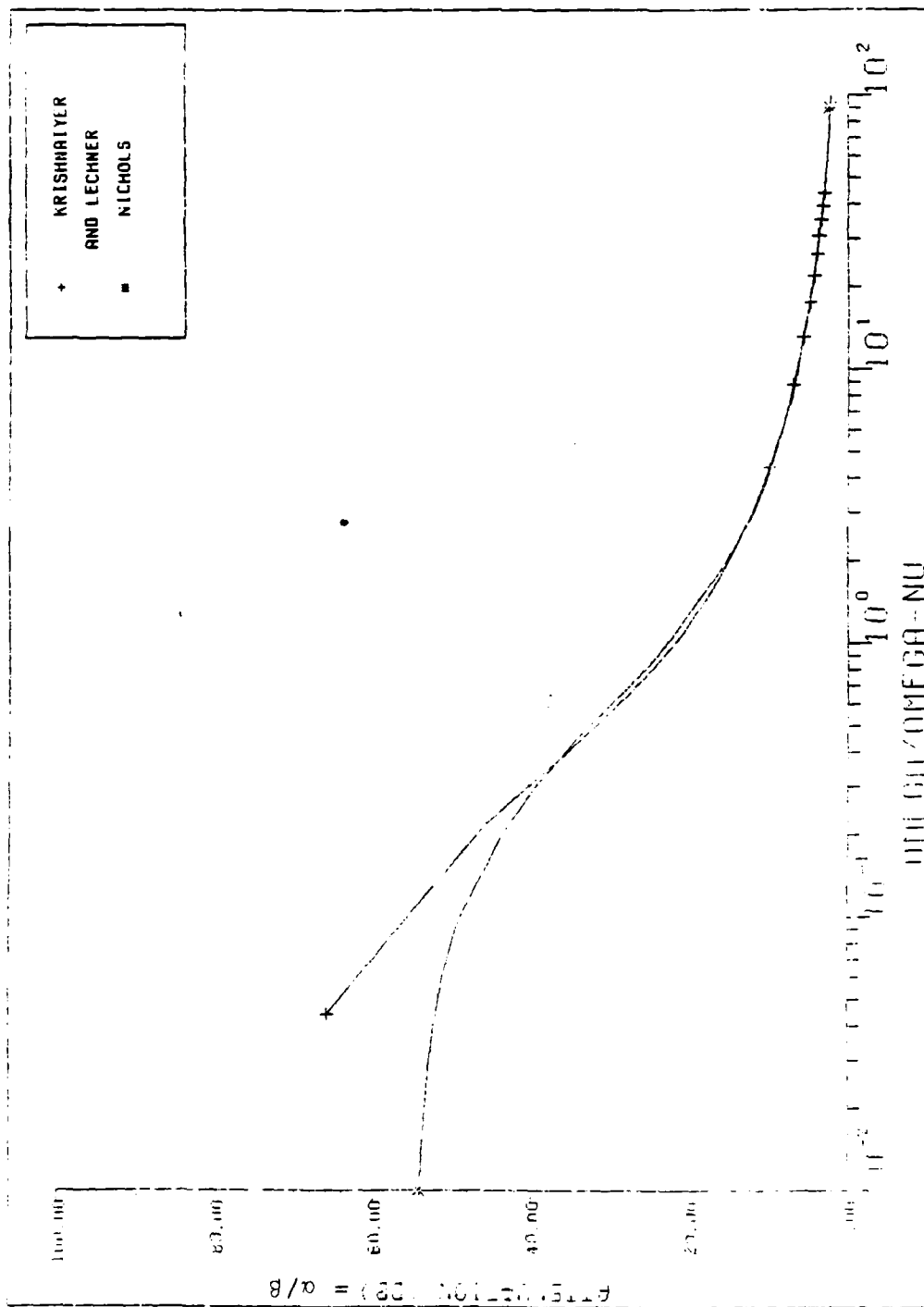
Fig. 74. Comparison of Theoretical Attenuation--Nichols vs. Krishnaiyer-Lechner

126
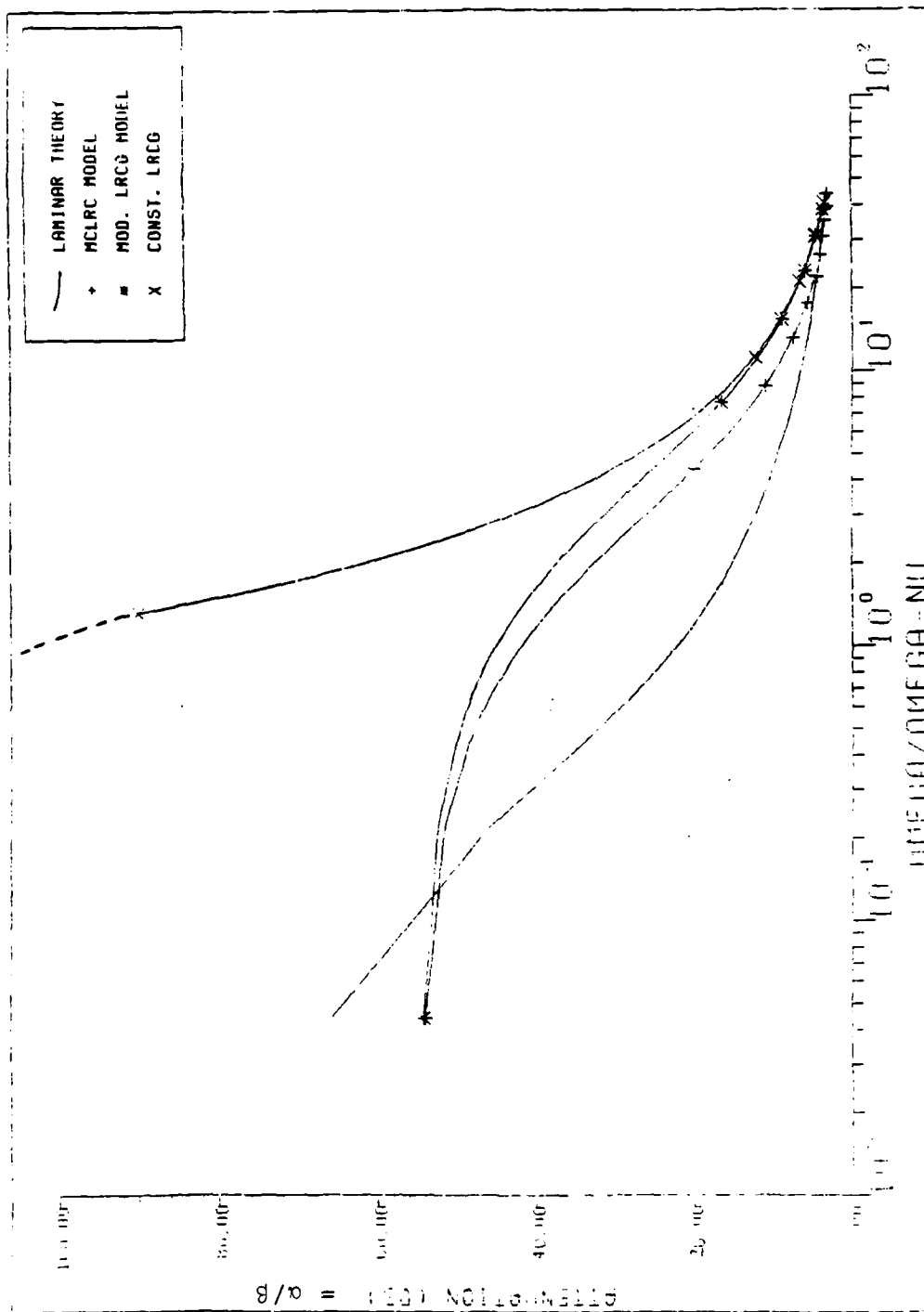
Fig. 75. Comparison of Attenuation for Theoretical Models—Case 11033

127
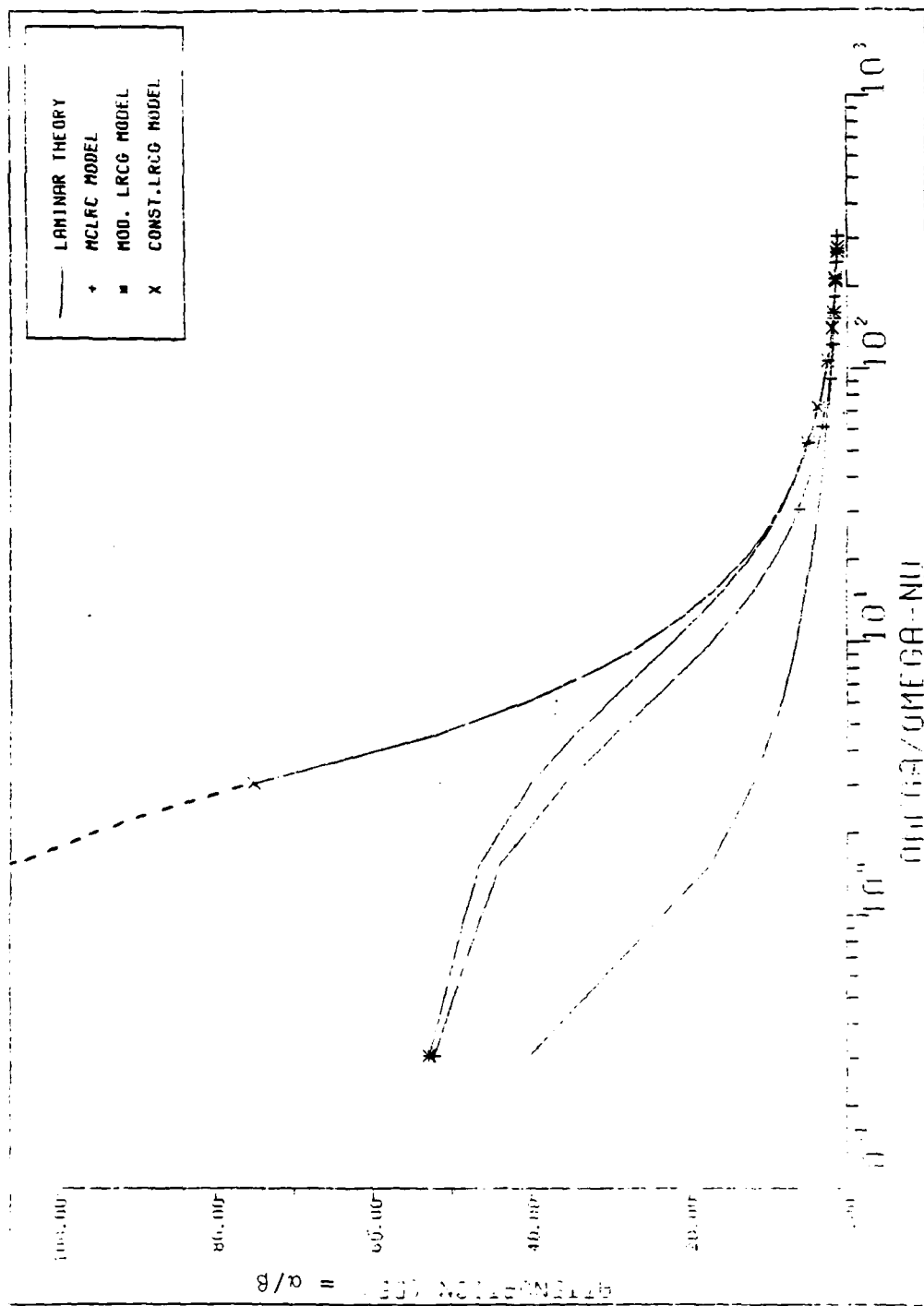
Fig. 76. Comparison of Attenuation for Theoretical Models--Case 33079

Appendix B: <u>Simulation of the Dynamic Response of</u>

<u>the Pneumatic Transmission Line</u>

```
      PROGRAM MSB
C

C     TRANSMISSION LINE STUDY/Z-IN METHOD WITH BRANCH
      DIMENSION DBT(300),RVT(100),DI(100),AD(100),AR(100),CV(100),
     &OMT(100),CNA(100),GMA(100),AGM(100),FN(100),RN(100),GN(100),
     &ALN(100),CN(100),AN(100),BTN(100),AMC(100),AZRN(100),BZRN(100),
     &AZIN(100),BZIN(100),DC(100),DG(100),DD(100),P(100),RHO(100),
     &ANU(100),CA(100),QTCA(100),OMG(300),RTP(100),GP(100),BETA(100),
     &AZOT(100),BZOT(100),REY(100),Q(100),BET(100),GR(300),GI(300),
     &DB(300),OMGX(300),OMGP(300),PHASE(300),PH(300)
      INTEGER TURB,CASE
      CHARACTER TITLE*50,THEOR*50
      DATA PI,TPI/3.1415926,6.2831853/
      DATA AMU,RE,GAM,SIG/0.2679E-08,247104.,1.4,0.8414/
      DATA N/10/
C
C     TO NEGATE THE PLOT ROUTINE SET ICAS TO ZERO.
C
C********************************************************************
C                                                                  *
C        THIS PROGRAM IS DESIGNED TO CALCULATE THE THEORETICAL      *
C        GAIN AND PHASE SHIFT FOR A GIVEN PNEUMATIC TRANSMISSION    *
C        LINE.  THE PROGRAM FIRST CALCULATES THE PRESSURE DROP      *
C        ALONG THE LINE BY TREATING THE LINE AS A SERIES            *
C        OF SHORTER SEGMENTS.  WITH THE INPUT PRESSURE FOR          *
C        EACH SEGMENT, THE PROPAGATION OPERATOR IS CALCULATED       *
C        USING THE LAMINAR THEORY OR A SELECTED TURBULENT           *
C        THEORY.  THE SELECTION OF THE THEORY TO BE USED            *
C        AND THE SELECTION OF THE ORIFICE CONDITIONS ARE            *
C        INTERACTIVE.  THE PROGRAM PROVIDES A TABULAR               *
C        OUTPUT ON FILE 'ACROUT' WHICH IS DESCRIBED BELOW.          *
C        THE PROGRAM ALSO PRODUCES TWO PLOTS: THEORETICAL           *
C        AND EXPERIMENTAL GAIN VS. FREQUENCY, AND                   *
C        THEORETICAL AND EXPERIMENTAL PHASE SHIFT VS.               *
C        FREQUENCY.                                                 *
C                                                                  *
C********************************************************************
C********************************************************************
C                                                                  *
C        ACROUT IS THE TABULAR OUTPUT FILE OF THE FOLLOWING         *
C                                                                  *
C             PRESENTED BY LINE SEGMENT                             *
```

```
C     LENGTH                                                            *
C     DIAMETER                                                          *
C     PRESSURE                                                          *
C     ADIABATIC SPEED OF SOUND                                          *
C     FUNDAMENTAL FREQUENCY                                             *
C     DENSITY                                                           *
C     REYNOLDS NUMBER                                                   *
C                                                                       *
C        THEORETICAL RESULTS                                            *
C     FREQUENCY                                                         *
C     NON-DIMENSIONAL FREQUENCY                                         *
C     NON-DIMENSIONAL ATTENUATION                                       *
C     PHASE SHIFT                                                       *
C     GAIN                                                              *
C     TURBULENCE INDICATOR                                              *
C                                                                       *
C        EXPERIMENTAL RESULTS                                           *
C                                                                       *
C     FREQUENCY                                                         *
C     SENDING PRESSURE                                                  *
C     RECEIVING PRESSURE                                                *
C     GAIN                                                              *
C     PHASE SHIFT                                                       *
C                                                                       *
C***********************************************************************
C                                                                       *
C     ATTEN IS AN OUTPUT FILE OF THE NON-DIMENSIONAL                    *
C     FREQUENCY AND ATTENUATION USED AS AN INPUT                        *
C     FILE FOR THE PLOT ROUTINE 'PLOTM' TO CREATE                       *
C     PLOTS AS PRODUCED BY BROWN OF NON-DIMENSIONAL                     *
C     FREQUENCY VS NON-DIMENSIONAL ATTENUATION                          *
C                                                                       *
C***********************************************************************
      OPEN(11,FILE='D20000')
      REWIND 11
      OPEN(12,FILE='ACROUT')
      REWIND 12
      OPEN(13,FILE='ATTEN')
      REWIND 13
      OPEN(14,FILE='GAIN')
      REWIND 14
      CALL PLOTS(0.,0.,9)
C***********************************************************************
C     TAPE 11 IS THE INPUT FILE CONTAINING THE FOLLOWING:               *
C       ICAS IS THE CASE NUMBER                                         *
C       OP IS THE LINE CONDITION; 1.0 FOR OPEN LINE,ELSE 0.0            *
C       TR IS THE AMBIENT TEMPERATURE IN DEGREES RANKINE                *
C       PG IS THE BAROMETRIC PRESSURE (PSIA)                            *
C       PT IS THE STATIC LINE PRESSURE (PSIG)                           *
C       FL IS THE MASS FLOW RATE (LBM/SEC)                              *
C       D1 IS THE OUTSIDE LINE DIAMETER (IN)                            *
C       DORF2 IS THE SQUARE OF THE ORIFICE DIAMETER (IN**2)
```

```
C          DI IS THE LINE SEGMENT DIAMETER (IN)                          *
C          AD IS THE LINE SEGMENT LENGTH (IN)                            *
C             LINE SEGMENTS 1 & 2 ARE THE DOWNSTREAM DYNAMIC             *
C             PRESSURE TRANSDUCER BRANCH.                                *
C             THE UPSTREAM END OF THE TEST SECTION IS DENOTED            *
C             AS SEGMENT NUMBER 10.                                      *
C                                                                        *
C*************************************************************************
C                                                                        *
C       THE FOLLOWING VARIABLES ARE USED IN THIS PROGRAM                 *
C          CT IS THE RATIO OF TURBULENT/ADIABATIC CAPACITANCE            *
C          TL IS THE INERTANCE CONSTANT                                  *
C          ZEND IS THE REAL PART OF THE TERMINAL IMPEDANCE (PSI/CIS)     *
C          ZENDI IS THE IMAGINARY PART OF THE TERMINAL IMPEDANCE (PSI/CIS)*
C          AMU IS THE DYNAMIC VICOSITY (PSI-SEC)                         *
C          RE IS THE GAS CONSTANT FOR AIR (IN/SEC-R)                     *
C          GAM IS THE RATIO OF SPECIFIC HEATS                           *
C          SIG IS THE SQUARE ROOT OF THE PRANDTL NUMBER                  *
C          N IS THE NUMBER OF LINE SEGMENTS                              *
C          REYT IS THE REYNOLDS NUMBER                                   *
C                                                                        *
C*************************************************************************
      READ(11,*)ICAS,OP
      READ(11,*)TR,PG,PT,FL,D1
      IF(OP.EQ.1.)GOTO 110
      READ(11,*)DORF2
  110 CONTINUE
      DO 898 I=1,N
      READ(11,*)DI(I),AD(I)
  898 CONTINUE
      IF(OP.EQ.1.)GOTO 100
C
C*************************************************************************
C             IF DORF2 =0. THEN THE DATA IS FOR A BLOCKED LINE CASE.     *
C             IN THIS CASE THE MODEL SELECTION IS BYPASSED AND THE       *
C             CALCULATIONS ARE DONE USING THE LAMINAR THEORY.            *
C             CASE IS SET TO 3                                           *
C             N1 IS SET TO 3                                             *
C             N1=3 SELECTS THE CORRECT HEADING FOR THE OUTPUT FILE.      *
C                                                                        *
C*************************************************************************
      IF(DORF2.EQ.0.) THEN
       CASE=3
       N1=3
       GOTO 96
      ENDIF
  100 CONTINUE
C
C
```

```
C************************************************************************
C                                                                      *
C     THIS INTERACTIVE SECTION ALLOWS THE SELECTION OF                 *
C     A LAMINAR OR TURBULENT MODEL.   IT ALSO ALLOWS THE               *
C     SELECTION OF ONE OF TWO LOAD IMPEDANCE MODELS.                   *
C     CASE IS THE MODEL INDICATOR FOR THE LAMINAR OR                   *
C     TURBULENT MODEL. IF A COMBINATION OF LAMINAR AND                 *
C     TURBULENT MODELS IS SELECTED, THE PROGRAM WILL                   *
C     SWITCH TO THE TURBULENT MODEL IF THE REYNOLDS NUMBER             *
C     IS GREATER THAN 2300 AND THE TURBULENT ATTENUATION               *
C     IS GREATER THAN THE LAMINAR VALUE. OTHERWISE THE LAMINAR         *
C     MODEL IS USED.                                                   *
C     N1 IS THE LOAD IMPEDANCE INDICATOR. YOU HAVE A CHOICE            *
C     OF EITHER CHOKED OR NON-CHOKED FLOW THROUGH THE                  *
C     ORIFICE.                                                         *
C                                                                      *
C************************************************************************
C
      PRINT*,'   '
      PRINT*,"   '
      PRINT*,'   '
      PRINT*,'   '
      PRINT*,'   '
      PRINT*,'    PLEASE ENTER VALUE OF CASE '
      PRINT*,'   '
      PRINT*,'   '
      PRINT*,'    CASE'
      PRINT*,'   '
      PRINT*,'     1        LAMINAR/MOD. CONST. LRC'
      PRINT*,'     2        LAMINAR/MODIFIED LRCG'
      PRINT*,'     3        LAMINAR THEORY ONLY'
      PRINT*,'   '
      PRINT*,'   '
      PRINT*,'   '
      PRINT*,'   '
      PRINT*,'   '
      PRINT*,'   '
      PRINT*,'   '
      PRINT*,' '
      PRINT*,' '
      PRINT*,'? CASE'
      PRINT*,' '
      READ*,CASE
      IF(OP.EQ.1.0) GOTO 96
      PRINT*,' '
      PRINT*,' '
      PRINT*,' '
      PRINT*,'    PLEASE ENTER VALUE OF N1'
      PRINT*,' '
```

132

```fortran
      PRINT*,'      N1'
      PRINT*,' '
      PRINT*,'      1    CHOKED FLOW IN THE ORIFICE'
      PRINT*,'      2    NON-CHOKED FLOW IN THE ORIFICE'
      PRINT*,' '
      PRINT*,' '
      PRINT*,'? N1'
      PRINT*,' '
      READ*,N1
  96  WRITE(12,612)ICAS
 612  FORMAT(1X,T10,'RESULTS OF RUN NUMBER',T32,I7)
      IF(CASE.EQ.3)THEN
      WRITE(12,804)
 804  FORMAT(1H0,T10,'CALCULATED USING LAMINAR THEORY THROUGHOUT')
      ELSE
      IF(CASE.EQ.1)THEN
      WRITE(12,807)
 807  FORMAT(1H0,T10,'CALCULATED USING MOD. CONST. LRC THEORY IN THE TUR
     &BULENT REGION')
      ELSE
      WRITE(12,808)
 808  FORMAT(1H0,T10,'CALCULATED USING THE MODIFIED LRCG THEORY IN THE
     &TURBULENT REGION')
      ENDIF
      IF(OP.EQ.1.0) GOTO 500
      IF(N1.EQ.1)THEN
      WRITE(12,809)
 809  FORMAT(1X,T10,'REFLECTION COEFFICIENT CALCULATED ASSUMING CHOKED
     &FLOW IN THE ORIFICE')
      ELSE
      WRITE(12,820)
 820  FORMAT(1X,T10,'REFLECTION COEFFICIENT CALCULATED ASSUMING NON-
     &CHOKED FLOW IN THE ORIFICE')
      ENDIF
 500  CONTINUE
      ENDIF
C
C        THE FOLLOWING VARIABLES ARE USED AS PROGRAM COUNTERS.
C
      ICT=1
      IND=1
      NNN=1
C
C     OP=0 SIGNIFIES BLOCKED OR RESTRICTED FLOW.
C     CALCULATES INITIAL REYNOLDS NUMBER BASED ON THE LINE DIAMETER
C      UPSTREAM OF THE TEST SECTION.
C      (4/(AMU*PI*32.2*12)) = 1.22999E06
C
      IF(OP.EQ.0.) THEN
      REYT=1.22999E+06*FL/D1
      ELSE
```

133

```
C     TOTL IS THE LINE LENGTH (INCHES) FROM THE STATIC
C     PRESSURE TRANSDUCER TO THE TERMINATION OF THE
C     LINE. THE DISTANCE FROM THE STATIC TRANSDUCER
C     TO THE BEGINNING OF THE TEST SECTION IS 2.0 INCHES.
      TOTL=2.0
      DO 901 I=3,N
      TOTL=TOTL+AD(I)
901   CONTINUE
      REYT=PT*(PT/2.+PG)*(DI(N)**3.)/(32.*(AMU**2)*TOTL*RE*TR)
      IF(REYT.LT.2300.) GOTO 902
      REYT=(REYT*32./.1582)**(4./7.)
902   CONTINUE
      ENDIF
      PT=PT+PG
C
C*********************************************************************
C                                                                   *
C     THE PRESSURE DROP BETWEEN THE STATIC PRESSURE                 *
C     TRANSDUCER AND THE BEGINNING OF THE TEST LINE IS              *
C     CALCULATED. P(N) IS THE LINE PRESSURE AT THE UPSTREAM         *
C     END OF THE TEST LINE. PF IS THEN SET EQUAL TO P(N).           *
C                                                                   *
C*********************************************************************
      IF(REYT.LT.2300.) THEN
      DP=PT-SQRT(PT**2.+2.27E-10*REYT*TR/(D1**3.))
      ELSE
      DP=PT-SQRT(PT**2.+1.12226E-12*REYT**1.75*TR/(D1**3.))
      ENDIF
      P(N)=PT+DP-PG
      PF=P(N)
      IF(REYT.EQ.0.)GOTO 999
      IF(REYT.LT.2300)THEN
      F=64./REYT
      ELSE
      F=0.3164/(REYT**0.25)
      ENDIF
      F2=SQRT(F)
      TL=((F2+1.)*((F2+2.)**2))/(4.*((2*F2)+1.0))
      CT=GAM-((GAM-1.)/TL)
C*********************************************************************
C        THIS PROGRAM USES THE TERM (CT*AGM(I))                     *
C        THIS IS THE TURBULENT CAPACITANCE. IF THE                  *
C        ADIABATIC CAPACITANCE IS TO BE USED, SET CT=1.0            *
C        AFTER THIS POINT.                                          *
C        THE TERM (TL*RHO(I)/AR(I)) IS THE TURBULENT               *
C        INERTANCE. FOR ADIABATIC INERTANCE SET TL=1.0              *
C*********************************************************************
999   CONTINUE
      DO 899 I=1,N-2
      IF(OP.EQ.1.) GOTO 895
```

134

```
C
C          CALCULATES THE REYNOLDS NUMBER IN THE TEST SECTION.
C
           REYT=1.22999E+06*FL/DI(10)
     895   CONTINUE
C
C************************************************************************
C                                                                      *
C          THE PRESSURE DROP ACROSS EACH SEGMENT OF THE LINE IS        *
C          NOW CALCULATED.  THE INDEX I IS SET FROM 1 TO N-2 TO        *
C          SKIP THE DOWNSTREAM TRANSDUCER BRANCH. THE INDEX K          *
C          IS USED TO REVERSE THE ORDER OF THE SEGMENTS SINCE #10      *
C          IS THE UPSTREAM END OF THE LINE.                            *
C                                                                      *
C************************************************************************
C          PF=PF+PG
           K=N+1-I
           IF(REYT.LT.2300.) THEN
            DO=PF-SQRT(PF**2.+1.135E-10*AD(K)*REYT*TR/(DI(K)**3.))
            ELSE
            DP=PF-SQRT(PF**2.+5.61128E-13*REYT**1.75*AD(K)*TR/
       &    (DI(K)**3.))
            ENDIF
            P(N-I)=PF+DP-PG
           L=(N-I)
            WRITE(*,66)L,P(L)
      66 FORMAT(T5,'P(',I1,')= ',F10.7)
           PF=P(N-I)
C
C          PEND IS THE LINE PRESSURE AT THE DOWNSTREAM END OF THE
C          TEST SECTION.
C
           PEND=P(2)
           IF(OP.EQ.1.) PEND=0.0
     899 CONTINUE
C       THE PRESSURE IN THE DOWNSTREAM DYNAMIC TRANSDUCER BRANCH
C       IS SET EQUAL TO THE PRESSURE IN THE LINE AT THE BRANCH POINT.
        P(2)=P(5)
        P(1)=P(2)
C       DETERMINE REYNOLDS NUMBER FOR A LINE
        TOTL=0.0
        DO 2 I=3,N
        TOTL=TOTL+AD(I)
   2    CONTINUE
C       RHO(N) IS THE DENSITY AT THE BEGINNING OF THE TEST LINE.
        RHO(N)=(PG+P(N))/(RE*TR)
        REYT=(P(N)-PEND)*((P(N)+PEND)/2.+PG)*(DI(N)**3.)/32./AMU/AMU
        REYT=REYT/TOTL/RE/TR
        IF (REYT.LT.2300.) GOTO 3
        REYT=(REYT*32./.1582)**(4./7.)
```

135

```
C      QM IS THE MASS FLOW RATE (LBF-S/IN)
C      QM*386.04=QM(LBM/S)
 3     QM=REYT*PI*DI(N)*AMU/4.
       QM1=386.04*QM
       WRITE(*,67)REYT
   67 FORMAT(T5,'THE REYNOLDS NUMBER IS ',F8.2)
       WRITE(*,68)QM1
   68 FORMAT(T5,'THE MASS FLOW RATE IS ',1PE11.4,' LBM/SEC')
C
C***********************************************************************
C                                                                     *
C                                                                     *
C      THE VARIABLES IN THE FOLLOWING SECTION ARE DEFINED AS:         *
C         RHO=DENSITY CALCULATED BY THE IDEAL GAS LAW  (LBF-S**2/IN**4) *
C         ANU=KINEMATIC VISCOSITY (IN**2/S)                           *
C         CA=ADIABATIC SPEED OF SOUND  (IN/S)                         *
C         AR= CROSS-SECTIONAL AREA OF LINE   (IN**2)                  *
C         CV=VISCOUS CHARACTERISTIC FREQUENCY (OMEGA-NU) (RAD/S)      *
C         OMT=THERMAL CHARACTERISTIC FREQUENCY  (RAD/S)               *
C         CNA=VISCOUS RESISTANCE  (LBF-S/IN**6)                       *
C         Q=VOLUMETRIC FLOW RATE (IN**3/S)                            *
C         AGM=ADIABATIC CAPACITANCE                                   *
C         RVT=LINE RESISTANCE                                         *
C         FN=FUNDAMENTAL FREQUENCY (RAD/S)                            *
C         PBR=LINE SEGMENT PRESSURE (PSIA)                            *
C                                                                     *
C***********************************************************************
       DO 23 I=1,N
       PBR=P(I)+PG
       RHO(I)PBR/(RE*TR)
       ANU(I)=AMU/RHO(I)
       CA(I)=SQRT(PBR*GAM/RHO(I))
       AR(I)=PI*DI(I)**2./4.
       CV(I)=(8.*PI*ANU(I))/AR(I)
       OMT(I)=CV(I)/(SIG*SIG)
       CNA(I)=(8.*PI*AMU)/(AR(I)*AR(I))
       Q(I)=QM/RHO(I)
   23 CONTINUE
C      THE FLOW IN THE DYNAMIC TRANSDUCER BRANCH IS SET
C      EQUAL TO ZERO.
       Q(1)=0.0
       Q(2)=0.0
       GMNI=.5*(GAM-1.)
       DO 26 I=1,N
       REY(I)=(4.*RHO(I)*Q(I))/(PI*DI(I)*AMU)
       PBR=P(I)+PG
       AGM(I)=AR(I)/(GAM*PBR)
       QTCA(I)=0.25*CA(I)
C
C      RVT(I) IS THE DC LINE RESISTANCE
```

136

```
C          1.75*RVT(I) IS THE AC (INCREMENTAL) LINE RESISTANCE
C
      RVT(I)=.3164*AMU*(REY(I)**.75)/(2.*AR(I)*(DI(I)**2.))
       RVT(I)=RVT(I)*1.75
     FN(I)=QTCA(I)/AD(I)
  26 CONTINUE
     NST=1
     DW=0.
     Y=1.
     M=0
C
C***********************************************************************
C          LOOP 80 CALCULATES THE THEORETICAL VALUES FOR THE            *
C          PLOT ROUTINE. THE MODIFIED EQUATIONS OF KRISHNAIYER          *
C          AND LECHNER ARE USED FOR BLOCKED AND LAMINAR FLOW.           *
C          THE PROGRAM ALSO CALCULATES THE PROPAGATION CONSTANT         *
C          BASED ON THE SELECTED TURBULENT MODEL AND COMPARES           *
C          THE LAMINAR AND TURBULENT VALUES. IT SELECTS THE             *
C          GREATER VALUE FOR USE IN THE OUTPUT ROUTINE.                 *
C                                                                       *
C                                                                       *
C          THE VARIABLES USED ARE:                                      *
C                                                                       *
C                                                                       *
C          RN=REAL PART OF Z (EQN 6 WILKIN)                             *
C          DC=COEFFICIENT (EQN 11 WILKIN)                               *
C          DG=COEFFICIENT (EQN 10 WILKIN)                               *
C          DD=DENOMINATOR OF EQN 7 (WILKIN)                             *
C          GN=REAL PART OF Y (EQN 7 WILKIN)                             *
C          ALN=IMAGINARY PART OF Z (EQN 6 WILKIN)                       *
C          CN=IMAGINARY PART OF Y (EQN 7 WILKIN)                        *
C          TEM1=REAL PART OF ZY                                         *
C          TEM2=IMAGINARY PART OF ZY                                    *
C          AN=REAL PART OF SQRT(ZY)                                     *
C          BTN=IMAGINARY PART OF SQRT(ZY)                               *
C          OX=NONDIMENSIONAL FREQUENCY                                  *
C          OY=NONDIMENSIONAL ATTENUATION                                *
C          TURB=TURBULENT MODEL INDICATOR                               *
C                                                                       *
C***********************************************************************
  40    DO 80 J=1,NST
       M=M+1
C
C    INCREMENT THE FREQUENCY BY 5 HZ AND CONVERT TO RAD/SEC.
C
       Y=Y+DW
       W=TPI*Y
       DO 27 I=1,N
       ARG=.5*SQRT(W/CV(I))
       RN(I)=CNA(I)*(.375+ARG+(.375/(4.*ARG)))
```

137

```fortran
      DC(I)=.25+SQRT(W/OMT(I))+.125*SQRT(OMT(I)/W)
      DG(I)=SQRT(W/OMT(I))-.125*SQRT(OMT(I)/W)
      DD(I)=DC(I)*DC(I)+DG(I)*DG(I)
      GN(I)=W*(GAM-1.)*AGM(I)*DG(I)/DD(I)
      ARG=.5**SQRT(CV(I)/W)
      ALN(I)=RHO(I)*(1.+ARG-(ARG*(15.*CV(I)/(W*64.))))/AR(I)
      TURB=0
      CN(I)=AGM(I)*(1.+((GAM-1.)*DC(I)/DD(I)))
      TEMP=-W*W
      LT=TL*RHO(I)/AR(I)
      DENOM=RVT(I)**2+((W**2)*(LT**2))
C***********************************************************************
C      THIS SECTION CALCULATES THE PROPAGATION                        *
C      OPERATOR SQRT(ZY).  THE THEORY SELECTED AT                     *
C      THE BEGINNING OF THE PROGRAM IS USED IN                        *
C      THIS SECTION.                                                  *
C          410      MODIFIED CONSTANT LRC                             *
C          420      MODIFIED LRCG                                     *
C          430      LAMINAR                                          *
C***********************************************************************
      GOTO(410,420,430)CASE
  410 TEM1=RN(I)*GN(I)+TEMP*ALN(I)*CN(I)
      TEM2=W*(RN(I)*CN(I)+GN(I)*ALN(I))
      CALL RTCMP(ARG1,ARG2,TEM1,TEM2)
      AN(I)=ARG1
      BTN(I)=ARG2
      TEM1=TEMP*TL*RHO(I)/AR(I)*CT*AGM(I)
      TEM2=W*RVT(I)*CT*AGM(I)
      CALL RTCMP(ARG1,ARG2,TEM1,TEM2)
      TAN=ARG1
      TBTN=ARG2
      IF(REY(I).LE.2300) GOTO 27
      IF(AN(I).GE.TAN) GOTO 27
      AN(I)=TAN
      BTN(I)=TBTN
      TURB=1
      GOTO 27
  420 TEM1=RN(I)*GN(I)*TEMP*ALN(I)*CN(I)
      TEM2=W*(RN(I)*CN(I)*GN(I)*ALN(I))
      CALL RTCMP(ARG1,ARG2,TEM1,TEM2)
      AN(I)=ARG1
      BTN(I)=ARG2
      CT=GAM-((W**2)*(GAM-1.)*LT*RHO(I)/(AR(I)*DENOM))
      TEM1=(((RVT(I)*(GAM-1.)*AGM(I)*RHO(I)*(W**2))/(AR(I)*DENOM))
     &))+(TEMP*TL*RHO(I)*CT*AGM(I)/AR(I))
      TEM2=((RVT(I)*(GAM-1.)*AGM(I)*RHO(I)*LT*(W**3))/(AR(I)*DENOM))
     &+(W*RVT(I)*CT*AGM(I))
      CALL RTCMP(ARG1,ARG2,TEM1,TEM2)
      TAN=ARG1
      TBTN=ARG2
      IF(REY(I).LE.2300) GOTO 27
      IF(AN(I).GE.TAN) GOTO 27
```

138

```fortran
            AN(I)=TAN
            BTN(I)=TBTN
            TURB=1
         GOTO 27
  430       TEM1=RN(I)*GN(I)+TEMP*ALN(I)*CN(I)
            TEM2=W*(RN(I)*CN(I)+GN(I)*ALN(I))
            CALL RTCMP(ARG1,ARG2,TEM1,TEM2)
            AN(I)=ARG1
            BTN(I)=ARG2
   27    CONTINUE
          OX=AR(10)*W/ANU(10)/PI
          OY=AR(10)*CA(10)*AN(10)/PI/ANU(10)
         WRITE(13,75)OX,OY
   75    FORMAT(T5,F10.5,T20,F10.5)
C        CALCULATE ZO
         DO 32 I=1,N
         TEM1=W*ALN(I)
         TEM2=W*CN(I)
         TEM3=RN(I)
         TEM4=GN(I)
         CALL CMPDV(ARG1,ARG2,TEM3,TEM1,TEM4,TEM2)
         CALL RTCMP(AZRNI,BZRNI,ARG1,ARG2)
         AZRN(I)=AZRNI
         BZRN(I)=BZRNI
         IF(TURB.EQ.0) GOTO 32
         TEM1=RHO(I)*(P(I)+PG)/AR(I)/AR(I)
         TEM2=-RVT(T)*(P(I)+PG)/W/AR(I)
         CALL RTCMP(ARG1,ARG2,TEM1,TEM2)
         AZRN(I)=ARG1
         BZRN(I)=ARG2
   32    CONTINUE
C CALCULATE Z IN 1
         I=1
         TEMP=AN(I)*AD(I)
         IF(TEMP.GT.88.) GO TO 80
         ARG1=COSH(TEMP)
         ARG2=SINH(TEMP)
         TEM5=BTN(I)*AD(I)
         TEMP=COS(TEM5)
         TEM1=ARG1*TEMP
         TEM3=ARG2*TEMP
         TEMP=SIN(TEM5)
         TEM2=ARG2*TEMP
         TEM4=ARG1*TEMP
         CALL CMPDV(ARG1,ARG2,TEM1,TEM2,TEM3,TEM4)
         TEM1=AZRN(I)
         TEM2=BZRN(I)
         CALL CMPMP(TEM3,TEM4,TEM1,TEM2,ARG1,ARG2
         AZIN(I)=TEM3
         BZIN(I)=TEM4
```

139

```
C CALCULATE Z IN 3
C    SEGMENT 3 IS THE DOWNSTREAM END OF THE TEST SECTION
      I=3
      TEM1=AZRN(I)
      TEM2=BZRN(I)
C
C**********************************************************************
C        CALCULATES THE TERMINAL IMPEDANCE: IF OP=1 (UNRESTRICTED       *
C        FLOW), SETS REAL PART EQUAL TO ZERO                            *
C               CALCULATES IMAGINARY PART                               *
C           IF OP=0 (RESTRICTED FLOW), SETS IMAGINARY PART TO ZERO      *
C               CALCULATES REAL PART                                    *
C                  FOR BLOCKED LINE   RE= INFINITY                      *
C                  FOR ORIFICE FLOW  RE CALCULATED USING REFLECTION     *
C                               COEFFICIENTS                            *
C                                                                       *
C**********************************************************************
C     IF (OP.EQ.1.) THEN
      ZEND=0.0
      ZENDI=-W*.4*RHO(I)*DI(I)/AR(I)
      ELSE
      ZENDI=0.0
        IF(DORF2.EQ.0.)THEN
        ZEND=1.0E99
        ELSE
        SQD3=DI(I)**2
C     N1 IS AN INDICATOR TO SELECT THE METHOD OF CALCULATING
C     THE REFLECTION COEFFICIENT.
C     N1=1    CHOKED FLOW IN THE ORIFICE
C     N1=2    NON-CHOKED FLOW IN THE ORIFICE
C
      IF(N1.EQ.1.)THEN
       RC=(SQD3-DORF2)/(SQD3+DORF2)
       ELSE
       RC=(SQD3-2.*DORF2)/(SQD3+DORF2)
      ENDIF
        RCC=(1.+RC)/(1.-RC)
        ZEND=4.*RHO(I)*CA(I)*RCC/(PI*SQD3)
        ENDIF
      ENDIF
      TEM3=ZEND
      TEM4=ZENDI
      TEM5=AN(I)
      TEM6=AD(I)
      TEM7=BTN(I)
      CALL CALZIN(AARG,BARG,TEM1,TEM2,TEM3,TEM4,TEM5,TEM6,TEM7)
      AZIN(I)=AARG
      BZIN(I)=BARG
C CALCULATE Z IN 4 AND 5
      DO 34 I=4,5
```

140

```
         TEM1=AZRN(I)
         TEM2=BZRN(I)
         TEM3=AZIN(I-1)
         TEM4=BZIN(I-1)
         TEM5=AN(I)
         TEM6=AD(I)
         TEM7=BIN(I)
         CALL CALZIN(AARG,BARG,TEM1,TEM2,TEM3,TEM4,TEM5,TEM6,TEM7)
         AZIN(I)=AARG
      34 BZIN(I)=BARG
C CALCULATE Z IN 2
         I=2
         TEM1=AZRN(I)
         TEM2=BZRN(I)
         TEM3=AZIN(I-1)
         TEM4=BZIN(I-1)
         TEM5=AN(I)
         TEM6=AD(I)
         TEM7=BTN(I)
         CALL CALZIN(AARG,BARG,TEM1,TEM2,TEM3,TEM4,TEM5,TEM6,TEM7)
         AZIN(I)=AARG
         BZIN(I)=BARG
C CALCULATE RECEIVING Z FOR LINE 6
         I=6
         TEM1=AZIN(I-1)
         TEM2=BZIN(I-1)
         TEM3=AZIN(I-4)
         TEM4=BZIN(I-4)
         CALL ZEBRA(AZOTI, BZOTI,TEM1,TEM2,TEM3,TEM4)
         AZOT(I)=AZOTI
         BZOT(I)=BZOTI
C CALCULATE Z IN 6 INCLUDING R-TRANSDUCER
         TEM1=AZRN(I)
         TEM2=BZRN(I)
         TEM3=AN(I)
         TEM4=AD(I)
         TEM5=BTN(I)
         CALL CALZIN(AZINI,BZINI,TEM1,TEM2,AZOTI,BZOTI,TEM3,TEM4,TEM5)
         AZIN(I)=AZINI
         BZIN(I)=BZINI
C CALCULATE Z IN 7,8,9 AND 10 INCLUDING R-TRANSDUCERS
         DO 39 I=7,10
         TEM1=AZRN(I)
         TEM2=BZRN(I)
         TEM3=AZIN(I-1)
         TEM4=BZIN(I-1)
         TEM5=AN(I)
         TEM6=AD(I)
         TEM7=BTN(I)
         CALL CALZIN(AZINI,BZINI,TEM1,TEM2,TEM3,TEM4,TEM5,TEM6,TEM7)
         AZIN(I)=AZINI
```

141

```
39      BZIN(I)=BZINI
C CALCULATE P5/P6 INCLUDING R-TRANSDUCER
        I=6
        TEMP=BTN(I)*AD(I)
        CSBI1=COS(TEMP)
        SNBI1=SIN(TEMP)
        TEMP=AN(I)*AD(I)
        ARG1=COSH(TEMP)
        ARG2=SINH(TEMP)
        TEM1=ARG1*CSBI1
        AZOTI=AZOT(I)
        BZOTI=BZOT(I)
        AZINI=AZIN(I)
        BZINI=BZIN(I)
        CALL CMPDV(TEM7,TEM8,AZOTI,BZOTI,AZINI,BZINI)
        CALL CMPMP(TEM3,TEM4,TEM7,TEM8,TEM1,TEM2)
        TEM5=ARG2*CSBI1
        TEM6=ARG1*SNBI1
        TEM9=AZRN(I)
        TEM10=BZRN(I)
        CALL CMPDV(TEM7,TEM8,AZOTI,BZOTI,TEM9,TEM10)
        CALL CMPMP(TEM1,TEM2,TEM7,TEM8,TEM5,TEM6)
        TEM1=TEM3-TEM1
        TEM2=TEM4-TEM2
        TEMP=TEM1*TEM1+TEM2*TEM2
        BETA(I)=ATAN2(TEM2,TEM1)
        BET(I)=(180./PI)*BETA(I)
        RTP(I-1)=SQRT(TEMP)
        GP(I-1)=20.*ALOG10(RTP(I-1))
C CALCULATE P6/P7, P7/P8, P8/P9, AND P9/P10 INCLUDING R-TRANSDUCERS
        DO 43 I=7,10
        TEMP=BTN(I)*AD(I)
        CSBI1=COS(TEMP)
        SNBI1=SIN(TEMP)
        TEMP=AN(I)*AD(I)
        ARG1=COSH(TEMP)
        ARG2=SINH(TEMP)
        TEM1=ARG1*CSBI1
        TEM2=ARG2*SNBI1
        AZINI1=AZIN(I-1)
        BZINI1=BZIN(I-1)
        AZINI=AZIN(I)
        BZINI=BZIN(I)
        CALL CMPDV(TEM7,TEM8,AZINI1,BZINI1,AZINI,BZINI)
        CALL CMPMP(TEM3,TEM4,TEM7,TEM8,TEM1,TEM2)
        TEM5=ARG2*CSBI1
        TEM6=ARG1*SNBI1
        TEM9=AZRN(I)
        TEM10=BZRN(I)
        CALL CMPDV(TEM7,TEM8,AZINI1,BZINI1,TEM9,TEM10)
        CALL CMPMP(TEM1,TEM2,TEM7,TEM8,TEM5,TEM6)
```

142

```
        TEM1=TEM3-TEM1
        TEM2=TEM4-TEM2
        TEMP=TEM1*TEM1+TEM2*TEM2
        BETA(I)=ATAN2(TEM2,TEM1)
        BET(I)=(180./PI)*BETA(I)
        RTP(I-1)SQRT(TEMP)
   43   GP(I-1)=20.*ALOG10(RTP(I-1))
        RTPT=RTP(6)*RTP(7)*RTP(8)*RTP(9)*RTP(5)
        GPT=20.*ALOG10(RTPT)
        BETAR=BETA(6)+BETA(7)+BETA(8)+BETA(9)+BETA(10)
   35   IF (BETAR.LE.0.) GOTO 36
        BETAR=BETAR-TPI
        TOGO 35
   36   IF (BETAR.GT.-TPI) GOTO 37
        BETAR=BETAR+TPI
        GOTO 36
C       CONVERTS BETAR(RADS) TO BETAD(DEGS)
   37   BETAD=(180./PI)*BETAR
C    SKIPS WRITE STATEMENT FOR OUTPUT TABLE HEADINGS
        IF(NNN.GT.1) GOTO 600
        WRITE(12,810)
  810   FORMAT(1H0,T3,'SEGMENT',T16,'LENGTH',T29,'DIAMETER',T43,
       &'PRESSURE',T59,'C ADB',T73,'FN',T86,'DENSITY',T98,'REYNOLDS NO')
        DO 803 I=1,N
        IF(OP.EQ.1.0) GOTO 803
        IF(DORF2.EQ.0.0) THEN
         REY(I)=0.
        ENDIF
  803   WRITE(12,802)I,AD(I),DI(I),P(I),CA(I),FN(I),RHO(I),REY(I)
  802   FORMAT(1H0,T6,I2,T11,7(1PE12.4,2X))
        WRITE(12,706)
  706   FORMAT(1H//)
        WRITE(12,890)
  890   FORMAT(T25,'****************************************************')
        WRITE(12,706)
        WRITE(12,700)
  700   FORMAT(T40,'THEORETICAL RESULTS')
        WRITE(12,706)
        WRITE(12,830)
  830   FORMAT(1X,T10,'FREQUENCY',T35,'ATTENUATION',T52,'PHASE SHIFT',T79
       &,'GAIN',T101,'TURBULENCE')
        WRITE(12,850)
  850   FORMAT(1X,T101,'INDICATOR')
        WRITE(12,840)
  840   FORMAT(1X,T5,'(HZ)',T13,'(NON-DIMENSIONAL)',T32,'(NON-DIMENSIONAL)
       &',T55,'(DEG)',T70,'(DB)',T82,'(NON-DIMENSIONAL)')
        WRITE(12,706)
C NNN IS THE COUNTER TO SKIP THE HEADINGS WRITE STATEMENT.
        NNN=2
  600   WRITE(12,702)Y,OX,OY,BETAD,GPT,RTPT,TURB
```

143

```
  702 FORMAT(1X,T4,F5.0,T14,F10.5,T34,F10.5,T54,F7.2,T66,1PE12.4,T83,1PE
     &12.4,T105,T2)
      WRITE(14,97)Y,GPT
   97 FORMAT(T5,F5.0,T20,1PE12.4)
      DBT(M)=GPT
      OMB(M)=Y
      PHASE(M)=BETAD

   80 CONTINUE
      GO TO (85,611),IND
   85 Y=0.
C   DW IS THE FREQUENCY INCREMENT (HZ), NST IS THE NUMBER
C   OF THEORETICAL VALUES CALCULATED (0-1000 HZ)
      DW=5.
      NST=200
      IND=2
      GO TO 40


C
C**********************************************************************
C**********************************************************************
C**********************************************************************
C**********************************************************************
C**********************************************************************
C**********************************************************************
C**********************************************************************
C            THIS SECTION IS FOR THE CALCOMP PLOTTER.  ONE SET OF      *
C            EXPERIMENTAL DATA MUST BE INCLUDED WITH EACH RUN.         *
C                                                                     *
C   NPTS IS NUMBER OF EXPERIMENTAL POINTS TO BE INPUT                 *
C   LSMB IS THE PLOTTER SYMBOL TO BE USED FOR GPX AND PHD.            *
C   SEE A CALCOMP PLOTTER USERS MANUAL FOR DESCRIPTION.               *
C   FREQ IS THE EXPERIMENTAL FREQUENCY (HZ)                           *
C   PS IS THE SENDING PRESSURE, EXPERIMENTAL (MV)                     *
C   PR IS THE RECEIVING PRESSURE, EXPERIMENTAL (MV)                   *
C   PHT IS THE EXPERIMENTAL PHASE DELAY (MSEC)                        *
C                                                                     *
C**********************************************************************
C      NEGATES THE PLOT ROUTINE IF ICAS .LE. ZERO
  611 IF(ICAS)502,502,610
  610 CALL FACTOR(0.625)
      CALL RECT(0.,0.,9.6,12.0,0.,3)
      CALL PLOT(.6,.6,-3)
      OMG(M+1)=0.
      OMG(M+2)=100.
      DBT(M+1)=-20.
      DBT(M+2)=5.0
C      DRAWS AXES FOR GAIN PLOT
      CALL AXIS(0.,0.,'FREQUENCY (HERTZ)',-17,10.0,0.,OMG(M+1),OMG
     &   (M+2))
```

144

```
              CALL AXIS(0.,0.,'GAIN (DECIBELS)',15,8.,90.,DBT(M+1),DBT
     &    (M+2))
C     PLOTS CURVE FOR THEORETICAL GAIN
              CALL LINE(OMG,DBT,M,1,0,4)
               READ(11,705)TITLE
       705 FORMAT(A50)
              READ(11,*)NPTS
              WRITE(12,706)
              WRITE(12,890)
              WRITE(12,706)
              WRITE(12,860)
       860 FORMAT(T45,'EXPERIMENTAL DATA')
              WRITE(12,207)
       207 FORMAT(1H//,T14,'N',T20,'FREQUENCY (HZ)',T42,'PRESSURE (MV)',T66,
     &'GAIN (DB)',T82,'PHASE SHIFT (DEG)')
              WRITE(12,870)
       870 FORMAT(1H//,T39,'SENDING',T49,'RECEIVING')
              WRITE(12,706)
              J=0
              DO 69 I=1,NPTS
              READ(11,*)FREQ,PS,PR,PHT
              GPX=20.*ALOG10(PR/PS)
              PHD=-PHT*FREQ*.36
              IF(PHD.LT.-360.)THEN
              PHD=PHD+360.
              ENDIF
              WRITE(12,209)I,FREQ,PS,PR,GPX,PHD
       209 FORMAT(1X,T12,I3,T23,F5.0,T39,F6.1,T50,F6.1,T64,F10.5,T84,F10.5)
              DB(I)=GPX
              OMGX(I)=FREQ
              IF(PHD.GT.0) GOTO 69
              J=J+1
              PH(J)=PHD
              OMGP(J)=FREQ
              JMAX=J
        69 CONTINUE
              OMGX(NPTS+1)=OMG(M+1)
              DB(NPTS+1)=DBT(M+1)
              OMGX(NPTS+2)=OMG(M+2)
              DB(NPTS+2)=DBT(M+2)
C     PLOTS EXPERIMENTAL GAIN DATA
              LSMB=0
              CALL LINE(OMGX,DB,NPTS,1,-1,LSMB)
              CALL SYMBOL(3.,13.,.165,TITLE,0.,50)
              GOTO(111,112,113)CASE
       111 THEOR='MOD CONST LRC'
              GOTO 114
       112 THEOR='CONST LRCG'
              GOTO 114
       113 THEOR='LAMINAR'
```

145

```
    114 CONTINUE
        CALL SYMBOL(3.,12.5,.165,THEOR,0.,50)
        CALL PLOT(15.0,-.6,-3)
        CALL FACTOR(0.625)
        CALL RECT(0.,0.,9.6,12.0,0.,3)
        CALL PLOT(.6,.6,-3)
        OMG(M+1)=0.
        OMG(M+2)=100.
        PHASE(M+1)=-360.
        PHASE(M+2)=45.
C     DRAWS AXES FOR PHASE PLOT
        CALL AXIS(0.,0.,'FREQUENCY (HERTZ)',-17,10.,0.,OMG(M+1),
       &OMG(M+2))
        CALL AXIS(0.,0.,'PHASE ANGLE (DEGREES)',21,8.,90.,PHASE(M+1),
       &PHASE(M+2))
C     PLOTS CURVE FOR THEORETICAL PHASE
        CALL LINE(OMG,PHASE,M,1,0,4)
        OMGP(JMAX+1)=OMG(M+1)
        OMGP(JMAX+2)=OMG(M+2)
        PH(JMAX+1)=PHASE(M+1)
        PH(JMAX+2)=PHASE(M+2)
C     PLOTS EXPERIMENTAL PHASE DATA
        CALL LINE(OMGP,PH,JMAX,1,-1,LSMB)
        CALL SYMBOL(3.,13.,.165,TITLE,0.,50)
        CALL SYMBOL(3.,12.5,.165,THEOR,0.,50)
   1003 CALL PLOT(10.0,0,-3)
C********************************************************************
C********************************************************************
C
    501 CALL PLOTE
    502 STOP
        END
C********************************************************************
C********************************************************************
C CALCULATES ROOT OF A COMPLEX NUMBER
C    X = RE(SQRT(A+BI)
C    Y = IM(SQRT(A+BI)
C
        SUBROUTINE RTCMP(X,Y,A,B)
        CALL ANGL(TEMP,A,B)
        TEMP=.5*TEMP
        Y=A*A+B*B
        X=SQRT(Y)
        X=SQRT(X)
        Y=X*SIN(TEMP)
        X=X*COS(TEMP)
        RETURN
        END
C
```

146

```
C********************************************************************
C
      SUBROUTINE CMPMP(X,Y,A1,A2,B1,B2)
C     MULTIPLIES TWO COMPLEX NUMBERS
C     (A1+A2J)*(B1+B2J)=X+YJ
C
      X=A1*B1-A2*B2
      Y=A1*B2+A2*B1
      RETURN
      END
C
C********************************************************************
C
C FINDS THE QUOTIENT OF TWO COMPLEX NUMBERS
      SUBROUTINE CMPDV(C1,C2,A1,A2,B1,B2)
C  CALCULATES THE QUOTIENT OF TWO COMPLEX NUMBERS
C     A1+A2J/B1+B2J
      TEMP=B1*B1+B2*B2
      C1=A1*B1+A2*B2
      C1=C1/TEMP
      C2=B1*A2-A1*B2
      C2=C2/TEMP
      RETURN
      END
C
C********************************************************************
C
      SUBROUTINE HSINX(ARG,X)
C   CALCULATES THE HYPERBOLIC SINE OF X
      A=EXP(X)
      B=EXP(-X)
      A=A-B
      ARG=.5*A
      RETURN
      END
C
C********************************************************************
C
      SUBROUTINE HCOSX(ARG,X)
C   CALCULATES THE HYBERBOLIC COSINE OF X
      A=EXP(X)
      B=EXP(-X)
      A=A+B
      ARG=.5*A
      RETURN
      END
C
```

```
C********************************************************************
C

      SUBROUTINE ANGL(C,A,B)
C    CALCULATES THE MAGNITUDE OF ANGLE X (IN RADS) AND ASSIGNS
C    THE PROPER SIGN BASED ON THE CARTESIAN COORDINATES (A,B)
      DATA PI/3.1415926/
      C=ABS(B/A)
      C=ATAN(C)
      IF (A.GT.0.) GO TO 5
      IA=1
      GO TO 7
    5 IA=0
    7 IF (B.GT.0.) GO TO 10
      IB=2
      GO TO 15
   10 IB=0
   15 IA=IA+IB+1
      GO TO (35,30,25,20),IA
   20 C=C-PI
      GO TO 35
   25 C=-C
      GO TO 35
   30 C=PI-C
   35 RETURN
      END
C
C********************************************************************
C

      SUBROUTINE CALZIN(AZIN1,BZIN1,AZRN1,BZRN1,AZIN2,BZIN2,AN1,DI1,
     &BTN1)
      TEMP=AN1*DI1
      CALL HCOSX(ARG1,TEMP)
      CALL HSINX(ARG2,TEMP)
      TEMP=BTN1*DI1
      CSBI1=COS(TEMP)
      SNBI1=SIN(TEMP)
      ZR=0.
      CALL CMPMP(TEM1,TEM2,AZIN2,BZIN2,ARG1,ZR)
      CALL CMPMP(TEM3,TEM4,AZRN1,BZRN1,ARG2,ZR)
      CALL CMPMP(TEM5,TEM6,AZIN2,BZIN2,ARG2,ZR)
      CALL CMPMP(TEM7,TEM8,AZRN1,BZRN1,ARG1,ZR)
      A1=TEM1+TEM3
      B1=TEM2+TEM4
      A2=TEM5+TEM7
      B2=TEM6+TEM8
      CALL CMPMP(TEM1,TEM2,A1,B1,CSBI1,ZR)
      CALL CMPMP(TEM5,TEM6,A2,B2,CSBI1,ZR)
      CALL CMPMP(TEM7,TEM8,A1,B1,ZR,SNBI1)
      CALL CMPMP(TEM3,TEM4,A2,B2,ZR,SNBI1)
```

148

```fortran
      TEM3=TEM3+TEM1
      TEM4=TEM4+TEM2
      TEM7=TEM7+TEM5
      TEM8=TEM8+TEM6
      CALL CMPDV(TEM1,TEM2,TEM3,TEM4,TEM7,TEM8)
      CALL CMPMP(AZIN1,BZIN1,TEM1,TEM2,AZRN1,BZRN1)
      RETURN
      END
C
C*********************************************************************
C

      SUBROUTINE ZEBRA(C1,C2,A1,A2,B1,B2)
C     COMPUTES THE INVERSE OF THE SUM OF THE INVERSES OF TWO
C     COMPLEX NUMBERS.
C     C1+C2J=1/((1/A1+A2J)+(1/B1+B2J))
      D1=1.
      D2=0.
      CALL CMPDV(ARG1,ARG2,D1,D2,A1,A2)
      CALL CMPDV(ARG3,ARG4,D1,D2,B1,B2)
      ARG1=ARG1+ARG3
      ARG2=ARG2+ARG4
      CALL CMPDV(C1,C2,D1,D2,ARG1,ARG2)
      RETURN
      END
```

149

Appendix C: <u>Equipment</u>

<u>Item</u>	<u>Manufacturer</u>	<u>Model</u>	<u>Serial No.</u>
Pneumatic driver	Bendix	PC-DCC-PS	001
Amplifier/ Power Supply	Bendix/Lambda		ENY A 293 -297
Wave Analyzers	Hewlett Packard	302A	018-02012 018-01985
Frequency Counters	Computer Measurement	726C	ENY 0021 ENY 0035
Dynamic Pressure Transducers	Kristal	701A	65079 7588
Charge Amplifiers	Kistler	568	704 1429
Digital Oscilloscope	Nicolet	2090-3C	85A06578
Static Pressure Transducer	Bell & Howell	1000-02	9302
Digital Voltmeter	Hewlett Packard	3466A	1716A-18944
DC Power Supply	Hewlett Packard	6205B	1140A14646
Rotometer	Brooks	ShoRate	USAF9175-83
Travelling Microscope	Gaertner	slide scope	2776P 1211K

150

Bibliography

1. Nichols, N. B. "The Linear Properties of Pneumatic Transmission Lines," _Transactions of the Instrument Society of America_, 1: 5-14 (1962).

2. Krishnaiyer, R. and T. J. Lechner, Jr. "An Experimental Evaluation of Fluidic Transmission Line Theory," _Advances in Fluidics_. Edited by F. T. Brown, et al. New York: American Society of Mechanical Engineers, 1967.

3. Brown, F. T., D. L. Margolis, and R. P. Shah. "Small Amplitude Frequency Behavior in Fluid Lines with Turbulent Flow," _Journal of Basic Engineering_, Trans. ASME: 678-693 (December 1969).

4. Moore, E. F. _The Small Signal Response of Fluid Transmission Lines Including Developed Mean Flow Effects_. PhD dissertation. School of Engineering, Air Force Institute of Technology (AU), Wright-Patterson AFB OH, June 1977.

5. Briski, M. S. _Effects of Mean Flow on the Dynamic Characteristics of Fluid Transmission Lines_. MS thesis. School of Engineering, Air Force Institute of Technology (AU), Wright-Patterson AFB OH, December 1983.

6. Wilkins, P. G. _Dynamic Response of Fluid Transmission Lines_. MS thesis. School of Engineering, Air Force Institute of Technology (AU), Wright-Patterson AFB OH, December 1984.

7. Kirshner, J. M. and S. Katz. _Design Theory of Fluidic Components_. New York: Academic Press, 1975.

8. Franke, M. E. Private Communications. Air Force Institute of Technology (AU), Wright-Patterson AFB OH, March 1984 - November 1984.

9. Moore, E. F. and M. E. Franke. _Approximations for Frequency Dependent Attenuation in Circular and Noncircular Lines with Turbulent Mean Flow_. Unpublished paper, date unknown.

10. Franke, M. E., A. J. Malanowski, and P. S. Martin. "Effects of Temperature, End-Conditions, Flow, and Branching on the Frequency Response of Pneumatic Lines," _Journal of Dynamic Systems, Measurement and Control,_ Trans. ASME: 15-20 (March 1972).

11. Moore, P. M. and K. U. Ingard. _Theoretical Acoustics._ New York: McGraw-Hill Book Company, 1968.

12. Kinsler, L. E. and A. R. Frey. _Fundamentals of Acoustics._ New York: John Wiley and Sons, Inc., 1972.

13. Schlichting, H. _Boundary Layer Theory._ New York: McGraw-Hill Book Company, 1979.

14. Malanowski, A. J. _The Dynamic Response of Fluidic Networks._ MS thesis. School of Engineering, Air Force Institute of Technology (AU), Wright-Patterson AFB OH, March 1971.

15. Doeblin, Ernest O. _Measurement Systems Application and Design_ (Third Edition). New York: McGraw Hill Book Company, 1983.

VITA

Major Stephen J. McKenna was born ███████████

███████████████████████████ He graduated from

█████████████████████ in 1972 and was selected to attend

the Royal Military College of Canada in Kingston, Ontario

under the Regular Officer Training Plan. He graduated in

1976 with a Bachelor of Chemical Engineering (Nuclear

Science) and received his commission in the Canadian Armed

Forces as an Aerospace Engineering Officer. He has served

as a maintenance officer on C-130 and CC-138 aircraft, and

following specialized training in the United Kingdom, as

a training officer at the Canadian Forces School of Aero-

space and Ordnance Engineering. Major McKenna entered the

School of Engineering, Air Force Institute of Technology,

in August 1983.

Permanent address: ███████████

███████████████

██████

██████

153

AD-A164354

REPORT DOCUMENTATION PAGE

UNCLASSIFIED

1a. REPORT SECURITY CLASSIFICATION	1b. RESTRICTIVE MARKINGS
2a. SECURITY CLASSIFICATION AUTHORITY	3. DISTRIBUTION/AVAILABILITY OF REPORT
2b. DECLASSIFICATION/DOWNGRADING SCHEDULE	Approved for public release; distribution unlimited.

4. PERFORMING ORGANIZATION REPORT NUMBER(S)	5. MONITORING ORGANIZATION REPORT NUMBER(S)
AFIT/GAE/AA/85S-1	

6a. NAME OF PERFORMING ORGANIZATION	6b. OFFICE SYMBOL (If applicable)	7a. NAME OF MONITORING ORGANIZATION
School of Engineering	AFIT/ENY	

6c. ADDRESS (City, State and ZIP Code)	7b. ADDRESS (City, State and ZIP Code)
Air Force Institute of Technology Wright-Patterson AFB, Ohio 45433	

8a. NAME OF FUNDING/SPONSORING ORGANIZATION	8b. OFFICE SYMBOL (If applicable)	9. PROCUREMENT INSTRUMENT IDENTIFICATION NUMBER

8c. ADDRESS (City, State and ZIP Code)	10. SOURCE OF FUNDING NOS.			
	PROGRAM ELEMENT NO.	PROJECT NO.	TASK NO.	WORK UNIT NO.

11. TITLE (Include Security Classification)
See Box 19

12. PERSONAL AUTHOR(S)
Stephen J. McKenna, B. Chem. Eng., Maj, CAF

13a. TYPE OF REPORT	13b. TIME COVERED	14. DATE OF REPORT (Yr., Mo., Day)	15. PAGE COUNT
MS Thesis	FROM _____ TO _____	1985 September	171

16. SUPPLEMENTARY NOTATION

17. COSATI CODES			18. SUBJECT TERMS (Continue on reverse if necessary and identify by block number)
FIELD	GROUP	SUB. GR.	Fluid Transmission Lines, Frequency Response, Pneumatic Transmission Lines
20	04		

19. ABSTRACT (Continue on reverse if necessary and identify by block number)

Title: DYNAMIC RESPONSE OF FLUID TRANSMISSION LINES

Thesis Chairman: Dr. Milton E. Franke

20. DISTRIBUTION/AVAILABILITY OF ABSTRACT	21. ABSTRACT SECURITY CLASSIFICATION
UNCLASSIFIED/UNLIMITED ☒ SAME AS RPT. ☐ DTIC USERS ☐	UNCLASSIFIED

22a. NAME OF RESPONSIBLE INDIVIDUAL	22b. TELEPHONE NUMBER (Include Area Code)	22c. OFFICE SYMBOL
Dr. Milton E. Franke	513-255-2362	AFIT/ENY

DD FORM 1473, 83 APR   EDITION OF 1 JAN 73 IS OBSOLETE.

The theoretical predictions of the dynamic response of circular cross-section pneumatic transmission lines were compared with experimental results. Tests were conducted in blocked line situations as well as in both laminar and turbulent mean flow conditions. The lines used in the study were 24 in. in length with inside diameters of 0.041, 0.119, and 0.195 in. Tests were conducted over the frequency range 20 to 1000 Hz and over a range of mean flow Reynolds numbers from 0 to 16000.

Theoretical solutions were obtained from computer simulations using a laminar flow model and two turbulent flow models. These models were developed from the Navier-Stokes equation and include components to account for viscosity and radial heat transfer in the fluid.

An examination of the turbulent models was conducted based on a nondimensional frequency and attentuation. This led to modification of one of the turbulent models to include a frequency dependent term in the conductance.

The effect of flow conditions upstream of the test line and the effect of orifice design on the dynamic response were studied.

Experimental results showed good agreement with results of earlier studies. The use of a bypass device upstream of the test line was found to have no effect on line response.

The reconfiguration of the orifice devices to more closely match theoretical models produced no noticeable change in the results.